9-15-2017 10:30 AM

Experimental Measurements of Far Field Cough Airflows Produced by Healthy and Influenza- Infected Human Subjects

Ahmed Faraj Alarbi Mohamed
The University of Western Ontario

Supervisor
Dr. Eric Savory
The University of Western Ontario

Abstract

The present work details an experimental study of the cough airflow fields produced by subjects infected with influenza and when they have recuperated as convalescent, together with data from healthy cohorts. The Particle Image Velocimetry (PIV) and Hot Wire Anemometry (HWA) measurements were taken far downstream at 1m from the source within a cough chamber, along with droplet sampling at two different locations and nasal swabs from the sick subjects. The measured data over different seasons were used to evaluate and compare the results from sick, convalescent and healthy subjects. Although a total of 7 sick participants from winter 2014 and 2017 yielded positive nasal swab analysis, the total number of subjects involved in this work was 49. The results from HWA show modest differences between sick and convalescent states of a participant, but the normalized cough velocity time histories from both the techniques follow similar trends. It is anticipated that a larger samples size will provide a clear conclusive difference among coughs from the three categories.

Keywords

Acknowledgments

I would like to dedicate this thesis to my family in appreciation for putting up with my long hours and supporting my efforts from start to finish.

I am grateful and I wish to express my deepest gratitude to my supervisor Professor Eric Savory, for his continuing advice, useful suggestions, guidance and interest through all stages of this work.

In addition I would express my sincere gratitude for each member of teaching staff member at Faculty of Engineering – UWO who contributed in constructing my academic knowledge.

Moreover, I wish to express my thanks to all of my brilliant colleagues of Advanced Fluid Mechanics Research Group (AFM – UWO), and in CHRP project. Their help, suggestions, and support both professionally and personally cannot be understated.

Table of Contents

List of Tables

List of Figures

Nomenclature

The following symbols are used generally throughout the text.

Others are defined as and when used.

Symbol	Description	Units
L	Integral length scale	mm
t	time	Second -(sec)
T_E	Integral time scale	sec
t_p	The time at the peak of the cough velocity	sec
t_s	The time at the beginning of the cough velocity period	sec
Δt	The time separation between laser pulses	μs
u	The axial velocity component	m/s
u_i	The local axial velocity component in the field of view	m/s
u_p	The axial velocity component at the peak of the cough velocity	m/s
$u_{p,c}$	Accumulative peak cough velocity	m/s
u'_{rms}	The root mean square of axial fluctuation velocity	m/s
$u'_{(t)}$	Instantaneous axial fluctuation velocity	m/s
U	Dimensionless the axial component of cough velocity	

U_{norm}	Normalized velocity	
$U_{p\text{-}s}$	The moving average velocity from min to max value of cough velocity	m/s
$U(t)$	Instantaneous axial velocity component	m/s
$\overline{U}_{(t)}$	Moving averaging of axial velocity component	m/s
$<U>$	The spatial mean velocity within the field of view	m/s
$<U'>$	Dimensionless spatially averaged cough velocity	
$<V>$	Instantaneous velocity magnitude within the field of view	m/s
Y	The vertical distance of the field of view	m
X	The axial distance of the field of view	m
R	Autocorrelation	

Abbreviations

CCD	Coupled charged device camera
CFD	Computational fluid dynamics
CTA	Constant temperature anemometry
FLUGIE	Fluids from UnderGrad with Influenza Enclosure
HWA	Hot wire anemometry
IA	Integration area

IMI   Interferometric Mie Imaging

LDA   Laser Doppler Anemometer

MTS   Mid Turbinate Swab

PCR   Polymerase Chain Reaction

PIV   Particle Image Velocimetry

PSD   Power Spectral Energy

PTFE   Polytetrafluoroethylene

REB   Research Ethic Board

RNA   Ribonucleic acid

RSV   Respiratory syncytial virus

WeCoF   Western Cold and Flu aerosol studies

WHO   World health organization

WSHS   Western student health service

Chapter 1

1. Introduction

In this chapter, general introduction about flu outbreak and its effect on the communities and how it spread will present in this section. Moreover, the motivation behind the research and its objectives both will be presented in individual sections. In addition, organization of the thesis will be illustrated in the last section of this chapter.

1.1   General Introduction

In April 2009, the pandemic influenza A (H1N1) first appeared in North America, and spread rapidly around the world (Canadian Institute for Health Information 2010). By the beginning of 2010, it had caused about 17,000 deaths around the world after the first wave of SARS in 2003 (Aliabadi et al. 2011). Canada was affected from the first wave in 2003, when the SARS outbreak killed 44 Canadians, caused illness in a few hundred more, and resulted in the quarantine of 250,000 residents in one geographic location, the city of Toronto (Canadian Institute for Health Information 2010). In general, influenza (flu) is caused by airborne contagious pathogens. It infects the human respiratory system first. It can cause mild to severe illness that can result in hospitalization or death (NCIRD 2016) A hundred airborne infectious pathogens can be classified into three major groups as follows: Viruses, Bacteria and Fungal Spores (Tang et al. 2011; Bahnfleh and Kowalski 1998). The smallest are viruses with diameters in the range of 0.02-0.3 µm, while the largest are spores with diameters in the range of 0.5-30 µm (Tang et al. 2011).

Human respiratory activities are key sources for dispersal of airborne pathogens, namely; breathing, speaking, coughing and sneezing. The human expirations (breathing, coughing and sneezing) generate the smallest aerosols compared to other sources and these expiratory aerosols are particularly important in the spread of airborne infection from host to host (Morawska 2006). Coughing is considered to be a discontinuous multiphase turbulent flow that is generally composed of buoyant warm moist air and suspended droplets of various sizes. These droplets contain pathogens and minerals that can form

droplet nuclei after evaporation of the droplet's phase (Tellier 2006). These flows retain roughly the same shape and their lateral extent increases linearly with distance from the source (Tellier 2006). Many factors govern coughing flow, such as mouth opening area, flow rate and direction, temperature and, finally, the size distribution of the virus droplets and the quantity of virus in the droplet (Gupta et al 2009). These factors are transient and can have considerable person-to-person variation.

Influenza is of great concern to the healthcare community because of annual seasonal outbreaks and the potential for newly emerging strains to cause severe global pandemics. In enclosed environments the microflora concentration (as bio-aerosols) of a healthy work environment are lower than in the outdoor environment (Memarzadeh 2013). In a healthcare setting people with certain health conditions and healthcare workers can more readily be infected by pathogens (Kinnamer 2007; Government of Canada 2006; Deller et al. 2008). During a pandemic, healthcare workers are at greater risk from exposure to the virus as they care for an unforeseen surge in the number of infected patients. Infectious agents can be transmitted by direct or indirect contact of droplet or droplet nuclei in healthcare settings (Deller et al. 2008). Direct transmission occurs when the transfer of microorganisms results from direct physical contact between an infected individual and a susceptible host. Droplet transmission occurs when respiratory droplets generated via coughing, sneezing or talking contact susceptible mucosal surfaces, such as the eyes, nose or mouth. Most respiratory droplets are large and are not able to remain suspended in the air. Thus, they are usually dispersed over short distance (Booth et al. 2005). Airborne transmission refers to infectious agents that are spread via droplet nuclei containing infective microorganisms. These organisms can survive outside the body and remain suspended in the air for long periods of time depending on their sizes (Bozzuto and Ruggieri 2010).

Recently, respiratory communicable diseases have developed the potential to cause deaths and economic disasters globally. Therefore, the World Health Organization (WHO) and developed countries expend a huge effort to prevent and control disease outbreaks (Tang et al. 2006). Evidence exists to support the transmission of influenza viruses by contact, droplet and airborne transmission. However, experimental studies

involving humans are limited (Tang et al. 2006) and the relative contribution of each mode of transmission remains unclear. Furthermore, the relative importance of airborne transmission in setting the normal air exchange in buildings is unknown (Memarzadeh 2013). In order to improve our understanding of the dynamic process of person-to-person airborne virus transmission, there is a necessity to use realistic airflow and droplet size data to develop an effective theoretical model (Holmes and Morawska 2006) and a computational fluid dynamics (CFD) model (Holmes and Morawska 2006; Shah et al. 2006; Zhu et al. 2006). Accurate boundary conditions, which are provided by experimental work, are important to gain an accurate prediction of virus transmission. Many previous studies have been based on artificial puff sources (Sze To et al. 2008) and some other studies have been based on a combination of experimental investigations and CFD simulation (Yan et al. 2009). The majority of the previous experimental work was conducted to study the relative importance of far-zone airborne transmission and near-zone large droplet transmission for many diseases (e.g. Influenza, Tuberculosis, and Chickenpox, Measles.) by using different techniques (e.g. high speed photograph, shadowgraph and schlieren imaging.) (Yan et al. 2009).

To perform efficient infection control measures in healthcare facilities, the pathways by which the disease transfers from person-to-person need to be identified so that transmission can be interrupted. The present research focuses on examining the factors influencing the persistence of viable influenza virus in human cough droplets issuing into the environment. These factors will establish evidence based guidance for safe separation distances to mitigate person-to-person transmission of influenza, notably in healthcare settings. The literature review of the work done on this field over the past decades is given in the next section to identify the gaps and discrepancies and, thus to come up with the objectives and paves the way for road map of the present research work.

1.2 Motivation

Most previous work has examined the near field region, especially close to the mouth, by using different techniques. Many factors affect the coughing flow and droplet size distribution. Some of these factors are transient, which increases the complexity of the coughing flow (Gupta et al 2009). Physiological factors such as gender, weight, height, age and health status of the participants play a key role in coughing flow (Nishimura et al 2013). Moreover, mouth opening area and head direction are factors affecting the cough flow direction (Gupta et al 2009). Environmental parameters, such as relative humidity (RH) and temperature, in addition to the break-up and collision of saliva droplets, have a great influence on the size distribution of droplets (Tang et al. 2009; Tellier 2009; Lowen et al. 2007). All these factors and parameters are considered to be important in the spread of general infectious respiratory diseases. Studies on the detailed investigation of the dynamics of aerosol droplets within a cough flow which examine the underlying physical processes are infrequent, particularly in the far field regime (Bourouiba et al 2014). Some studies investigated the initial conditions of coughing, such as mouth opening area, volume flow rate, the maximum expiration air velocity and the angle of the coughed air in the near field flow (Tang et al. 2009). Previous investigations on the dynamics of coughing jet flow used many different techniques and also focused on the near field region.

The measuring technique is a significant factor in an experimental investigation. Although intrusive techniques have provided many coughing jet flow details, they still have some drawbacks. For example, contamination which is due to deposition of impurities in flow on sensor alters the calibration characteristics and reduces frequency response. Moreover, intrusive techniques are unable to fully map velocity fields that depend strongly on space coordinates and simultaneously on time (Yue and Malmström 1998). On the other hand, the non-intrusive Particle Image Velocimetry (PIV) technique provided the data required to perform both qualitative and quantitative analysis which gave a significant advantage over other optical measuring techniques such as shadowgraph and schlieren imaging (Raffel et al. 1998).

Many factors affect the collection of airborne microorganisms and the measurement of the size distribution and concentrations of droplets, as mentioned in the literature review section, such as RH, ambient temperature and droplet temperature. The intrusive and non- intrusive techniques, which were used in this study, showed similar results as compared to the Wells curve and all those measurements were taken near to or immediately in front of the mouth. Moreover, by using only real human coughs from the sick subjects when they are naturally infected by influenza virus will yield results close to reality. Although the World Health Organization rolled that 1-2 m is a safe distance from an infected person when taking droplet precautions (Kinnamer 2007; Deller et al. 2008; World Health Organization 2006), no tangible supporting evidence exists. The coughing flow characteristics and airborne penetration at 1 m distance are not reported. Such an investigation would have a significant contribution to our knowledge as it is widely assumed that 1 m is safe distance between patients and healthcare workers.

1.3 Objective

Contrary to the previous fluid dynamic studies that have measured the velocity flow field using artificial aerosol sources or only on healthy subjects, the present work includes up to 9 human subjects when they were infected with influenza, and again after they recuperated from the respiratory illness. A cohort of up to 11 healthy volunteers was used as control. Moreover, measurement data from 17 subjects (summer 2013 and winter 2014) were used to make general regression analysis of cough flow at 1 m downstream. In the present research, the general dynamics of the cough jet aerosols is being examined simultaneously along with the bioaerosol sampling processes associated with the virus droplet formation and transmission.

The objectives of this thesis are:

• Study the penetration of viral droplets into the ambient environment and how far and for how long they will be suspended in the air by the cough jet flow.

• To rigorously test the "3 feet" or "1 metre" rule which is imposed by the WHO (Kinnamer 2007; Deller et al. 2008) as being a safe distance between patients and healthcare workers to prevent airborne transmission.

• Identify host determinants of individuals, according to the gender and age, who will emit higher quantities of virus which spread over a wider area, (our recruitments will have a limitation of 18-35 years inclusive).

1.4 Organization of the Thesis

The present research will be conducted in two simultaneous parts experimentally. The fluid dynamics of the cough jet aerosols are being examined in parallel along with the bioaerosol sampling processes associated with virus droplet formation and transmission. This thesis consists of five chapters in addition to the introduction.

• In chapter 2, the comprehensive literature review will present the previous work studying the aerodynamic characteristics of cough flow and the size distribution of droplets and viral contents. The concluding discussion of those researches will be presented in the last section of the chapter.

• Chapter 3 describes the experimental details FLUGIE (Fluids from UnderGrads with Influenza Enclosure) cough chamber, the PIV system, HWA sensor and their calibration facility. Also, the sampling pumps, cassette filters and mid turbinate swab equipment will present in this chapter.

• Chapter 4 describes the experimental methodology followed in this thesis. The methodology for achieving the research objectives consists of two parts. The first part consist of HWA measurements, bio-aerosol sampling and mid turbinate swab, while the second part will cover the followed methodology for PIV measurements.

• Chapter 5 presents the results of virology analysis and MTS of both studies of winter 2014 and winter 2017. The results from HWA measurements of winter 2017 will illustrate and discuss first. The results from the PIV measurements will present and

discusses for studies of summer 2013, winter 2014, winter 2017, and finally summer 2017.

• Chapter 6 presents the conclusions of the present research. In this chapter, the findings presented in Chapter 5 are summarized with the objectives of identifying and describing the common trends and overall dynamics of the coughing phenomena. The viral content of the aerosols which were produced during the coughs were collected by the cassette filter. Moreover, the identities of the pathogen are summarized for each infected participants. Based on the fluid dynamic findings and the bio-aerosols observed in the present study, suggestions for future research are made.

Chapter 2

2   Literature Review

The present chapter reviews the cough jet flow phenomena such as aerodynamic flow behavior and the factors affecting the flow in near and far field region. The physical size of the droplets and the droplet nuclei produced during coughing and the factors that play main roles to suspend them in the air for longer time and at a far distance from cougher mouth are also reviewed in detail. Also, in this chapter some challenges faced by earlier researchers in their work are also described. All these factors will be discussed to provide an essential background and motivation for this current study.

2.1   Aerodynamic Characteristics of Coughing Jet Flow

The route of airborne disease transmission starts from infectious viruses exhaled from an infected person, and then the viruses are transported in the air (see Fig.1) and, finally, inhaled by a susceptible person. According to the cough definition in the introduction, the important factors that govern the cough flow dynamics are cough exhaled velocity, flow rate, direction, mouth opening area, and temperature. These factors are considered as transient boundary conditions for coughing flow (Gupta et al 2009).

Experimental observations were conducted to measure the flow dynamics of human coughs and flow rates, flow directions and mouth opening areas of coughs collectively (Gupta et al 2009). All the experimental measurements were performed near the mouth of 12 female and 13 male healthy subjects in order to obtain realistic flow features for single and sequential coughs. The experimental measurements, which were performed at 330 Hz by using high-speed camera, showed a very high initial acceleration in exhalation and, subsequently, decay. The inhalation volume was very small and may be neglected. A large variation existed among the subjects by the conducted measurements. Cigarette smoke was used the seeding fluid to measure the flow directions by using moderate speed photography (120 Hz / 1 MP), and the sequences of images were taken over time periods up to 0.3s. The results showed that the downward jet can be defined with two angles θ_1 and θ_2 (see Fig. 1). The 95% confidence bounds for the mean angles were determined

to be: $\theta_1 = 15° \pm 5°$, $\theta 2 = 40° \pm 4°$. The mouth opening area, defined as the area between the lips during the cough, was found to be almost constant (4 cm^2 Male- 3.75cm^2 female) for a period of 0.2 sec when there was flow from the mouth.
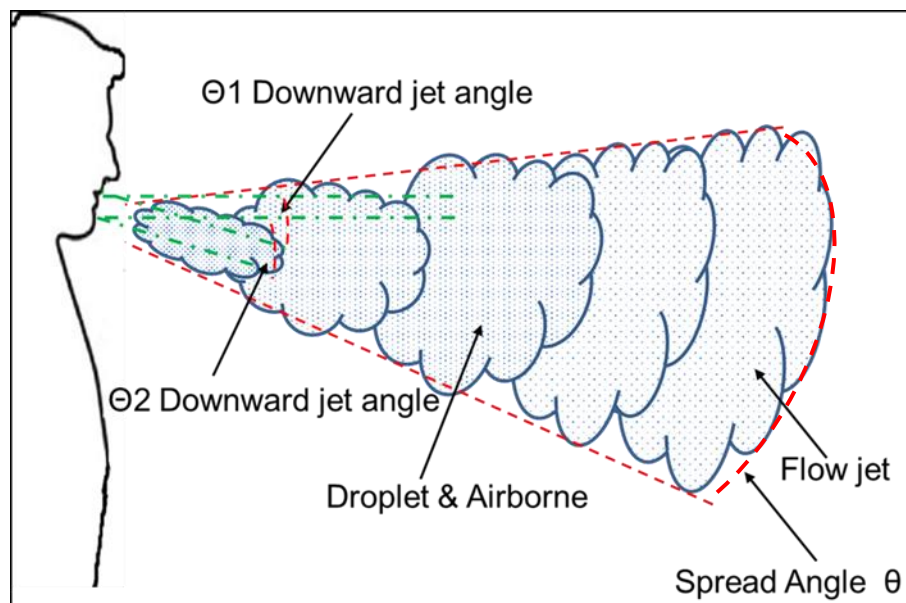
Figure 1 Definition of Cough Jet Flow Field showing the cough jet width and spread angle.

In addition, the results did not indicate any clear trend between mouth opening area and the heights of all the subjects, but the measurements showed that the mean mouth opening area for the female subjects was smaller than that of the male subjects. A sequential cough was found to be the combination of two single coughs. The first one behaved approximately the same as that of a single cough, while the second one was a scaled down version of the first one.

Another study was conducted to measure the airflows generated by a human cough where no particles or extraneous gasses were used, ambient temperature and relative humidity and ventilation currents were not considered (Tang et al. 2009). This study included 6 males and 4 female volunteers, divided into five age groups from 20 to 80 years. The unobstructed cough was first observed and quantitative velocimetry was performed by

tracking turbulent eddies in the expelled jet of air. Then, the effect of wearing either of two popular mask types (simple surgical and N95 masks) on the cough airflow was assessed by qualitative observation of Schlieren video records. Consecutive frames were taken at 330μs apart by using this technology to trace the motion of the expelled cough. The fine-scale turbulence evident without 'smearing' in the measurements attests that the motion of the jet of air from these coughs was 'frozen' by the 1-μs frame exposure.

The study concluded that the cough jet behaves approximately as a classical round incompressible transient turbulent jet with a total spreading angle of approximately 24°. Sample results of a single cough by a 57-year-old male volunteer without a mask showed a maximum average airspeed across the early-stage cough of 8 m/s, with an expected greater value for the centreline velocity. Unmasked coughing produced a turbulent air jet extending across the Schlieren field-of-view and, probably, well beyond it. The direction of the jet varied with each human subject, as well as with their individually adopted body attitudes, in both standing and supine position. The results of both masks in coughs had minimal momentum. Nonetheless, neither the surgical nor the N95 mask has any possibility of passing or containing all of the 2L or so of air expelled in less than a second during a cough. Thus, leakage or venting must occur, compromising any existing, originally fit-tested seal between the mask and the face of the wearer. The study revealed that cough jet may contain infectious aerosolized particles or droplets, but the visualized airflow study did not deal with concentrations or size distribution of droplets or of viable infectious agents.

The study of the dynamics of aerosol particles in sneezing and coughing was conducted by using a digital high-vision, high-speed video system and vector analyses (Nishimura et al 2013). The enhanced obtained images were converted to digital images every 330μs and subjected to vector analysis by using processing software. One healthy adult volunteer participated in each measurement. This methodology was applied to a cough by using smoke exhaled with the cough after smoking one breath of a cigarette, from which the dynamics of the fine cough bio-particles invisible with their system could be estimated by using the micro-clouds visible in the smoke as aerodynamically acceptable surrogates for the particles. The measurements were taken in a laboratory at a

temperature of 27 C^{o} and RH of 50%. It was concluded that the smoke cough micro-clouds had an initial velocity greater than 5 m/s. Moreover, the velocity of the sneeze after 0.05 s was about three times higher than the cough and, in contrast to the sneeze, the velocity of the cough drastically decreased about 0.05 s after the release. The study recommended that in the context of the transmission of respiratory infections such as influenza, studies on individuals who contracted the disease would be important for infection control. In addition, it is important to test these procedures on many subjects, including individuals of different gender, race, age group, and body type, as well as for various environmental conditions.

The measurements of the initial velocity of exhaled airflow from coughing and speaking were conducted with 26 tested subjects by using Particle Image Velocimetry (PIV) (Kwon et al. 2012), and the results were analyzed to study the angle of the expired air, the subject's height and the horizontal velocity of exhaled airflow from coughing and speaking. For coughing, the results showed that the average initial cough velocity was 15.3 m/s for the males and 10.6 m/s for the females. The angle of the coughed air was around 38° for the males and 32° for the females. Moreover, the coughing velocity increased with the subject's height.

The direct experimental observation of sneezing and coughing showed that such flows are multiphase turbulent buoyant clouds with suspended droplets of various sizes (Bourouiba et al 2014). The study observed that the initial emitted turbulent jet fluid entrains the ambient air, leading to the increase of its size and decrease of its mean speed with distance from the source. High-speed imaging of various violent expirations was recorded with 1–4 kHz frame rate using high-speed video system. The study concluded that the turbulent multiphase cloud, which is formed by coughing and sneezing, plays a significant role in extending the range of the majority of pathogen-bearing droplet. The smaller droplets and their associated droplet nuclei can remain suspended in the cloud for a prolonged period and can be resuspended by ambient air currents. For example, a droplet of diameter d =10 μm evaporates in 0.027 s, during which it would fall a distance of approximately 0.08 mm at a settling speed of approximately 3 mm/sec.

A PIV technique was used to measure the velocity distribution around the mouth of the three coughing subjects (Zhu et al 2006). The mass of saliva, which was collected from cough subjects by using a mask, was assessed with an electronic balance, and flour, which was expelled by the coughers, was used as tracer to visualize the dispersion of salvia droplets expelled during the cough. The experiments were performed in a styrene-board chamber 1.8 x 1.8 x 1.8 m that in order to prevent subjects being harmed by the tracer gas or laser beams and to avoid any effects of the ascending warm airflow on the coughed airflow. The study concluded that a total of more than 6.7 mg of saliva was expelled on aggregate at a maximum velocity of 22 m/s in each cough, with the average velocity being 11.2 m/s near the mouth. Furthermore, as the coughed air mass proceeded, the frontal flow field was disturbed, and the surrounding air was entrained into the cough airflow by the induced eddies around it. In addition to experimental measurements, numerical analysis was carried out by using CFD. First, the numerical study analyzed the indoor flow field assuming coughing and respiration to be steady phenomena and by using the experimental results as boundary conditions. The study subsequently analyzed the transport process for droplets with multi diameters in μm. The CFD analysis concluded that the diameters of droplets played an essential role to determine which force will affect the transport process.

The expiration air jet velocities and the size profiles of expiratory droplets during speaking and coughing in close proximity to the mouth were investigated by using PIV and the Interferometric Mie Imaging (IMI) method (Chao et al. 2009). Eleven healthy volunteers (3 men and 8 women) were recruited, all of them under 30 years old. The study excluded smokers, asthma sufferers, people who were experiencing illness, who had recently experienced expiratory problems or were likely to experience discomfort in confined spaces. The PIV image pairs were taken at a frequency of 5 Hz. The results showed that the maximum expiration air velocity during coughing by the male volunteers was 13.2 m/s and by the female volunteers was 10.2 m/s. The average expiration air velocity during coughing was 11.7 m/s, while during speaking it was 3.9m/s. All these measurements were carried out within 10 - 60 mm of the mouth.

The flow field of human coughs was measured by first filling an enclosure with theatrical fog and then having 29 healthy volunteer subjects (10 males and 19 females, their ages between 22-55) individually cough into the enclosure (Vansciver et al 2011). The enclosure had dimensions of 1.2 m length 0.76 m width and 0.67 m height and so its limited volume represented a constraint on the study. PIV measurements were conducted to determine the velocities of the fog particles. The average cough jet volume to enclosure volume ratio was roughly 240, and, thus, little indirect influence of recirculating flow can be expected. The study showed that the average velocities over all participants ranged from 1.5 m/s to 28.8 m/s, and the overall average maximum cough velocity was 10.2 m/s. The study illustrated that the width of the cough expanded linearly initially in the flow direction, and then remained constant at distances farther from the mouth. This affected the normalized velocity (by max. velocity) profiles, which were found to partially collapse when scaled with distance from a virtual origin. Moreover, the study showed no correlation between the gender and weight, and that a human cough cannot be reduced to a well-defined flow field.

In particular, the high degree of variance in the velocity data, including the width of the jet, the maximum velocities, and the direction of the jet demonstrates that studies of a human cough based on numerical or in vitro simulations should consider incorporating a wide range of conditions, rather than focus on a single "typical" cough flow. The study concluded that, in further work, the cough flow should be mapped at greater distances from the mouth in order to evaluate the far field velocities and jet widths and better determine the cough's penetration into a room.

A cough "simulator" with an electrically controlled hydraulic actuator was designed and used to accurately reproduce cough waveforms in a laboratory setting (Afshari et al. 2002). The chamber was built by using a 0.1x0.1x0.2 m Plexiglass box covered with non-reflective black material. The simulator was filled with seed particles (oil droplet less than 5µm), which allowed particle dispersion measurements and air velocity vector estimation. The air velocities within the environmental chamber were estimated by using

PIV at 14.9 Hz for the image pairs during a cough and similar measurements were made for a subject with asthma. The study concluded that the PIV makes it possible to undertake detailed analyses of average cough flow patterns in an enclosed space, and once the flow patterns have been established it would be possible to estimate how biological aerosols are transported in an enclosed space during a cough. From the previous studies, it is unclear how long cough-generated viral aerosols remain viable in the airborne phase. For this purpose, viable P aeruginosa in cough aerosols were measured (Knibbs et al. 2014), which were collected with an Anderson Impactor in a wind tunnel of modest cross-sectional area at 1, 2 and 4 m from the subject (distance) and after allowing aerosols to age for 5, 15 and 45 min in a slowly rotating drum to minimize gravitational settling and inertial impaction. The study reported that patients infected with cystic fibrosis (CF) produce cough aerosols containing viable organisms that are capable of traveling up to 4 m and persisting in the air for long 45 min.

Preliminary results were presented by WeCoF aerosol study (Savory et al. 2014). Twelve healthy subjects (9 male, 3 females) were involved in this study and the strength of their coughs were quantified at a distance of 1m from the mouth. For this purpose, a 1.81 m x1.78 m x 1.81 m cough chamber was constructed and PIV was used to conduct these measurements. The study illustrated that, as expected, the velocity decreases rapidly in the near field at the mouth, but at the far field, i.e. at distance 1m from the cough source, the cough front velocity had a magnitude in agreement with the average of the spatially averaged maximum velocity magnitude. The measurements showed that there was significant air motion, of the order of 0.5 m/s, even at a location as far away as 1 m from the mouth. The PIV window size and the variable physical traits of the study participants have had some limitations on the study, but it was found that each cough had a significant variation in strength and its location. Also a lot of data were missing from those studies as most of the imaged field of view was entirely missed for some coughs. The study showed that the cough velocity profile has no single characteristic shape and, thus, the measurement and analysis of a larger number of coughs than those examined in these initial trials, were considered to be an essential part in this study in order to suggest a defined envelope of cough profiles.

Recently, an experimental study of the two-stage cough jet was performed to examine the effects that different boundary conditions such as temporal exit velocity profiles, cough duration and velocity scale have on cough flow penetration (Wei and Li 2017). The exhaled particles spread by the cough flow were also investigated. The researchers simulated the flow of the cough by injecting a volume of dyed water into a large water tank. The dyed water was injected through a nozzle (D=10mm or D=4mm) by a piston which was controlled by servo motor, and the motor was operated to generate three velocity profiles by piston movements. The cough flow is characterized as a two-stage jet when the cough starts and flow is released then after the source supply is terminated. During the starting stage, the flow rate is a function of time and three temporal profiles of the exit velocity (pulsation, sinusoidal and real-cough) were studied. In both the starting- and interrupted-jet stages, the cough flows showed the self-preserving property. The farthest penetration distances of cough flow were in the 50.6- 85.5 D range. The study concluded that the real-cough and sinusoidal cases have greater penetrating ability compared with the pulsation cases under the same characteristic Reynolds number and cough expired volume. The study concluded that the cough expired volume and Reynolds numbers significantly affect the cough flow (Wei and Li 2017). Table (I) in appendix (A) summarize most the previous work on the aerodynamic characteristics of coughing jet flow as presented in this section.

2.2 Size Distribution of Droplets and Viral Contents

Respiratory activities, such as coughing, extrude droplets. These droplets will not totally evaporate, since they contain substances besides pure water, such as electrolytes, mucus, glycoproteins, enzymes, antimicrobial agents, and microorganisms (Bozzuto and Ruggieri 2010). Droplet nuclei, which were first identified by Wells in 1934 (Verreault et al 2008), exist when droplets evaporate as seen in Fig. 2.
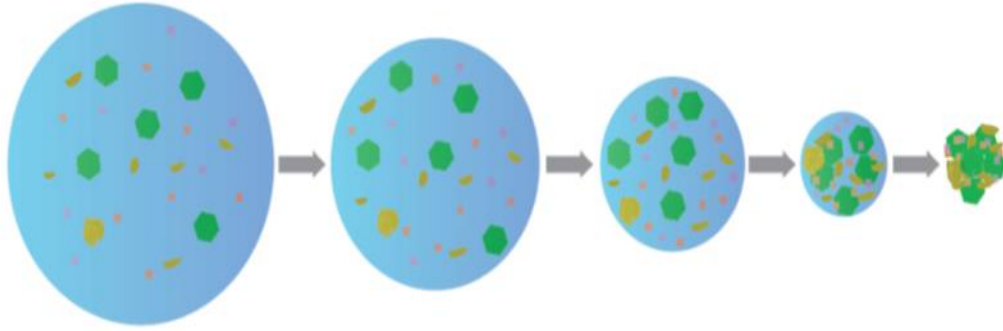
Figure 2 Evaporation of a liquid droplet (left) to a droplet nucleus (right). As the liquid evaporates, the non- evaporative content concentrates until a droplet nucleus is obtained (Verreault et al 2008 (with authors' permission)).

The earliest investigation, made by Wells (Tellier 2009), showed that the expiratory droplets and droplet nuclei can function as conveyors of pathogens for the infectious disease. The size of the droplets can also affect the possibility of spread as shown in Fig. 3. Consequently, precise measurements of the size distribution of expiratory droplets and droplet dispersion, along with number of the droplets and the concentration, are strongly recommended by (Wei and Li 2015).
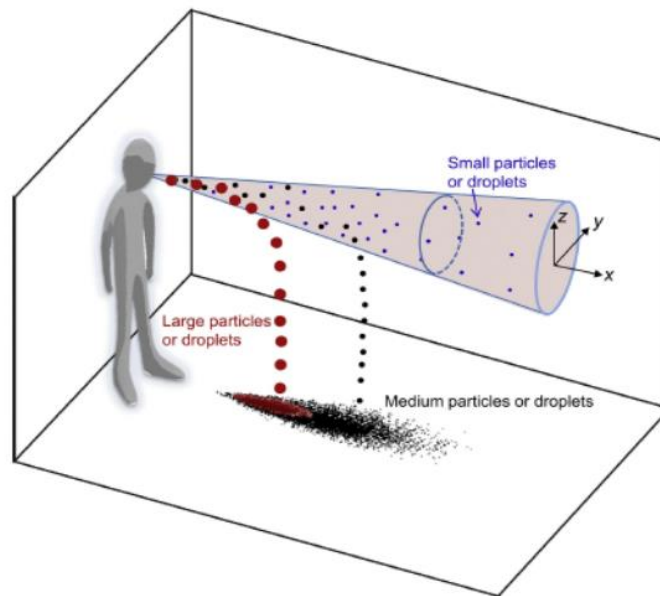
Figure 3 Three ranges of aerosol droplets are released in turbulent cough jet flow (Wei and Li 2015 (with authors' permission))

In general, two steps govern the measurement of virus aerosols, virus droplets are first removed from the air and then the collected virus aerosol sample is analyzed. Most aerosol sampling devices involve techniques that separate particles from the air stream and collect them in, or on, a preselected medium using common techniques involving slits, cyclone, impingers, impactors and filters (Wei and Li 2015). Many factors can affect the concentration, size distribution of droplets and their airborne dispersion, such as droplet temperature, relative humidity, air pollutants, irradiation, and exposure period (Xie et al. 2007). However, the droplet size dictates the capacity of a particle to remain airborne. In humans, the droplets which have a size distribution larger than 10 µm (aerodynamic diameter) will not pass the upper airway, while the minimum sizes of a viral aerosol is limited by the virus diameter itself which can be as small as 20 to 30 nm (Xie et al. 2007). Fundamentally, bioaerosols are suspensions in air of liquid particles that are small enough to remain airborne for a prolonged period of time because of their low settling velocity. The settling velocity of droplets in still air can be computed from Stokes' law (Tellier 2009).

$$F_d = 6\pi\mu Vd \qquad\qquad (2.1)$$

Where F_d is the drag force of the fluid on a droplet, μ is the fluid viscosity, V is the velocity of the droplet relative to the fluid, and d is the diameter of the droplet. For example, a 3 m fall of 20 µm particle (aerodynamic diameter) takes 4 min, 10 µm takes 17 min and 5 µm takes 67 min (Tellier 2009). It is important to distinguish between the initial diameter of droplets, which are generated by human subjects immediately at the mouth, and the diameter after water evaporation of the droplets in the ambient air (Tellier 2009). The evaporation of falling droplets was first studied by Wells (Verreault et al 2008) using a simple calculation method and he obtained a classical curve that revealed the relationship between droplet size, evaporation, and falling rate. The difference between disease transmission via large droplets and by airborne routes was first identified by Wells study. Wells found that under normal air conditions, droplets smaller than 100 µm in diameter would totally dry out before falling to the ground 2 m away, i.e., the average human height (Verreault et al 2008).
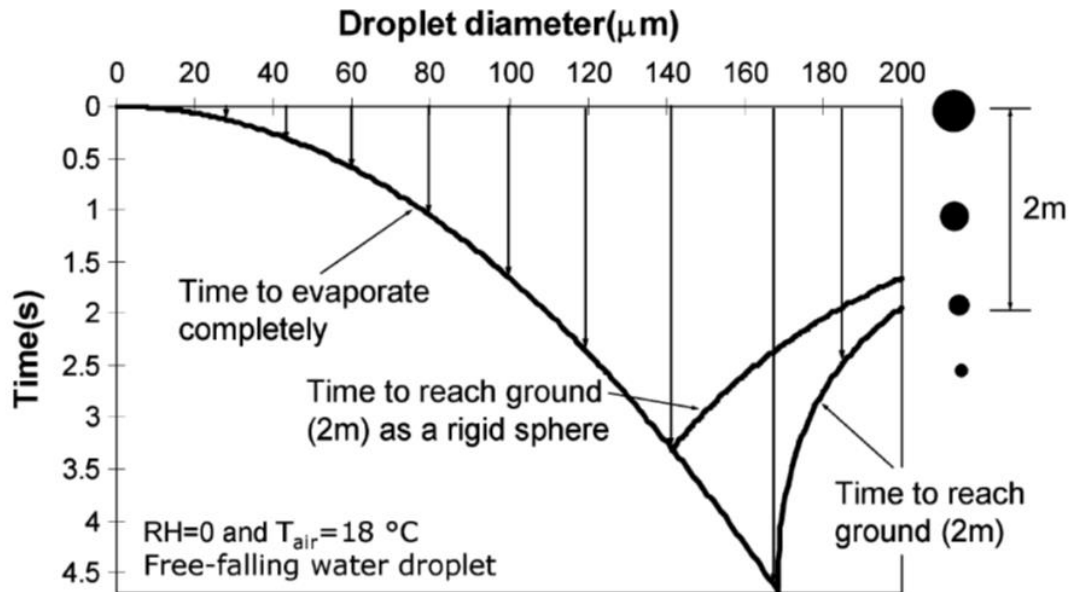
Figure 4 The Wells evaporation–falling curve of droplets [reproduced and modified from Wells (1934)], (Xie et al 2007 (with authors' permission))

Recently, a simple physical model was developed to calculate the droplet lifetimes and how droplet size changes with relative humidity and air temperature (Tellier 2009). The results reveal that for coughing flows, the sizes of the largest droplets that would totally evaporate before falling 2 m away are between 60 and 100 µm at an initial cough velocity of 10 m/s. In addition, it was confirmed that small droplets evaporate rapidly and large droplets fall to the ground quickly. The size distribution of cough droplets from subjects of different ages and gender were investigated to identify the effects of age and gender (Lowen et al 2007). Experimental results demonstrated that the average size distribution of the droplet nuclei ranged between 0.58–5.42 µm, and 82% of droplet nuclei centred in the range of 0.74 – 2.12 µm. Moreover, the experimental results indicated that the size distribution of coughed droplets peaked at approximately 1 µm, 2 µm, and 8 µm. However, the horizontally expelled large droplets can also penetrate a long distance. At a low relative humidity, more droplets and droplet nuclei could remain suspended in the air, increasing the probability of subsequent inhalation. (Lowen et al 2007) directly tested the hypothesis that RH and ambient air temperature impact the efficiency with which influenza virus is transmitted. Hartley strain guinea pigs were used as a mammalian

animal model, which have been shown to be highly susceptible to infection with human influenza viruses. The results showed that airborne transmission (large droplets and/or droplet nuclei) was enhanced at low temperature ($5\,^{\circ}$C) and at high temperature ($30\,^{\circ}$C) interrupted transmission at all values of RH. At $20\,^{\circ}$C, transmission was highly efficient at an RH of 20 and 35 %, low at 50 %, efficient again at 65 % and completely absent at 80 %. The authors tentatively attributed the effect of low temperature to the increased viral load observed in the animals at this temperature (Lowen et al 2007), but proposed no explanation for the effect of high temperature, which interestingly enough, did not interfere with contact transmission between animals in the same cage (Lowen et al 2008). As the authors noted, the effect of RH is indicative of infectivity decay of influenza virus aerosols.

In another study (Mubareka et al. 2009), the same group again used the guinea pig model to show stronger experimental evidence for aerosol transmission when they documented instances of transmission within the cage of the contact animal located above the cage of the source animal at a separation distance of 80 or 107 cm. Another important observation in this study made by them is that different influenza strains differ considerably in their capacity for aerosol transmission. Another study supporting this observation (Yang et al 2011) showed that not all influenza strains are capable of 'airborne transmission'. Another crucial issue related to respiratory infectious transmission is exhaled droplet concentration. Even fewer studies have determined the droplet concentration in coughing, which is an important aspect to consider as it determines the infectious contents of the actual droplet.

Study conducted by (Yang et al. 2007) showed that the coughed droplet concentrations for test subjects wearing a filter mask were markedly lower than for subjects who coughed directly into the sample bag. This difference referred to coughed droplets easily impacting the inner surface of the mask, reducing sharply the number coughed droplets measured. Moreover, they found that the average concentration for males was significantly higher than that for females, as males have a longer cough flow rate than females. Also, the comparison of droplets concentration among difference age groups

showed that subjects in 30-50 years age group had the largest droplet concentrations, as subjects in this age group have the largest cough flow rate.

In another study, the concentration and size distribution of droplet nuclei of influenza viruses were measured in a health centre, a day care facility, and aeroplanes during 2009-2010 flu season (Zayas et al. 2012). Eight out 16 collected samples contained influenza (A) viruses (the concentration ranged from 5800 to 37000 genome copies per m^3). On average, 64 % of viruses-laden particles were found to be smaller than 2.5µm, which can remain as airborne for hours. The size distribution and concentration of expiratory droplets expelled during coughing and speaking and the velocities of the expiration air jets of healthy volunteers were measured. These measurements were performed in close proximity to the mouth to avoid air sampling losses. The results estimated that 947-2085 droplets were expelled per cough and 112-6720 droplets were expelled during speaking. By using different estimating methods, they found that the droplet concentration ranged from 2.4-5.2 per cm^3 for each cough and 0.004-0.223 per cm^3 for speaking.

An experimental study was conducted on 45 healthy non-smokers (Knibbs et al. 2014). A laser diffraction system in the open bench was used to obtain accurate, time-dependent, quantitative measurements of the size and number of droplets expelled in the cough aerosol. Droplets ranging from 0.1 - 900 µm were generated by voluntary coughs. Droplets of less than 1 µm represented 97% of the total number of measured droplets contained in the cough aerosol. Moreover, the study illustrated that age, sex, weight, height, and corporal mass have no statistically significant effect on the aerosol composition in terms of size and number of droplets. The study concluded that the cough aerosol is the single source of direct, indirect, and/or airborne transmission of respiratory infections like the Influenza (A) H1N1 virus.

The effects of two stage jet of human cough on the particles transportation were investigated experimentally (Wei and Li 2017). A small, medium and large glass beads were fed into the discharged dyed water. The flow field was not altered by the presence of these particles since, the volume fraction was less than 0.5 %. The results of water tank experiments showed that particles of different sizes behaved similarly during the short

cough period (0.5 s). They all reached approximately 38 D when the cough was stopped (Wei and Li 2017).

Table (II) in appendix (A) summarize most of the previous work on size distribution of droplets and viral contents as presented in this section.

2.3 General Discussion and Summarize of Previous Work

Based on the classification discussed in the literature review (near-field and far-field), the results concerning the aerodynamic characteristics of coughing jet flow may be summarized as shown in Fig. 5.The last four studies in near field region, on the right, were conducted using PIV, where the overall average is 12 m/s, max is 28.5m/s and min 0.2 m/s, while the first two used Schlieren optical camera with max spatial average 8 m/s (using PIV processing) and a high-speed digital video system with initial velocity 6 m/s (vector analysis), respectively. It may be seen that there is a significant difference between the male and female subjects. The number of participants involved in these studies and their conditions as most of them healthy volunteers. Finally, the velocity values for near-field measurements by PIV show comparable results and higher than those obtained by using other techniques. Far-field studies were rarely conducted, and the results of (Savory et al. 2014) indicated that there was significant air motion during a cough, of the order of 0.5 m/s, at a location as far as 1 m from the mouth and the spatial average maximum velocity across 27 coughs was 0.41 m/sec and max velocity 4.5 m/s for males and around 1 m/s for females. To sum up, succinctly, many techniques were used to define all parameters in near field region, which is less than 0.5 m. All results, as presented in the literature, showed that there is rapid decay of the velocity after 0.05 second. The PIV technique gave more reliable data because all previous experiments showed a closer agreement with respect to the average of peak cough velocity. Physiological factors such as gender, height, weight, and mouth opening area play a main role in cough flow in near-field studies. It's infrequent to find a far field cough study, which means at 1 m or 2 m downstream from the cough source. A novel experimental facility – the FLUGIE chamber- overcomes all of the difficulties faced by the earlier

researchers in this field. It was designed to study the far-field aerodynamic of human coughs as presented in (Savory et al. 2014).
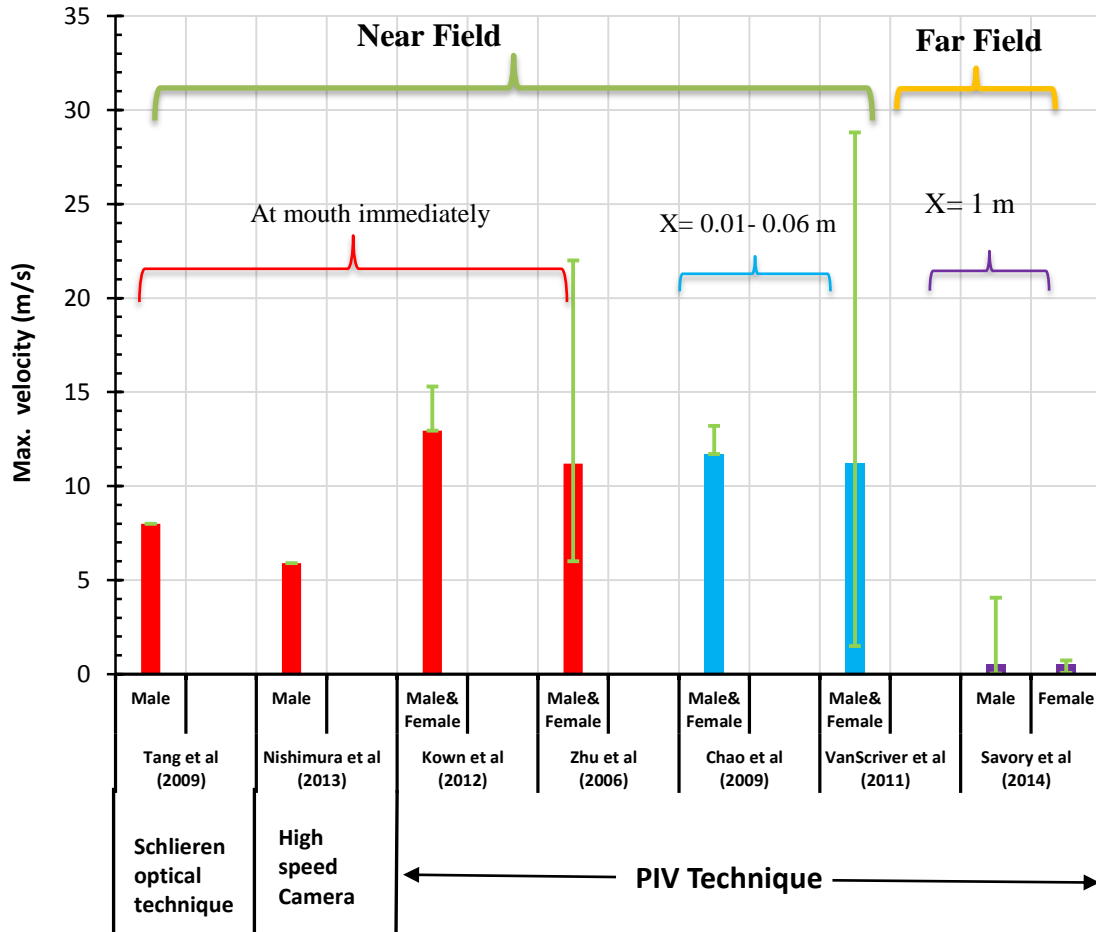
Figure 5 Summary of maximum cough velocity for male and female subjects

Figure 6 presents the measurements of spread angle in the near-field flow studies using different techniques. It can be see that both (Gupta et al 2009; Tang et al. 2009) show 23.5^{o} ($\pm 3.5^{o}$) and 25° ($\pm 5^{o}$) mean spread angle across all subjects, using Schlieren optical and high-speed camera techniques respectively, while the PIV data of (Kwon et al. 2012) shows significant differences between male and females, of 6°, and mean spread angles that are 10° higher when compared to the other studies.
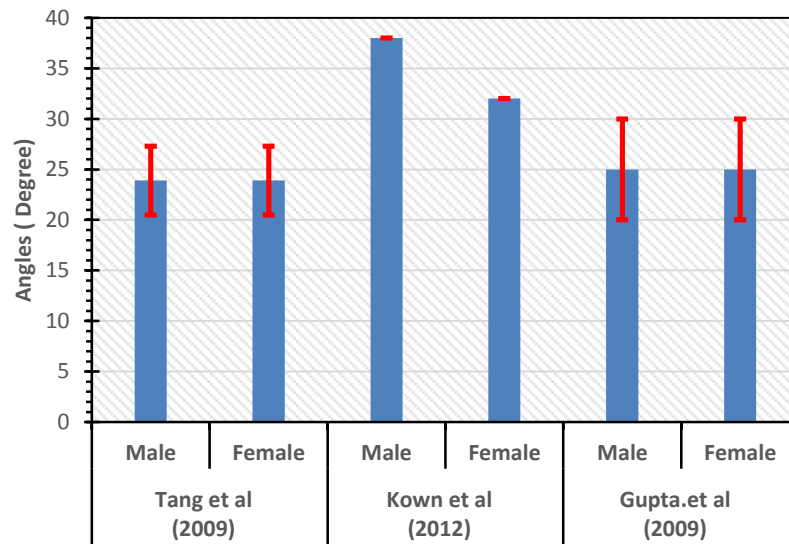
Figure 6 Cough jet flow spread angle

Figure 7 shows droplet size distributions measured in the near-field region in previous work. Different methods and techniques were used to conduct these experimental studies. A similar trend was obtained for the first two studies (Zayas et al. 2012; S. Yang et al. 2007) with a maximum limit of less than 5 μm, while (Knibbs et al. 2014) showed that most droplets had a size distribution less than 1 μm. (Chao et al. 2009) showed good agreement with the earliest study was conducted by (Duguid 1946). The study illustrated that the maximum droplet size was 750 μm for 30 droplets and 6 μm for about 1300 droplets and minimum size distribution of 3 μm for 86 droplet and mean droplet size was 13.5 μm. Although virus diameters lie in range of 20-30 nm (Verreault et al 2008), droplets which have a distribution size more than 10 μm will not pass the human upper airways (Verreault et al 2008). Some studies illustrated that different influenza strains differ considerably in their capacity for aerosol transmission (Van Hoeven et al. 2009; Yang et al 2011). The effects of RH and ambient temperature on the aerosol transmission were studied by many researches (Tellier 2009; A C Lowen et al. 2008). Transmission of droplet and droplet nuclei were enhanced at low temperature and interrupted at high temperature while low RH showed higher droplet and droplet nuclei transmission. The

mean cough flow rate was about 2.5 l/s (Tang et al. 2009; Gupta et al 2009), and the minimum number of droplets was around 950 and the maximum was 2100 droplets per cough (Chao et al. 2009). Generally, it can be seen that most of these studies were conducted in the near rather than the far region of the cough. Rare studies recruited infected subjects and used different techniques which showed various results.
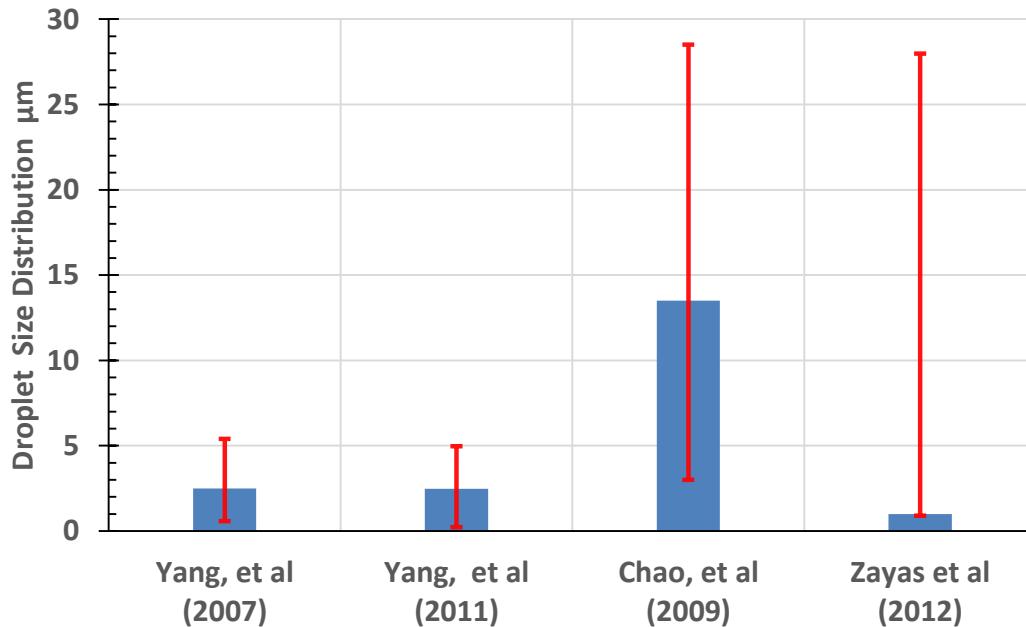
Figure 7 The average, max and min droplet size distribution of coughing based on different sources

In this section, the current state of knowledge about cough flow phenomena was succinctly summarized and discussed. It is clear from this discussion that all previous studies showed limitation on the number of participants. This explains the lack of sufficient data to make statistically significant conclusions about three main points missed in this knowledge. First, the differences in the flow field among sick, convalescent, and healthy coughs at 1 m downstream. In addition, the ability of the viruses to spread by coughing beyond 1 m from the source of cough. Finally, identify host determinants of high emitters of viral particles via coughing which disperse further. These points will be considered as tangible supporting evidences when taking droplet precautions as WHO recommended (1-2 m safe distance role). Such an investigation

would have a significant contribution to our knowledge as it is widely assumed that 1 m is safe distance between patients and healthcare workers.

Chapter 3

3 Experimental Facilities and Equipment

In this chapter, the experimental facilitates that were used in this research are described, namely the FLUGIE chamber and the particle image velocimetry (PIV) equipment, the hot wire anemometer system (HWA sensor) and its calibration facilities, together with the bio-aerosol pumps and cassette filters and mid-turbinate collection tubes for droplet sampling.

3.1 Experimental test chamber (FLUGIE)

Biocontainment containment level 2 laboratory has a 22 m^2 plan area. The FLUGIE chamber is centred within the lab as shown in Fig 8, occupying about 3.22 m^2 with a significant volume of around 7.15 m^3 this volume is important to overcome on some of the drawbacks mentioned in the literature. All surfaces in the lab are made from non-absorbable materials such as varnished wood, polymers, aluminum, and coated steel that to make them safe and easy to clean. The far-field aerodynamics and aerosol transport of droplets produced by the coughs from naturally infected humans are studied using an experimental cough chamber facility called the FLUGIE. The experimental test chamber FLUGIE was designed to overcome many difficulties as mentioned in the literature. Hence, a chamber of adequate size is preferable as a quiescent environment in which a cough flow may be studied negating the effect of any turbulence phenomenon from uncontrolled surroundings (Savory et al. 2014).
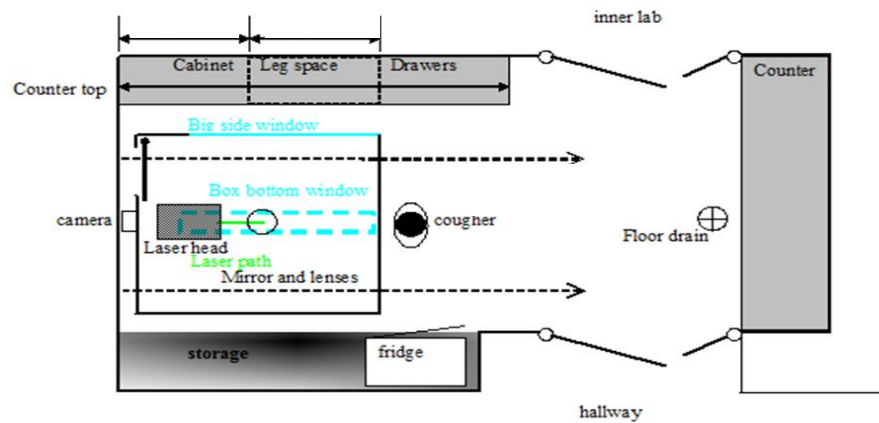
Figure 8 Schematic Diagram of Laboratory layout
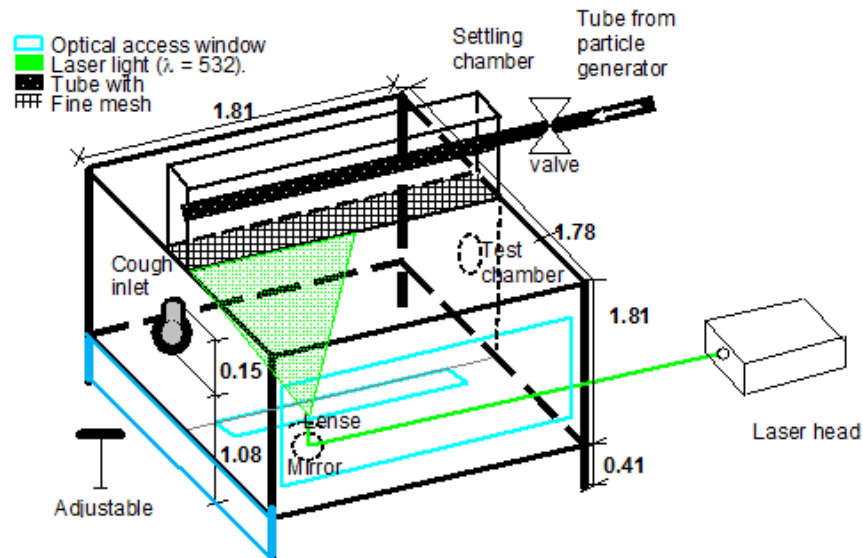
Figure 9 Schematic diagram of the Experimental test Chamber (FLUGIE)

The chamber has internal dimensions 1.81 m long, 1.81 m width, and 1.78 m high. These dimensions create a large volume to overcome the influence of recirculating flow of the cough jet inside the chamber with respect to average cough jet volume. The surfaces are made from wood as a solid barrier to avoid any harmful reflection from laser beams and isolate the cough flow from the external effects such as participant's body heat generated

by metabolism, and the inner surfaces are painted by black to avoid any scattering from the laser sheet when illuminating the seeding particles. A large glass window on one side allows optical access to make the measurements using dual coupled- charge-device (CCD) cameras. The test chamber is raised up to 0.41 m above the laboratory floor and mounted upon casters to allow quantitative measurements at various streamwise positions and to allow laser sheet to enter the test chamber through a glass window and illuminate a centreline plane extending from the test chamber floor to the roof as shown in Fig. 9. The test chamber is seeded with titanium dioxide particles TiO_2 (rutile mineral form), which has size distribution ranging from 0.34 to 0.43μm. The TiO_2 particles enter a settling chamber mounted on top of the test chamber through a tube with perforations. The FLUGIE settling and test chambers are separated by a fine mesh, which permits TiO_2 particles, under the action of gravity and local airflow, to gently enter the test chamber along its centreline. As shown in Fig. 3.2, there is a small opening for the cougher's mouth in the front surface of the FLUGIE. The opening is pear-shaped such that the participant's nose and mouth area are unobstructed whilst a cough is directed into the enclosed test chamber (Savory et al. 2014). The major vertical axis of the pear-shaped opening is 15 cm high and the base of the opening, where the participant's chin rests, is 67 cm above the chamber floor. The minor horizontal axis of the pear-shaped opening is 10.5 cm wide. This chamber inlet has a cover which is only opened when a cough is introduced into the chamber. In order to examine the cough velocity produced by the pulmonary effort alone, the cough should be observed by restricted head motion. A chin rest and a forehead rest are used to let the position of the participant's head is fixed, such that the angle of the cough is horizontal and consistent over multiple trials (Savory et al. 2014).

3.2   Particle Image Velocimetry System (PIV)

The measuring technique is a significant factor in an experimental work. The main experimental part on the aerodynamics of the cough is conducted in this research by using the non-intrusive particle image velocimetry PIV technique. This technique provides the data required to perform 2D qualitative and quantitative analyses which

gives a significant advantage over other measuring techniques used in the literature. In this section, the components of the PIV system illustrated in Fig. 10, A double pulsed Nd: YAG crystal laser of power 120 mJ per pulse is used to generate laser beams of 532 nm wavelength at 15 kHz that produced high level of illumination with very short intervals between two pulses at lower laser power. Although the Nd : YAG double-pulsed system is more expensive and more difficult to set up due to the added timing and synchronization equipment, it is used because it can provide an illuminated sheet with an almost stable and fixed thickness without aberration or diffusion and due to the coherent and monochromatic character of the emitted light (Stamhuis 2006). The main component to deliver the bright laser sheet is the optical lens system which is located at the end of the laser beam generated by the laser head.
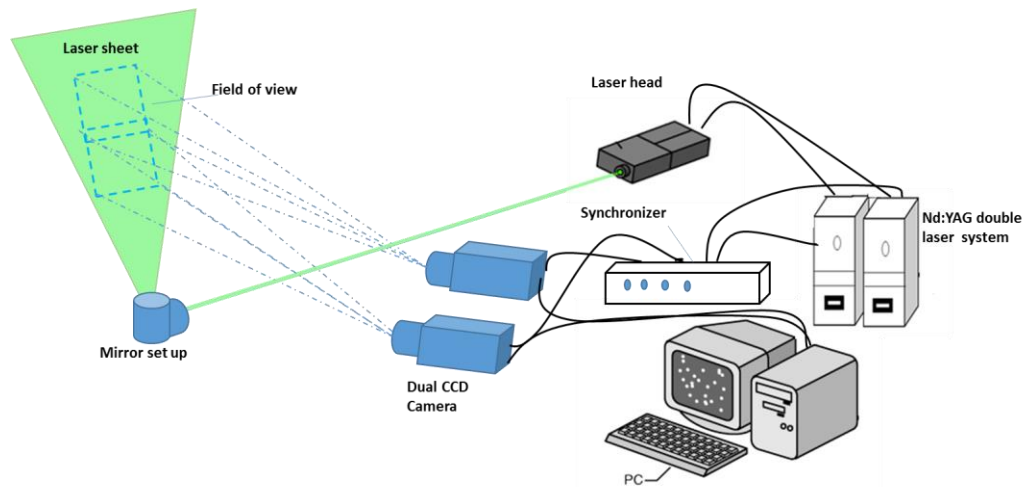
Figure 10 Schematic diagram of the used Particle Image Velocimetry

Photography System

3.2.1   Selecting the appropriate Laser Sheet Optics

Each laser system has a set of cylindrical and spherical lenses that are used to produce the light- sheet, which illuminates the tracer particles and the flow. The slightly diverging light beam produced by a laser is usually transformed into a sheet by converging it with a weak positive lens and subsequently makes the beam fan out in one plan as sheet by an additional cylindrical lens as shown d in Figure 11.
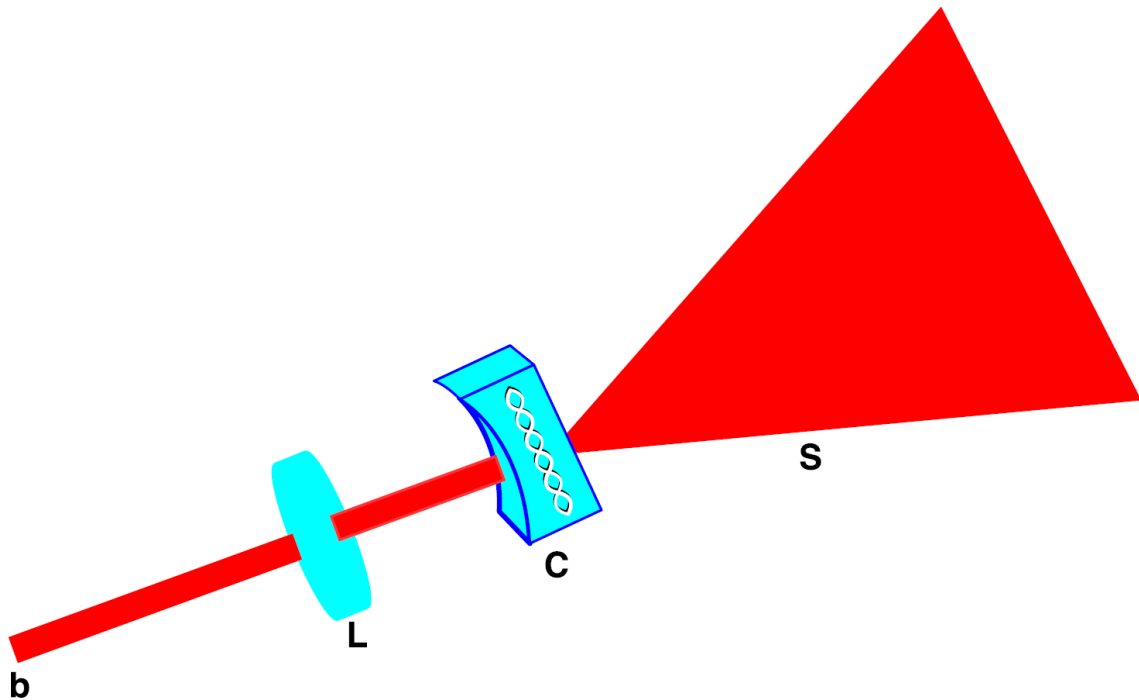
Figure 11 Basic optical lenses arrangement to produce a light sheet from a laser beam: The mildly divergent laser beam coming from the left (b) is collimated by a weak positive spherical lens (L) and subsequently fanned out in one plane only by a cylindrical lens (C). This results in a sheet (s) with a slightly converging thickness (Reproduced from Stamhuis 2006).

The optimum light sheet can be obtained by choosing the correct lenses. Both of the cylindrical and spherical lenses control the converging and diverging of the light beams. The selected light sheet optics should diverge the laser beam over the imaged area (field of view). The laser beam leaves the laser head with 1 to 4 mm diameter as maximum for Nd: YAG laser beam (Cao et al 2014). For most PIV experiments a light sheet of less than 1 mm thick is desired to guarantee the measured flow field can keep in a plane (Stamhuis 2006; Cao et al. 2014), and the spherical lens is used to reduce the light sheet thickness. In the present wok, the selected cylindrical and spherical lenses are -15 mm fl and 500 mm fl respectively. According to the manufacturer's manual (TSI Coorporation (TM) 2004), these specifications yield a 1.34 mm as waist thickness and a 336 mm laser

sheet width, which can be calculated by using the following formula (TSI Coorporation (TM) 2008):

$$Y = \frac{W*X}{F} \qquad (3.1)$$

Where

W- The beam diameter before passing through the cylindrical lens. (Equal to 6.3 mm) (Raffel et al. 1998), **X**- The distance from the focal point cylindrical lens. (800 mm)

F- The focal length of the cylindrical lens. (-15 mm.fl) (TSI Coorporation (TM) 2008)

The main challenge for using lasers as the illumination source, after producing a range of light sheet sizes suitable for the laser, is the timing set up.

3.2.2   The time separation (Δt)

The time separation between the pulses (Δt), is the main important parameter to set when using lasers as the illumination source. The time separation determines the particle image displacement in PIV images. Therefore, the time delay should not only be long enough to determine the displacement of the seeded particles between the two pulses but it also needs to be short enough to avoid the seeded particles leaving out the light sheet between subsequent illuminations (Cao et al 2014). It is very important to select an appropriate Δt, so that particle image displacement is consistent with experimental measurements. Many correlation are used to determine the time pulse delay. (Cao et al 2014) recommended that the optimum pulse delay depends on the desired interrogation area size d_{Int} (in pixels) and on the maximum velocity U_{max} in airflow fields recorded, given as:

$$\frac{Pixel}{U_{max}} < \Delta t = \frac{\Delta X}{U_{max}} < \frac{1}{4} * \frac{d_{Int}}{U_{max}} \qquad (3.2)$$

(Li et al. 2010) presented an easier method to determine Δt. A practical relation (Eq. (3.3)) between Δt and the maximum velocity at area of interest (U_{max}) was founded. In particular, (Δt increases with the decrease of the maximum velocity within the field of view:

$$\Delta t \ (\mu s) \ = \frac{250}{U_{max}} \qquad (3.3)$$

The time separation Δt should be selected so that the displacement follows the "role of thumb" of 25% of the intended interrogation region which produced from broken up the image frame into a grid of "integration regions", and to ensure consistency with experimental measurements (Cao et al. 2014). In order to optimize Δt, the main step is developing an eye observation for it (Cao et al. 2014). Although qualitative, this is a critical step in optimizing a particle image velocimetry measurement. According to that, if the displacement appears random Δt should be reduced, and if there is little or no displacements then Δt should be increased (Cao et al. 2014). In the present work, Δt was selected according to the equation 3.2 with average spatial velocity of 0.41 m/s, which is the average across 27 cough tests (Savory et al. 2014), and optimized to be 750 μs.

3.2.3   Tracer particles

Tracer particles, which are seeded inside the cough chamber, play a key role in any PIV measurement because, as a non-intrusive technique, PIV actually measures the velocities of tracer particles instead of actual airflow velocities. Generally, the size of tracer particles should be not only small enough to achieve good tracking behavior of the turbulence but also large enough to scatter sufficient light signal for image recording devices (Cao et al 2014). In PIV measurements, the tracking behaviors of tracer particles are particularly critical for measurement accuracy. In gas flows, such as in the present case, safety, health and handling considerations are significant factors when selecting appropriate particles.

Many techniques are used to generate and supply tracer particles for seeding gas flows. For example, dry powders can be dispersed in fluidized beds or by air jets. Liquids can be evaporated and afterwards precipitated in condensation generators, or liquid droplets can directly be generated in atomizers (Raffel et al. 1998). Atomizers can also be used to disperse solid particles suspended in evaporating liquids or to generate tiny droplets of high vapor pressure liquids (Raffel et al. 1998). Moreover, for flow visualization in wind tunnel flows smoke generators and monodisperse polystyrene or latex particles injected with water-ethanol are most often used for seeding (Raffel et al. 1998). In the present

work, the size of the tracer particles should be optimized to make a balance between the tracking behavior and the scattering characteristics.

Table 1 illustrates the most common seeding materials which are used as tracer particles for gas flows (Raffel et al. 1998).

Type	Material	Mean diameter (in μm)
Solid	Polystyrene	0.5 – 10
	Alumina Al_2O_3	0.2 - 5
	Titanium dioxide TiO_2	0.1 - 5
	Glass micro-spheres	0.1 - 3
	Glass micro-balloons	30 - 100
	Granules for synthetic coatings	10 - 50
	Dioctylphathalate	1 - 10
	Smoke	< 1
Liquid	Different oils	0.5 - 10
	Di-ethyl-hexyl-sebacate	0.5 – 1.5
	Helium-filled soap bubbles	1000 - 3000

The FLUGIE chamber is seeded with Titanium dioxide particles (TiO_2) in rutile mineral form. According to the producer specification the particle size distribution ranges from 0.15 to 0.47 μm, where 69% of the particles are in the 0.34 to 0.43 μm size bin and 29% of the particles are in the 0.27 to 0.34 μm size bin (Savory et al. 2014). Different methods are available for the generation of the particles to seed indoor airflow (Cao et al 2014).

Particles should be seeded into airflow with a sufficient, steady and spatially uniform concentration. Generally, a higher seeding concentration is preferred for better measurement spatial resolution. However, an excessively high-density of seeding may lead to poor spatial resolution due to bad scattering performance. The ideal concentration of the tracer particles is 5 to 20 particles in an interrogation area (Raffel et al. 1998). Ideally, the generators should produce particles with a monodisperse size distribution and at a constantly high enough production rate to meet the spatial resolution requirement of the PIV experiment. For this purpose, a vacuum-oven is used to dry the titanium dioxide (TiO_2) powder, which is stored in a vacuum container to minimize clumping and later aerosolized using a custom crafted version of the Pitt 3 aerosol generator (Raffel et al. 1998), as illustrated in Fig 12.
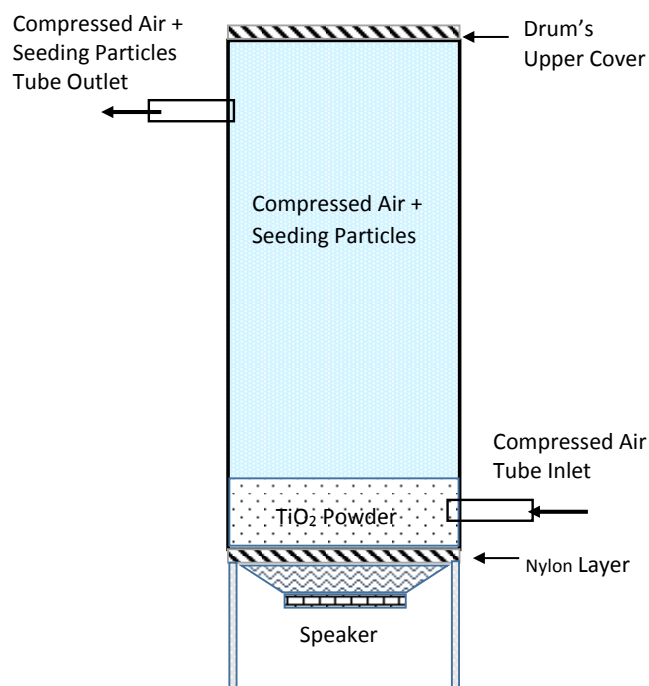
Figure 12 Schematic diagram of the aerosol drum generator

The aerosol generator consists of a vertical cylindrical drum with two small ports for both inlet and outlet near its bottom and top ends, respectively. The drum is filled with TiO_2 powder, which is carried up and out of the drum by the flow driven by a compressed air line attached to the inlet port at a 5.0 kPa. A loader speaker is placed at the bottom of the drum, which generates sound waves to vibrate and break up the powder particles. The

outlet port of the aerosol generator is connected to a settling chamber which is mounted on top of the FLUGIE (as shown in Fig.13), by a tube with perforations inside the settling chamber to disperse the TiO_2 particles. The FLUGIE chamber and settling chamber are separated by a fine mesh, which permits TiO_2 particles, under the action of gravity and local airflow, to gently enter the test chamber along its centreline (Raffel et al. 1998). The cough jet flow, which is generated by the participant, moves the TiO_2 particles, and the camera system captures the successive images to obtain quantitative information of the flow field.
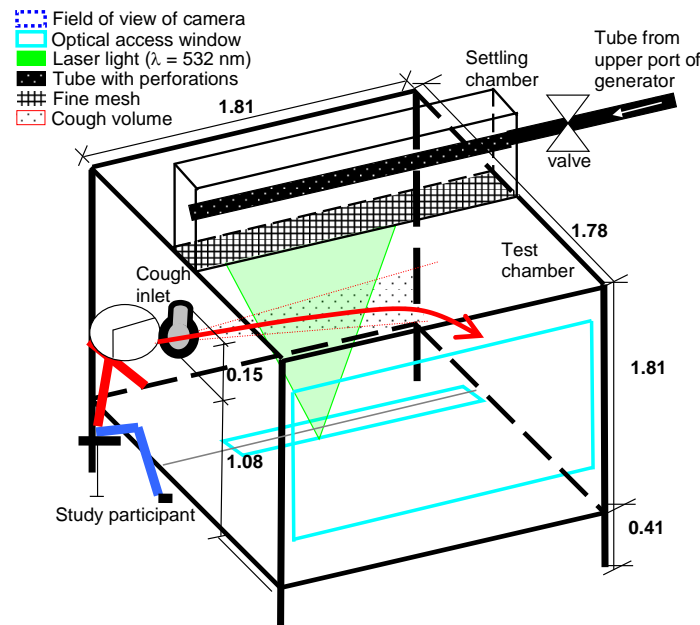
Figure 13 Diagrammatic layout of the 1.81 m × 1.78 m × 1.81 m FLUGIE cough chamber (Modified from Savory et al 2014), all dimensions shown in metres)

3.2.4   Image Recording Devices

The most common type of image recording devices used in PIV flow measurements are CCD cameras (Coupled Charged Devices). In PIV experiments, CCD cameras have been in widespread use for many reasons, such as their spatial resolution, convenient data transmission and image processing, minimum exposure time, high light sensitivity at 532nm and low background noise (Raffel et al. 1998). A CCD element is an electronic sensor, which works by converting light into electronic charge in a silicon chip

(integrated circuit). This charge is digitized and stored as an image file on a computer (Raffel et al. 1998), Fig. 14 describes the CCD structure and the basic working concept.
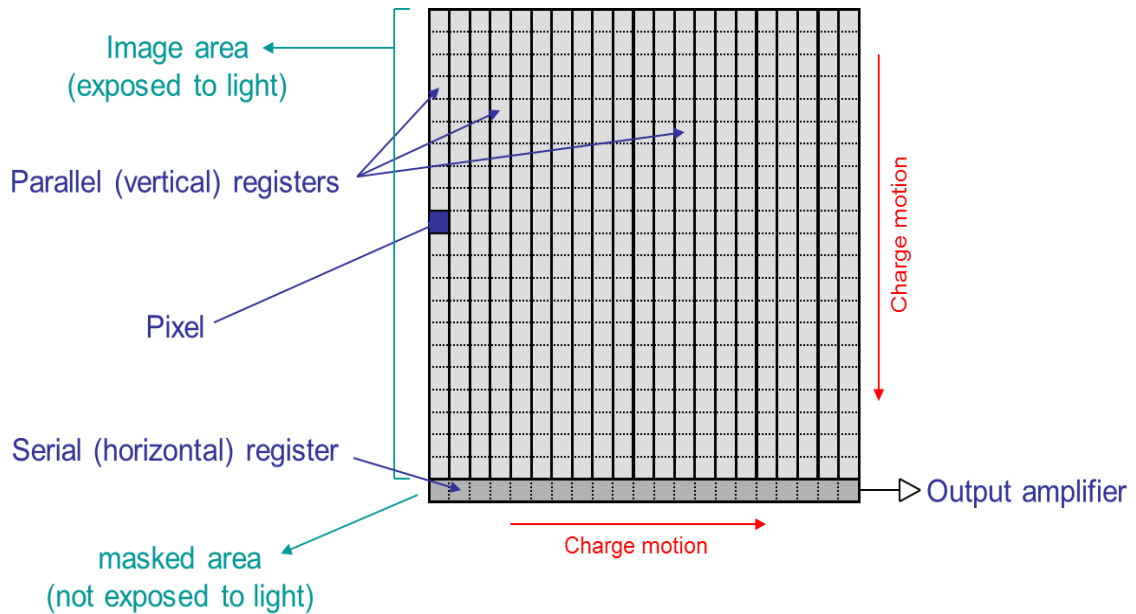
Figure 14 The structure of CCD Semiconductor (Raffel et al. 1998)

A CCD is a two-dimensional array of metal-oxide-semiconductor (MOS) capacitors, which normally consists of an array of many individual CCD elements, and also called pixels (Cao et al. 2014). Nowadays, the sensor resolution of commercially available CCD cameras typically has a range from 2M (1600 pixels × 1200 pixels) to 29M (6576 pixels × 4384 pixels), and the corresponding frame frequency is from 35 Hz to 2 Hz (Raffel et al. 1998). Selecting a CCD camera depends upon the specific application and conditions. For instance, the large-scale measurement in a full-size room needs to use a high-resolution CCD camera, which aims to obtain the complete airflow structures. Contrarily, for studying the small-scale turbulent characteristics of airflows, it is more suitable to use a high-frequency CCD camera (Cao et al. 2014). The other significant factor is the dynamic range of CCD sensors, which is should also be considered to evaluate the signal quality per pixel. Normally, a dynamic arrange of 8 or 12 bits data output per pixel is sufficient for most PIV purposes (Cao et al. 2014; Raffel et al. 1998).

3.2.4.1   PIV cameras calibration procedure

In order to show the used software how to convert from pixel units on the images, to the physical units in the flow space, calibration process are needed to give the software more information to be able to convert pixels to mm over the entire image region. The calibration process uses a calibration target, which is a rectangular grid of marker points with known (X, Y, Z) locations, as present in Fig 15. A single image of a single plane target may be used for one camera systems or multiple PIV camera to create a XY (no Z) calibration for dewarping (Raffel et al. 1998). The calibrations steps start with align the camera using calibration target plane. The centre of target plane, which has dimension 20x20 cm, locate at 1m downstream the cough inlet and raise by 0.5 m from the chamber floor that assume the laser sheet location. The camera focuses on the target plane, capture image with single mode and save it in calibration file. The distance between white dots in target plane presents 0.1 m, that lets possible to select known distance across the image. The selected distance measures in the calibration image menu with the number of pixel to find convertor factor.
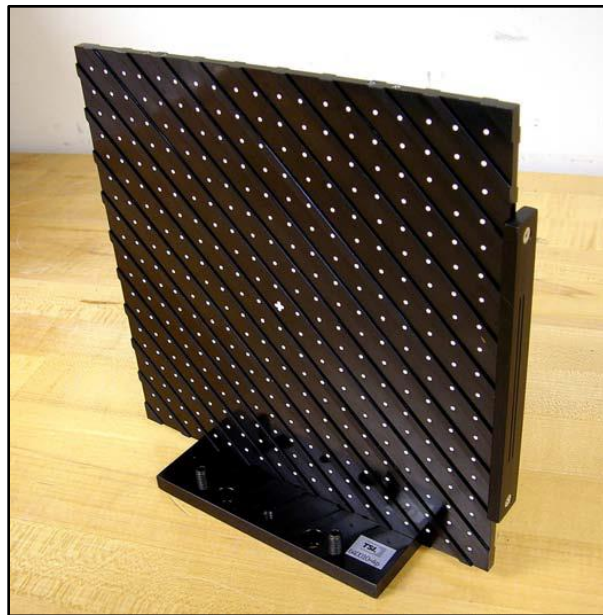
Figure 15 Plane calibration target

In the present work as illustrated in Fig.13, two CCD cameras (Model 630057 POWERVIEW TM Plus 2MP) are used that to cover the field of view centred at 1m

downstream the cough flow and 0.5 m above the chamber floor for both cameras. The calibration process of the camera system yields a spatial resolution of 8.5 pixels per 1 mm with a sensor array of 1600 pixels by 1200 pixels, yielding a 99 × 74 array of velocity vectors .The longer side of the camera view is oriented vertically for both cameras in this experiment, whereas the dual camera setup will increase the field size compared to the single one used in (Savory et al. 2014) and, thereby, increasing the field of view. The cameras set up focuses upon the light sheet at the chamber centreline with an overlap region of about 20% from each one, Fig. 16 shows the dimensions of camera's field of view.
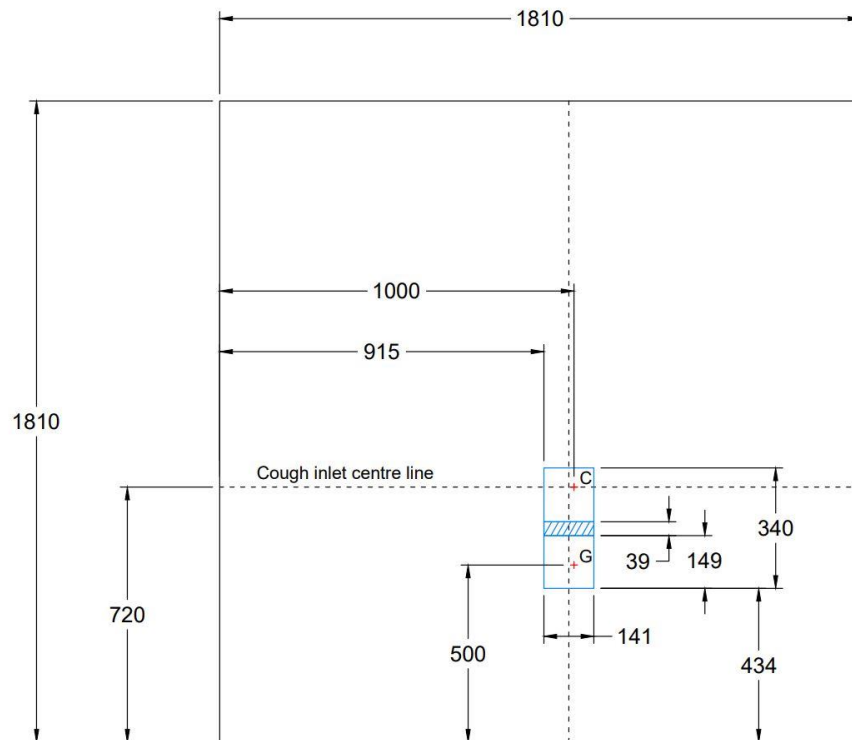
Figure 16 Schematic diagram of the cameras system field of view within FLUGIE (All dimensions in mm)

3.2.5   The Evaluation Method of Captured Image

The principle of the PIV technique is based on the direct determination of the two fundamental dimensions of the particle velocity which are displacement and time. However, direct calculation of the velocity for every particle is a hard task due to the high

concentration and the overlaps between particles. Deriving the displacement information from raw particle images are conducted by image evaluation methods. The most common evaluation method in PIV systems is to capture two images on two separate frames and to perform multistep cross-correlation analysis. The magnitude and direction of the velocity vector will be provided without ambiguity by using the cross-correlation function, which has a significant peak. For calculating the correlation functions, the cross-correlation methods, in general, are based on digital Fast Fourier Transform (FFT) algorithms (Raffel et al. 1998). The most widely used evaluation method is the cross-correlation map. The cross-correlation map method iteratively calculates velocity vectors with an initial interrogation area (IA) of size N times the size of the final IA and uses the intermediary results as information for the next IA of smaller size, until the final IA size is reached (Raffel et al. 1998). IA is a sub-area in the recorded images and its dimensional setting directly determines the spatial resolution and accuracy of the measurement (Raffel et al. 1998). The smaller IA size and higher overlap ratio can achieve higher spatial resolution, but require higher quality image recordings and consumes longer computing time (Cao et al. 2014). In the present work, the first step is the rotation of the images by $+ 90^{o}$ because they are oriented vertically. The cross-correlation analysis for PIV was performed for interrogation windows of 32 pixels $\times$ 32 pixels with a 50% overlap, yielding a 74 $\times$ 99 array of velocity vectors (Recursive Nyquist Grids). Using a global standard deviation filter followed by local median filters, erroneous vectors were identified and rejected. Typically, this filtering process resulted in less than 5% of the vectors being removed (Raffel et al. 1998). The data were then interpolated to fill the locations where velocity data were rejected (Raffel et al. 1998).

3.3   Hot Wire Anemometry (HWA)

In an experimental measurement, it is not question of the best instrument but rather which instrument will perform best for the specific application. In contrary to PIV technique, the hot wire anemometry probe, which has been used extensively for a long time as a research tool in fluid mechanics, is an intrusive measurement technique. This old history from using of HWA sensors is attributed to the good frequency response (several hundred of kHz), wide velocity range as a magnitude, direction, and a velocity fluctuations, and

two phase turbulent flow measurements, temperature measurements (Tropea et al 2007). The HWA sensors classified into main categories according to the operating principle as follows: constant voltage anemometers (CVA), constant current anemometers (CCA) and constant temperature anemometers (CTA). The mode of operation of CTA gives many advantages in front of the other modes. In this section, Description of the HWA- CTA probe components, the operating concept, and the calibration method will be provided.

3.3.1   Basic components and Principle of Operation

A hot wire anemometer consists of two probes with fine wire, which is of the order of a micron, stretched between them. The miniature wire generally made of tungsten or platinum with dimensions around 1.25mm long and 5 µm diameter, a small glass-coated thermistor bead is often used on CTA circuit probes (Tropea et al 2007)]. Fig. 17 shows the structure of hot wire probe. Very often a dedicated Application software for CTA set-up, data acquisition, and data analysis is part of the CTA anemometer (Yue and Malmström 1998). The CTA anemometer works on the basis of convective heat transfer from a heated sensor to the surrounding fluid, the heat transfer being primarily related to the fluid velocity. By using very fine wire sensors placed in the fluid and electronics with servo-loop technique, it is possible to measure velocity fluctuations of fine scales and of high frequencies. The advantages of the CTA over other flow measuring principles are ease-of-use, the output is an analog voltage, which means that no information is lost, and very high temporal resolution, which makes the CTA ideal for measuring spectra. And finally, the CTA is more affordable than LDA or PIV systems (Jørgensen 2002). By using very fine wire sensors placed in the fluid and electronics with servo-loop technique (Wheatstone bridge configuration) as shown in Fig.18, it is possible to measure velocity fluctuations of fine scales and of high frequencies (Tropea et al 2007).
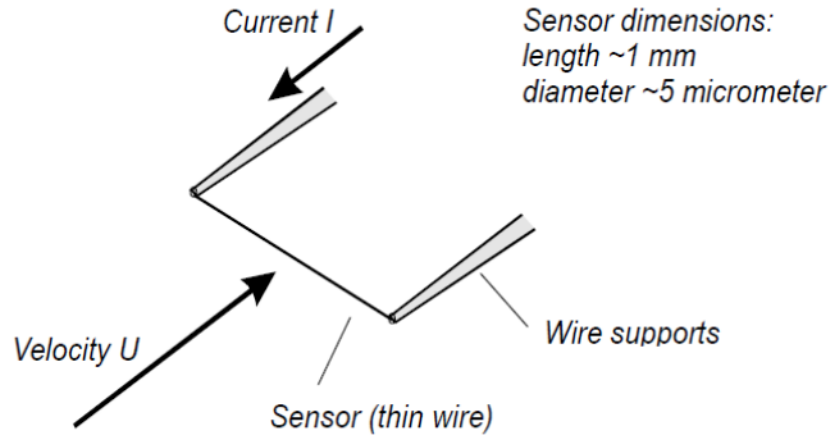
Figure 17 Schematic Diagram of the HWA structure (Yue and Malmström 1998)
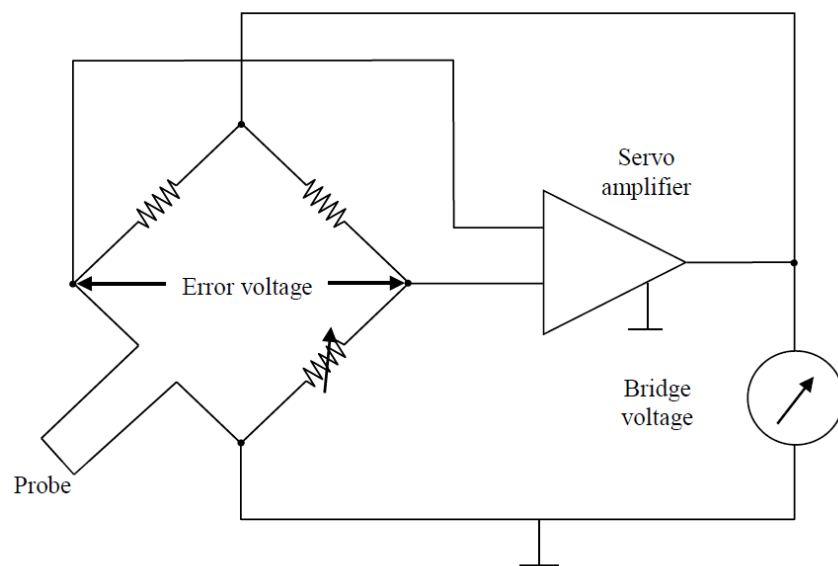
Figure 18 Principal Circuit of a CTA for hot-wire Measurements (Reproduced from Jørgensen 2002)

3.3.2   General Hot Wire Equation

The basic idea to determine the flow velocity by using HWA probe is the heat transfer from the heated sensor to the medium flowing around the sensor. The heat can be transferred from the sensor by radiation Q_R, conduction Q_C, free convection Q_{fc}, and

especially by forced convection Q_{con}. In thermal equilibrium state, the power generated by heating equal to (Jørgensen 2002):

$$W = \; Q_h * \frac{dQ_i}{dt} = Q_{el} \tag{3.4}$$

and the supplied electrical power

$$Q_{el} = I * E_w = \; I^2 * R_w \; = \frac{E^2}{R} \tag{3.5}$$

Where:

C_w - Heat capacity of wire (J/ kg K^o)

E_w - acquired voltage for the wire (V)

I - Heating current feeding the wire in (A)

Q_{el} - Electrical power supplied (W/m^2 K^o)

Q_h - Heat transfer rate to ambient surrounding (W/m^2 K^o)

Q_i - thermal energy stored in the wire (C_wT_w) in (W/m^2 K^o)

R_w - Resistance in the wire at the operating temperature (Ω)

T_w - Temperature of wire (K^o)

W- Power generated by joule heating given by I^2R_w where ($R_w = R_w (T_w)$) in (Watt)

and the power generated equal to the heat output carried off by the sensor (Jørgensen 2002):

$$W=Q_{el}= Q_R + Q_c + Q_{fc} + Q_{con} \tag{3.6}$$

Forced Convection Q_{con} plays the main role in heat transferred to the surrounding.

$$W=Q_{el}=Q_{con}=I^2*R_W=h * A_w * (T_w - T_a) \tag{3.7}$$

The resistance of a wire is a function of its temperature. For a metallic conductor (Bruun 1995):

$$R_w = R_a [1 + b_1 (T_w - T_a) + b_2 (T_w - T_a)^2 + \ldots] \qquad (3.8)$$

This can be linearized for a temperature range of up to 200°C (Bruun 1995):

$$R_w = R_a[1 + b_1(T_w - T_a)] \qquad (3.9)$$

This results in the following expression (Bruun 1995):

$$\frac{I^2 * R_w}{R_w - R_a} = A + B * U^{0.5} \qquad (3.10)$$

Hence for finite length hot wire anemometer,

$$\frac{I^2 * R_w}{R_w - R_a} = A + B * U^n \qquad (3.11)$$

In terms of the voltage E_w Eqn. 3.11 can be written as (Bruun 1995):

$$\frac{E^2}{R_w} = (A + B * U^n) * (T_w - T_a) \qquad (3.12)$$

For the CTA the temperature and resistance are constant. Since the frequency response of a sensors is mostly flat (linear) over a large range (order of 100 Hz to order of 10000 Hz) this allows the instantaneous response of the hot wire to be written, even for unsteady flows., in an algebraic form as (Jørgensen 2002; Bruun 1995):

$$E^2 = A + B * U^n \qquad (3.13)$$

Where A, B and n are constants determine from calibration.

Eqn.3.13 is known by King's Law (Jørgensen 2002; Bruun 1995), and in its original form n = 0.5. However, the results obtained by Collis and Williams have showed that a good estimation for (n) is 0.45 which gives better prediction for the flows within the range of 0.02<Re<44 (Jørgensen 2002; Bruun 1995). Eqn.3.13 uses for determining the voltage of hot wires permits the velocity behavior to be determined, for velocity measurements. An

alternative approach is so-called polynomial linearization which approximates the inverse of the King's Law (Jørgensen 2002; Bruun 1995):

$$U = f(E) = \left(\frac{E^2 - A}{B}\right)^{\frac{1}{n}}$$ (3.14)

by usually fourth order polynomial (Krause 2008; Bruun 1995):

$$U = A + BE + CE^2 + DE^3 + FE^4 \ldots\ldots$$ (3.15)

This polynomial equation was tested by using a computer program which could fit a polynomial of up to the tenth degree to raw calibration data (Krause 2008). However, the solution of the polynomial equation was found to become unstable above the fourth order (Krause 2008). In measurement practice, the calibration procedure, which will be discussed in the next section, will establish a relation between the HWA output and the flow velocity.

3.3.3   Velocity probe calibration procedure

A calibration system is normally not considered part of the measuring chain. However, it is considered as a significant step for the accuracy and the speed with which an experiment can be conducted. Calibration of hot-wire probes at relatively high velocity (for example, $U > 2$ m s−1 for air flow) can be easily carried out by measuring the outlet velocity of a calibration nozzle with a 'top hat' velocity profile (Yue and Malmström 1998). Calibrations can be performed in a dedicated calibrator with a low turbulent free jet, whose velocity is calculated on basis of the pressure drop over its exit (Jørgensen 2002). Calibrations can also be performed in the wind-tunnel, where the experiments are going to take place, with a pitot-static tube used to determine the reference velocity through measurement of dynamic pressure (Jørgensen 2002). For all actual measurements, direct calibration of the anemometer is necessary, in the present work a dedicated calibrator was used to generate a laminar low-velocity pipe flow to calibrate the CTA probe as used in (Yue and Malmström 1998). The next subsection will explain the details of the calibrator facility.

3.3.3.1   Calibration facility

The probe is placed in a low-velocity air stream of known and adjustable velocities and the anemometer output voltage E is measured as a function of the flow velocity U. There is a non-linear dependence of the anemometer output voltage on the flow velocity. The calibration facility used in this work shown in Fig. 19.
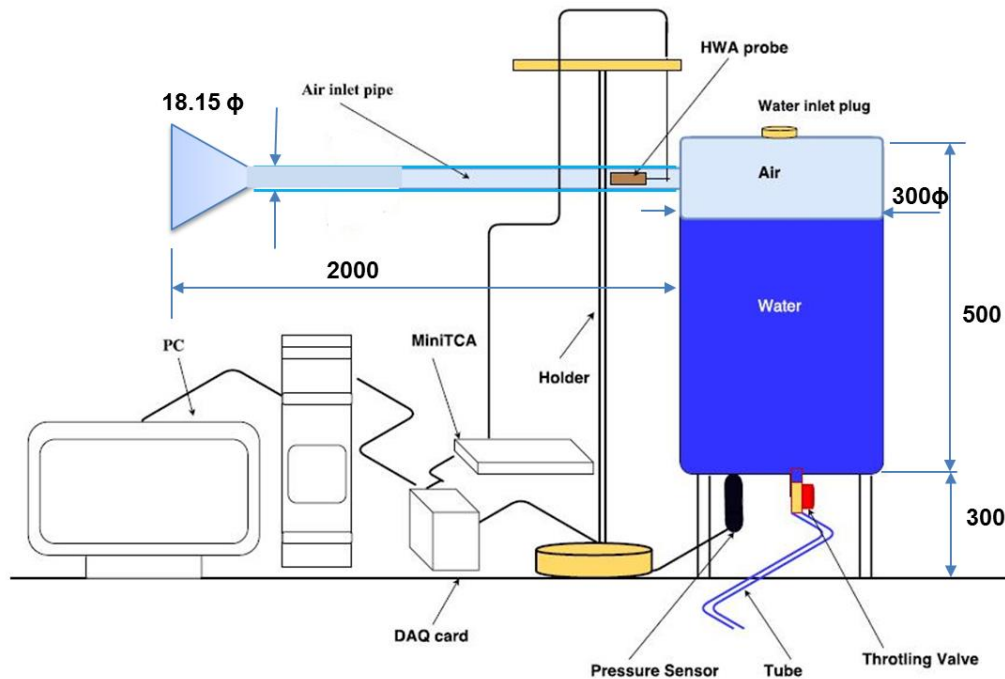
Figure 19 Calibration facility for CTA probe (All dimensions in mm)

The calibrator consists of a closed water tank with dimension of 0.3 m in diameter and 0.5 m in high, which is made from plastic, equipped with an inlet tube at the top of the tank to generate free air stream, a liquid pressure sensor and a throttling valve at the bottom. By using this setup, the calibration process can reliably be performed throughout a range of air velocities extending from approximately 0.2 m/s to 2.4 m/s.

3.3.3.2   Pressure Sensor Calibration Process

The first step in the calibration process is a determination of the true value for the air velocity. For this propose, the liquid pressure sensor was calibrated with using data sheet information provided, which provide by the manufacturer to obtain on the true value. The pressure transducer used in this work is from Omegadyne Co., Model PX409-001G5V-EH, with a pressure range of 0-6.9 kPa and a corresponding voltage output of 0-5Vdc, with an uncertainty of +/- 0.05% of 6.9 kPa, the datasheet for this sensor was provided in appendix B.

The tank labeled with ticks has 1 mm resolution, and it is filled up to 0.45 m depth of water, and the calibration is performed by turning the valve to a range of different openings during a single draining of the tank with 0.05 m step of water depth. This procedure gives nine measurement points as voltage readings from the pressure sensor. The pressure reading of the sensor, which is provided by the data sheet, is used to calculate height the water above the transducer sensor according to the formula of eqn. 3.16:

$$P = \rho * g * H \tag{3.16}$$

$$\text{And } H = h + \Delta h$$

Where:

P- is liquid pressure, g -is gravity, ρ-is density of water, h- is the height of water within the tank and Δ h- is the depth of water from bottom of the tank to the sensor.

Figure 20 illustrates the comparison of sensor voltage readings vs. water pressure between measured and data sheet points. It is clearly evident that the rate of change of voltage with pressure from the data sheet range compares well with the measured data being 0.7262 v/kPa and 0.7312 v/kPa respectively as shown in Fig.19. These data are perfectly acceptable by 0.7 % difference between them and the HWA calibration measurements can be carried out confidently.
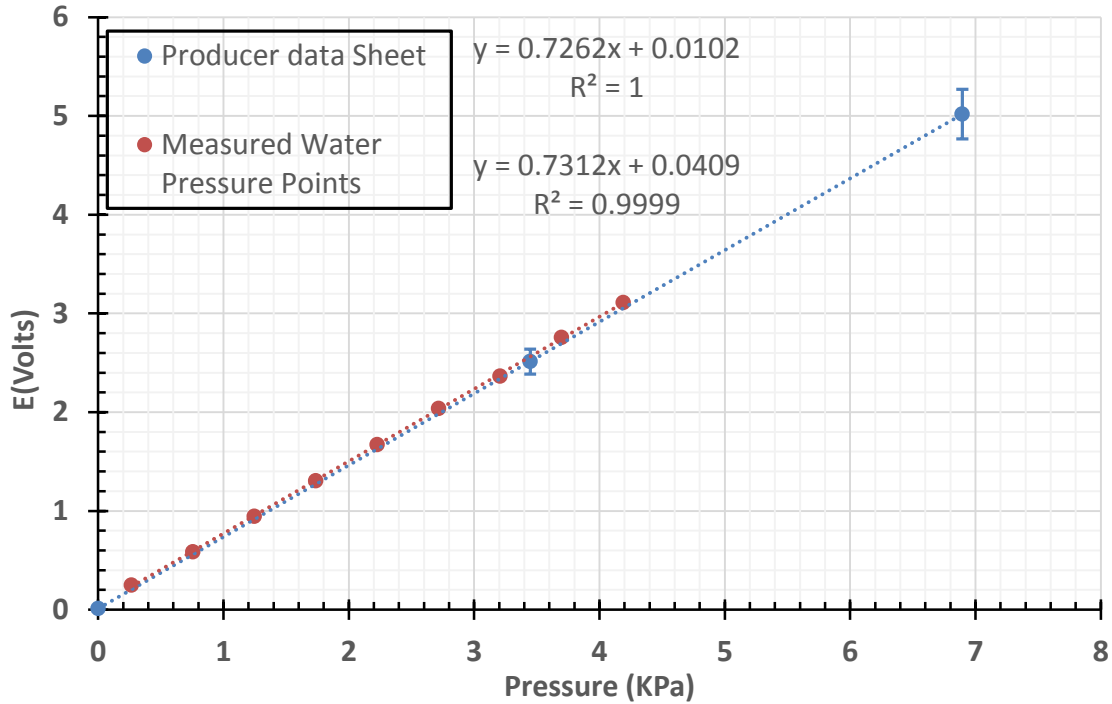
Figure 20 Comparison of voltage vs. pressure points between manufacture's data sheet and measured data

3.3.4 HWA Probe Calibration Process

The calibration process of hot wire probes, using the set up shown in Fig.19 and similar to that used in (Yue and Malmström 1998), can be summarized in general as first filling the tank with water to approximately 45 cm depth. A LabVIEW program, which was created for monitoring the pressure sensor and HWA probe voltages, is used for obtaining the calibration data. The tank is allowed to sit for a span of approximately 10 minutes in order for the water to become stationary. The throttling valve has 1260 degrees of rotation available and that corresponds to $3\frac{1}{2}$ complete turns. The valve knob has 6 arms with these it is easy to determine 1/6 of a turn. The calibration is performed by the turning valve to fully open to achieve the first single draining of the tank for 10 s, then the valve is closed gradually by third of a turn steps to obtain ten single draining increments of the tank water. This allows for rapid calibration without the need for refilling the tank between trials. After each interval at the selected valve opening, the tube will be completely plugged to allow for the water to become completely stable in the

tank. Moreover, this is to allow for easier separation of the data during the data analysis stage of the calibration.

The LabVIEW program records the time history for both the pressure sensor and the HWA probe for all draining points. It is important to measure the room temperature and room atmospheric pressure because they will be used to determine the probe uncertainty. Fig. 21 shows the time history for ten reading points from a calibration process. At each draining point, the transition data are excluded to avoid any signal noise and the average of the HWA probe output the rate of change of the pressure sensor voltage reading, as shown in Fig. 22, were computed.
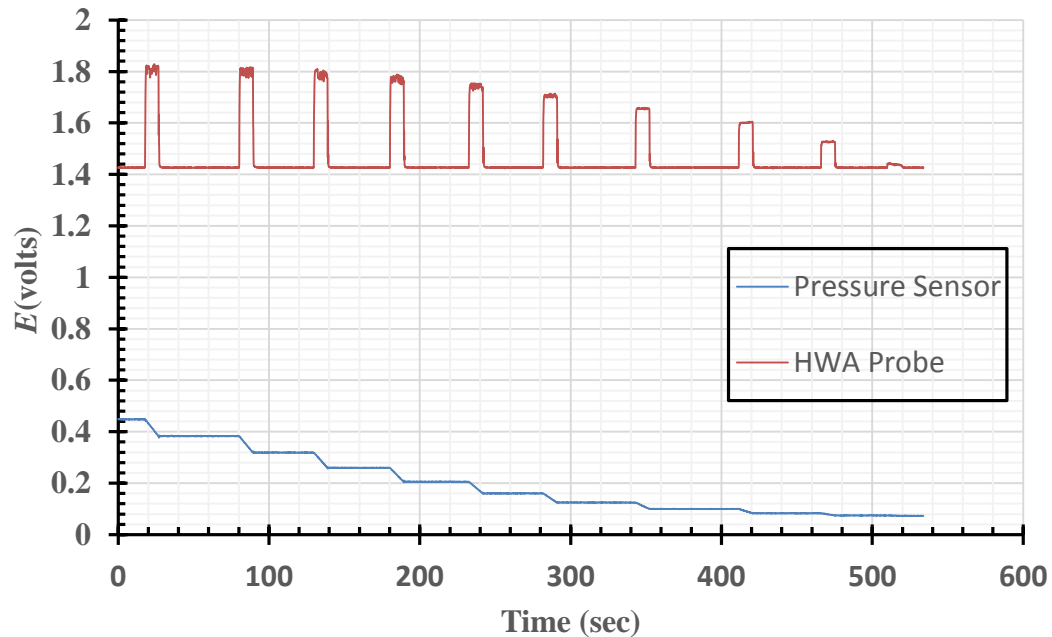
Figure 21 The time history of ten readings of the pressure sensor and HWA velocity probe
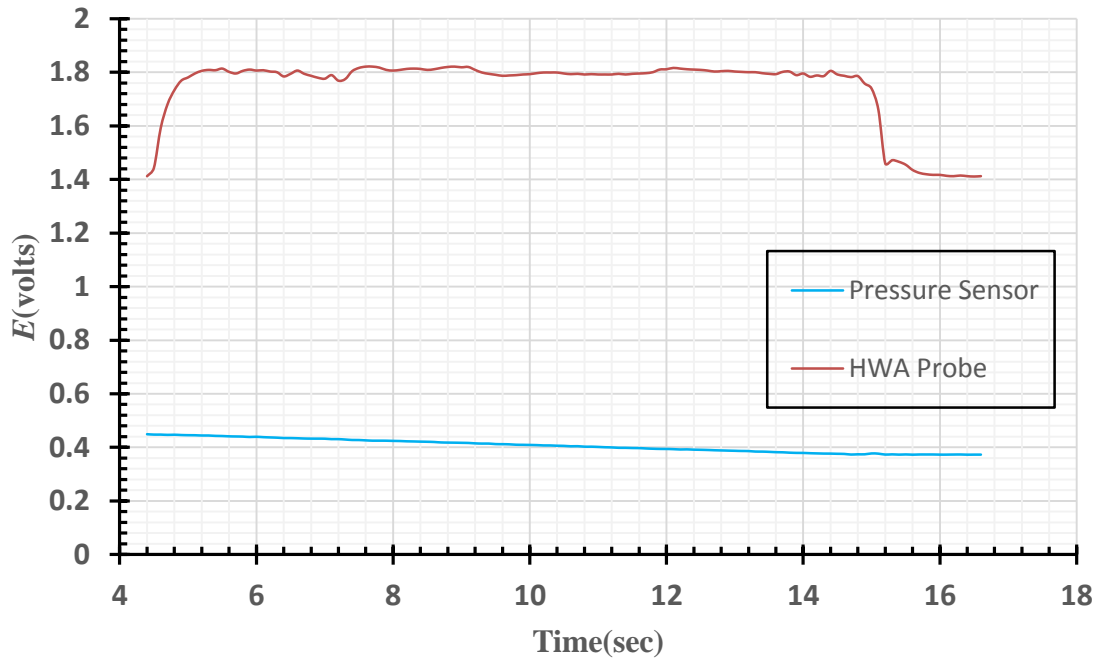
Figure 22 The time history of the pressure sensor and HWA probe

at the first draining point

The theoretical velocity is calculated by using the continuity equation for the water tank that will give:

$$U_{avg} = \frac{A_t}{A_p} * \frac{dh}{dt} \qquad (3.17)$$

U_{avg} is the air average velocity in the inlet tube, $\frac{dh}{dt}$ is the change rate of water height in the tank

A_t is water tank cross-sectional area and A_p is the inlet pipe cross-sectional area.

The maximum velocity of the air inside the pipe equal to (White 2010):

$$U_{max} = 2*U_{avg} \qquad (3.18)$$

Consider the fully developed laminar flow in a round pipe of radius R (White 2010):

$$U_{th} = U_{max} * (1 - \frac{r^2}{R^2})$$
(3.19)

Where: R is the pipe radius, r the position of the probe from the pipe centre.

From table 2, the curve between E^2 and U_{th}^n is plotted by using each data of ten points for three trials. The value of n varies from 0.45 to 0.5. For the present work, n = 0.5 is selected since it gives the best fit of data as shown in Fig. 23. According to the selected value of n, the trend line will give the calibration coefficients A and B of King's law as presented in eqn. 3.13.

From eqn. 3.19, ten points are calculated to obtain values of Upredict at each value of E. A polynomial trend line is created between Upredict and E. The polynomial curve fit is normally recommended, as it makes very good fits with linearization errors often less than1% (Jørgensen 2002; Bruun 1995). Figure 24 shows the recommended fourth order polynomial curve fit, which is used in this work, because a higher order results in an unstable solution (Bruun 1995). The measured data for three trials are arranged in Table 2, which shows the rate of water in the tank, the probe voltage, and the theoretical velocity, respectively, at each point for all three trials.

Table 2 The measured data of both the HWA probe and the pressure sensor at the ten points with three trials (M-1, M-2, and M-3)

	M-1			M-2			M-3				
P	dh/dt	E	Uth_1^n	dh/dt	E	Uth_2^n	dh/dt	E	Uth_3^n	$U_{predict}$	-/+Error
1	0.0077	1.66	2.02	0.0076	1.67	2.01	0.0077	1.67	2.01	3.90	0.39
2	0.0074	1.66	1.98	0.0074	1.66	1.98	0.0074	1.66	1.98	3.76	0.38
3	0.0068	1.65	1.90	0.0068	1.65	1.90	0.0068	1.65	1.90	3.60	0.36
4	0.0061	1.63	1.80	0.0062	1.63	1.82	0.0061	1.63	1.80	3.23	0.32
5	0.0051	1.61	1.65	0.0052	1.61	1.66	0.0051	1.61	1.65	2.82	0.28
6	0.004	1.58	1.46	0.004	1.58	1.46	0.004	1.58	1.46	2.28	0.23
7	0.003	1.54	1.26	0.003	1.54	1.26	0.0029	1.54	1.24	1.72	0.17
8	0.0019	1.48	1.00	0.0019	1.48	1.00	0.0019	1.48	1.00	1.06	0.11
9	0.001	1.41	0.73	0.001	1.41	0.73	0.0009	1.41	0.69	0.48	0.05
10	0.0005	1.36	0.52	0.0005	1.36	0.52	0.0005	1.36	0.52	0.22	0.02

$$E^2 = 0.6029U^{0.5} + 1.5803$$
$$R^2 = 0.9942$$
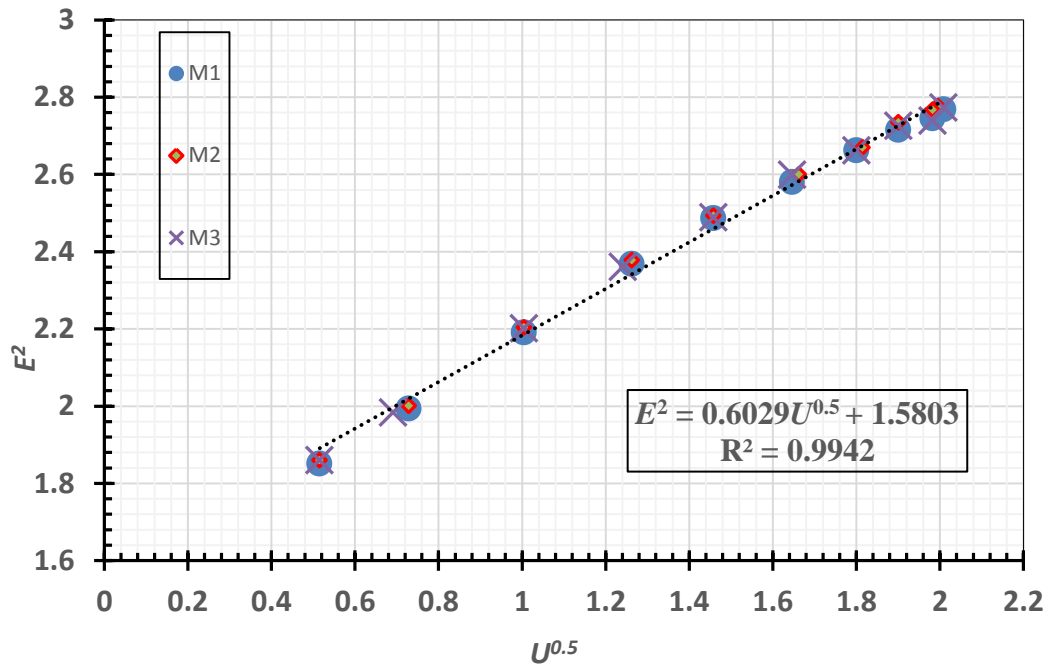
Figure 23 Trend line Plot of calibration data points

$$U_{predict} = KE^4 - LE^3 - ME^2 - LE + O$$
$$R^2 = 1.00$$
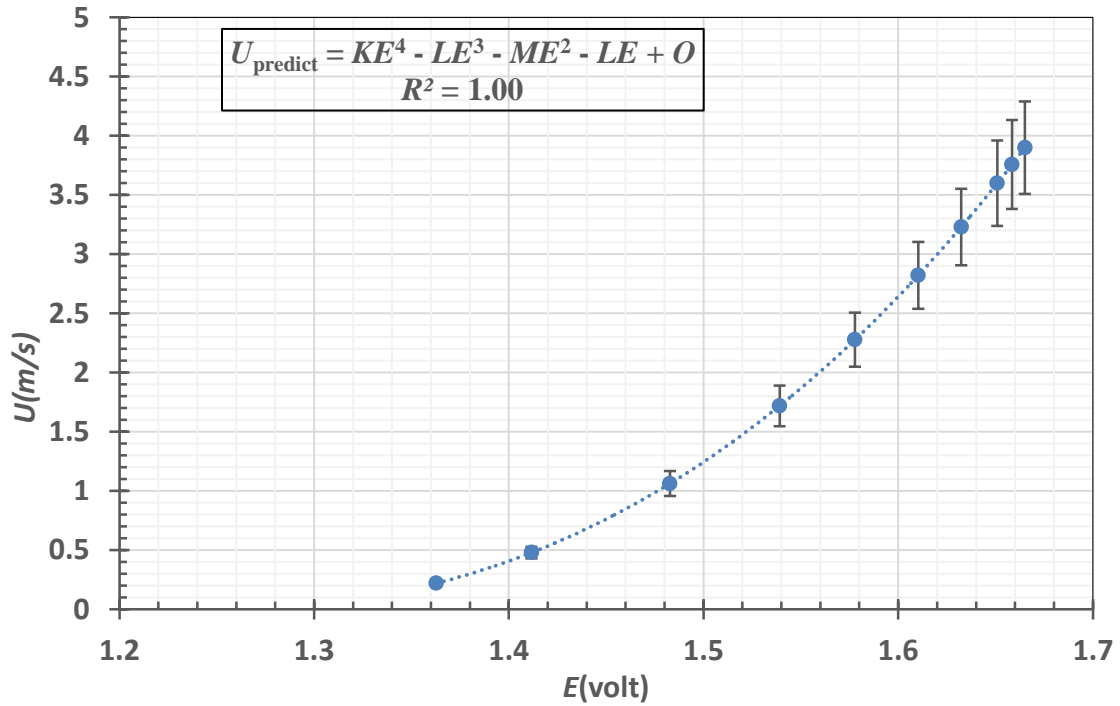
Figure 24 Fourth order polynomial Curve fitting of calibration data points with uncertainty values (K, L, M, N, O fitted constants)

3.4   Experimental Uncertainty

Properly reporting an experimental result along with its uncertainty allows other people to make judgments about the quality of the experiment, and it facilitates meaningful comparisons with other similar values or a theoretical prediction. Experimental measurements always have some degree of uncertainty that may come from a variety of sources.

3.4.1   HWA Probe Uncertainty

The relative expanded uncertainties on a single velocity sample obtained with a single – sensor hot wire probe in air (Jørgensen 2002). The calculations for the HWA uncertainties attached in Appendix C-1, can be summarized in the following table:

(Input data are: T_o= 20.1^{o}C, P_o = 98.6452 KPa, Tw = 300°C, U = 1.5 m/sec.)

Table 3 Error sources and uncertainties for single velocity sample acquired with a CTA including calibrator uncertainty (Jørgensen 2002)

Source of uncertainty	Input variants	Typical value	Relative output variants	Relative standard uncertainty
Calibration	U_{th}	1%	C-7	0.092
A/D resolution	E_{AD} a	3 volts 12 bit	C-11	0.00116
Probe Positioning	θ	1°	C-12	0
Temperature variations (sensor overtemp.)	ΔT	±1°C	C-13	0.0043
Temperature variations (ρ,T)	ΔT	1°C	C-14	0.0023
Ambient pressure	ΔP	13KPa	C-15	0.00045

The summation of relative standard uncertainty = 0.1047 = 10.47≈10 % which will be considered in this study.

3.4.2   PIV System Uncertainty

In PIV techniques, the uncertainty is comprised of two components. The first component is bias error, which is caused by various aspects of measurements techniques and equipment. The second component is the random error, which is due to the statistical variation of the measured quantities in multiple measurements. In PIV measurements, there are numerous error sources. These error sources are velocity gradient, particle seeding diameter, out of plane motion, Interpolation, peak locking (Cowen and Monismith 1997). The total error in Particle Image Velocimetry can be calculated by adding all the errors caused from different sources (Elatar, 2013). The error estimation attached in Appendix C-2 (for participant 221-cough2), and can be summarized in the following table:

Error due to	Error symbol	Error in pixel	Error in m/s
Velocity gradient	ε_u, ε_v	ε_u = 0.0045 (pixel/pixel) ε_{v}=0.0050 (pixel/pixel)	*ε_{V}=0.0011
Particle seeding diameter	ε_{dp}	0.01 pixel	0.0016
Interpolation	ε_I	0.08 pixel	0.013
Out of the plane	ε_{op}	0	0
Peak locking	ε_{pl}	0	0

* $\varepsilon_V = \sqrt[2]{\varepsilon_u{}^2 + \varepsilon_u{}^2}$, which is the total error for velocity vector. The total uncertainty

($\varepsilon_T = \varepsilon_V + \varepsilon_{dp} + \varepsilon_I + \varepsilon_{op} + \varepsilon_{pl}$) (Elatar, 2013)equal to 0.016 m/s. Considering the maximum mean velocity in the measurement plane, 0.89 m/sec, the total error is equal to 2 %.

3.5 Averaging the instantaneous velocity

Inherent in the collection of data taken over time is some form of random variation, as in a cough velocity measurement which is non-stationary phenomena. There exist methods for reducing of canceling the effect due to random variation. An often-used technique in scientific researching is "smoothing" (Marple 1989) This technique, when properly applied, reveals more clearly the underlying trend and periodic components. The main smoothing method is the time average method. A moving average is a technique to get an overall idea of the trends in a data set; it is an average of any subset of numbers (Marple 1989). The moving average is extremely useful for forecasting long-term trends. There are many approaches for moving average such as simple method, centred method, cumulative method, weighted method, exponential method…etc. Centred moving average, which is preferred by most analysts because this approach allow to align each moving average with the midpoint of the observations that it averages; midpoint refers to the middle of a time span (Bohm and Zech 2010). The idea behind this approach to getting a moving average that's centred on an existing midpoint, that's done by taking set of consecutive data and averaging them by the procedure as shown in Fig 25. In a brief, moving averages remove some of the short-term variation from obtained data, and that depends on the window size. A window size is a kind of low-pass filter, so it is important to make a judgment about the time scale on which data variations change from being merely "noise" to more meaningful indications of true temporal changes in the underlying activity (Bohm and Zech 2010). In the present case, the squared values of root mean square fluctuation velocity (u'^2_{rms}) is plotted viruses of time scale (window size) to get good estimation based on adequate values for window size when u'^2_{rms} will give constant value as shown in Fig.26. Fig 27 shows comparison of instantaneous velocity and moving average value of cough velocity.
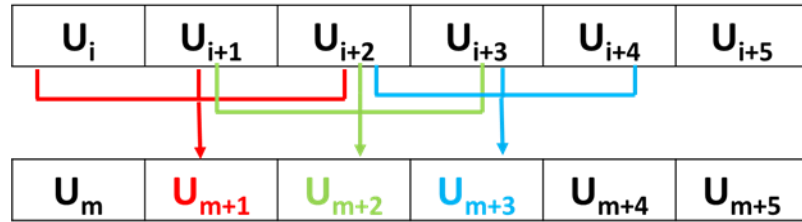
Figure 25 Centered moving average approach (windows size k=3)
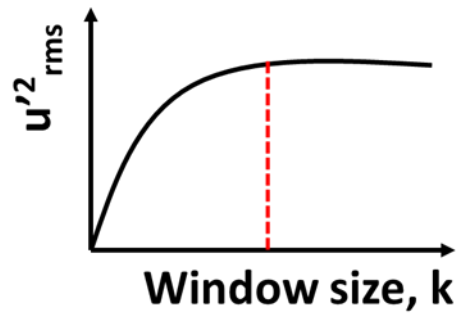
Figure 26 Windows size's check independency
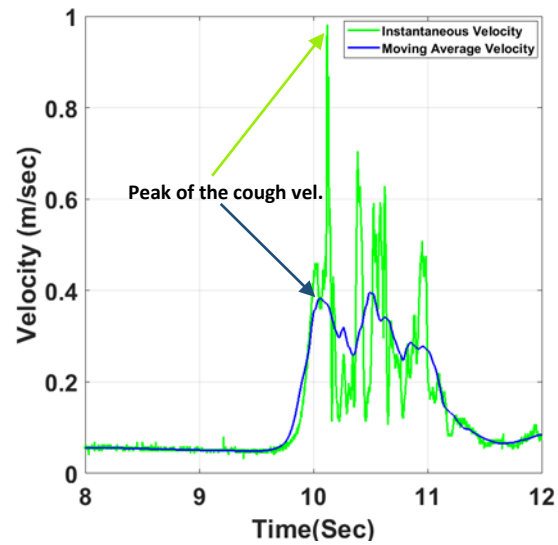
Figure 27 Comparison of moving average and instant velocity profiles of cough

3.6   Cough Velocity Normalization

For better analysis and more generalized comparison, each cough velocity time history, following a moving average filtering is normalized to give exactly 1 at the peak of the cough. For this purpose, the equation 3.20 will be used to normalize the velocities which were gotten by both HWA and PIV measurements in order to compare all cough velocity time histories from all participants.
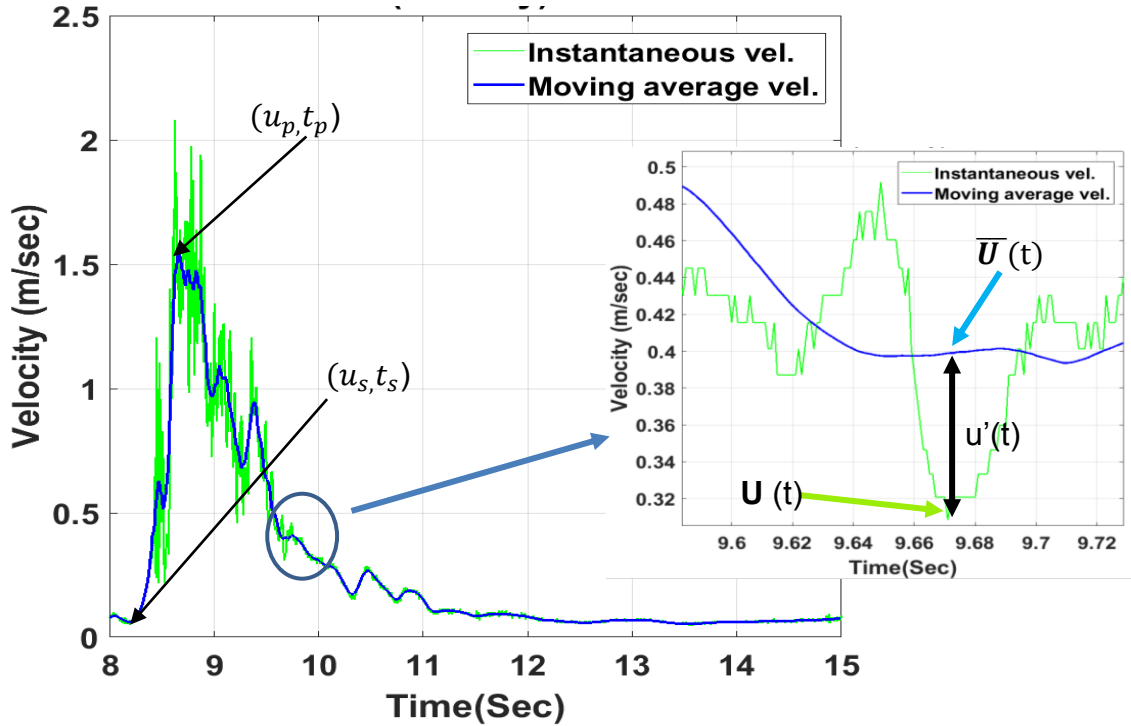
Figure 28 The definition of the cough start and peak points with zoom in sample

$$U_{norm.} = \frac{U(i) - U_s}{U_p - U_s} \tag{3.20}$$

Where:

U(i) is the instantaneous velocity, U_s the velocity of cough at the beginning of the cough period as shown in Fig.28, and U_p maximum velocity of the cough.

For the time axis, the time is normalized according to equation (3.21)

$$\tau_{(t)} = \frac{t_i - t_s}{t_p - t_s} \tag{3.21}$$

Where:

$\tau_{(t)}$ is the normalized velocity, t_p is the time at the peak of the cough velocity,

t_s the time at beginning of cough period and t_i is the instantaneous time .

3.7   Bioaerosol sampling and mid turbinate swab (MTS)

In order to quantify the factors relating to person-to-person airborne transmission of virus, the measurements of the viral content of the droplets produced during real human coughs from participants will be carried out. The bioaerosol processes associated with virus droplet formation and transmission will be started by droplet sampling onto wet polytetrafluoroethylene (PTFE) membrane filters of 1.0 μm pore size and 37 mm diameter. The use of the smaller (37-mm) filter will increase the probability of the contaminant being deposited onto a smaller area, thus increasing the concentration of the droplets collected from the filter (Jensen and Schafer 1998). Filters are often held in disposable plastic filter cassettes during bioaerosol sampling as shown in Fig.29. The constant-flow air sampling pumps (SKC Inc., Airchek 224-PCXR3) will be operated at a flow rate of 4000 ± 40 mL/min. Moreover, a self-collected mid turbinate swab (MTS) will be used to determine the identity of the pathogen acquired by each study participant. Then, these specimens will be interrogated by multiplex polymerase chain reaction (multiplex-PCR) assay for a panel of respiratory viruses (RVP Fast, Luminex) (Savory et al. 2014). The viral content from the membranes will be quantified using a virus-specific monoplex quantitative real-time PCR assay (Savory et al. 2014).
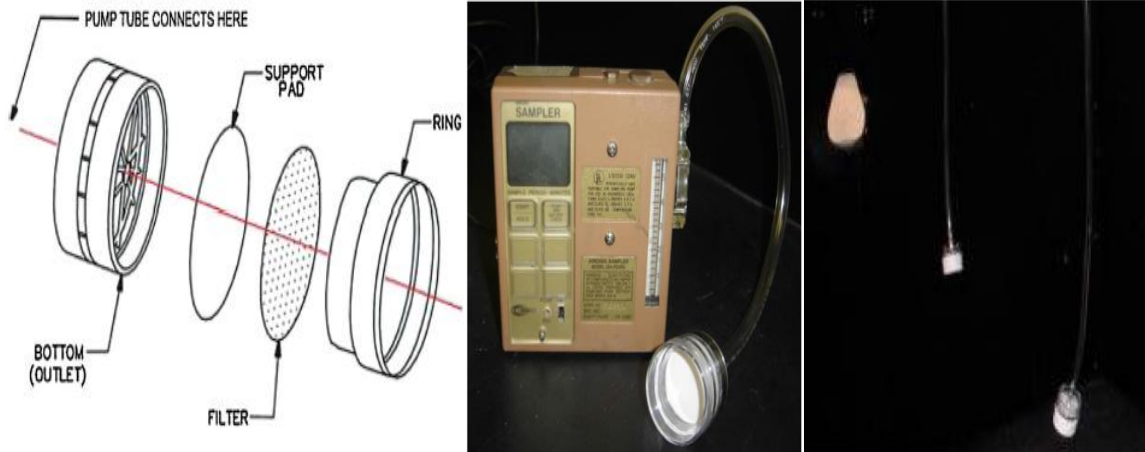
Figure 29 Diagram and photograph of the bioaerosol sampling cassette assembly and sampling pump and their positions in FLUGIE chamber (Savory et al 2014 (with authors' permission)).

Chapter 4

4   Experimental Methodology

According to the ethical responsibility, the office of Human Research Ethics in Western University (HSREB) reviewed and approved the present study (approval number: 108945). The intake steps of the volunteer students will start first after they are assessed by a physician in Western Students Health Service (WSHS). Then they are referred to our recruiters at the welcome desk to fill a study eligibility form where they are explained about the study and obtain an informed consent form from them. The eligibility form contains the inclusion and the exclusion criteria. The inclusion criteria are; the participants should have fever and cough and/or sore throat in the absence of another known cause of illness (e.g. allergies) in last 24 hours and be aged between 18 and 35 (inclusive). The exclusion criteria exclude any participants who are immunocompromised, or with underlying cardiopulmonary disease, pregnant, or a smoker. The Thompson Engineering Building (TEB 308) is used for sample collection of the coughs (one self-collected mid-turbinate swab and six cough airflows). The eligibility form, letter of information, and consent form and Research Ethics Boards (REB) approval form included in Appendix (D). The experimental measurements consist of three steps, which will be conducted during the research period. In this chapter, more details about the experimental methodology include the HWA probe measurements, bio-aerosol and mid turbinate swab sampling and PIV measurements will be presented.

4.1   HWA probe measurements

A thermal anemometer, which presented in chapter 3 section 3.3, is used to measure air velocities by measuring heat transfer from a small wire immersed in the cough flow field at 1 m in axial distance and 0.50 m height from the chamber floor as presented in Fig.30, (0.17 m under the centreline of the cough chamber inlet), that because the cough will tend to fell down at 1 m downstream as observed from previous study. Hot wire anemometry provides an analogue output which represents the velocity in a point. Velocity

information is thus available by using HWA_Acq.vi program, which is used to the hot-wire recording. 30 sec was applied to record the data and cover the whole cough period of each cough for all three coughs. Sampling rate at 1 kHz was applied in range of $0 - 3$ V to capture all turbulent scales of the cough.
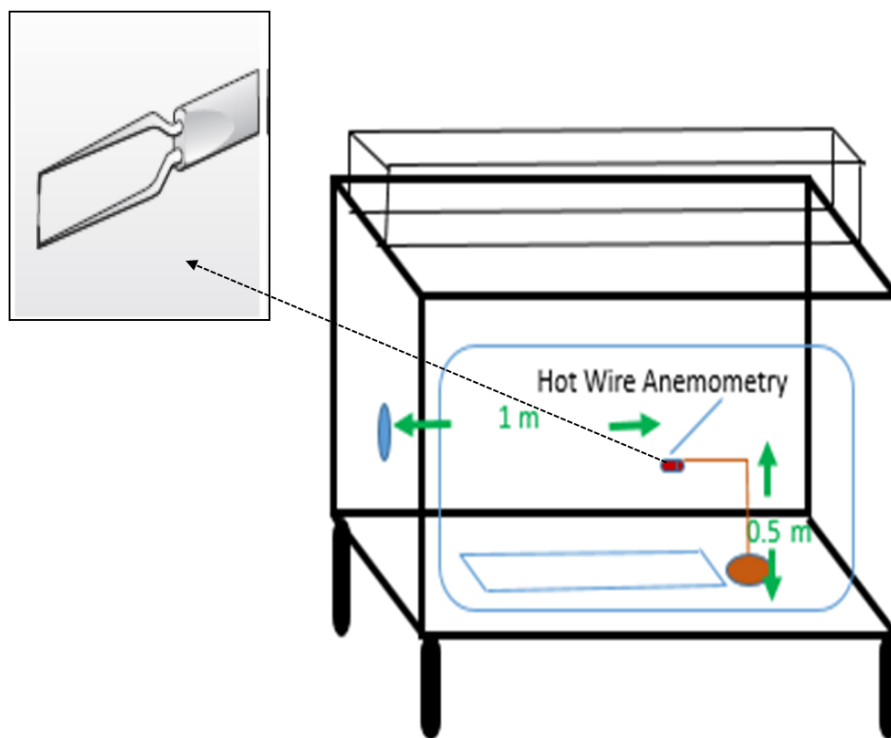
Figure 30 Hot Wire Anemometry in FLUGIE Chamber

4.2   Bio-aerosol and mid turbinate swab sampling

Two PTFE membrane filters are suspended from the roof of the chamber at (0.5, 0.89, 0.72) and (1.0, 0.89, 0.72) m as presented in section 3.5. These filters are connected to separate constant flow rate sampling pumps as shown in Fig. 29. Each participant gives

three separate coughs, 30 seconds apart. The aerosol sampling and HWA probe measurements are conducted simultaneously. Expelled pathogens are collected by the membranes and each membrane is saved in an individual swab tube and labeled by the participant number and location (0.5 or 1.0 m). The measurements procedures were illustrated in Appendix (E) (Lin et al 2014). Finally, the tube is shaken for 10 s by a vortex shaker and then stored at -80°C in the freezer. In order to identify the virus pathogen, a mid-turbinate swab (MTS) specimen is collected after the participant finishes these first two measurements. The MTS kit is used to make a self-collected swab. The samples are first stored at -20° C freezer (up to 24 hours maximum) in the lab and after all the measurements are completed, it is transferred to a -80°C freezer before final analysis in the Department of Microbiology; Division of Infectious Diseases; Sunnybrook Health Sciences Centre and Research Institute (SRI)-University of Toronto.

4.3 Particle Image Velocimetry Measurements of Coughs

The last step in the experimental measurements is the PIV measurements. In order to quantify the cough flow field, separate measurements are performed by using the optical access area into the FLUGIE chamber. The cough chamber is seeded by TiO_2. The Nd: YAG laser beam is directed into the chamber from a lower glass window by using a mirror and diverged and fanned by set of lenses setup (see Fig.13). The laser sheet illuminates the seeded particles with 336 mm width at 1 m downstream the cougher mouth. The dual CCD cameras system, which is focused on the laser sheet with defined flow field as described in Fig. 16, captures the cough flow characteristics within two flow fields overlapping by 20% vertically (see Fig. 16). The lower energy Nd: YAG laser is used with 15 Hz that allows capture of 80 images during 5 s (the period of capturing images). The participant presents three cough at this step, 30 seconds apart. Insight3G platform software is used with laser system to control the capture process. The timing setup which is used in this experiment is as presented in Table 4.

Table 4 PIV Capture Timing Setup

PIV Frame Mode	Straddle
Pulse Repetition Rate (Hz)	15
Laser Pulse Delay (µs)	10000
Delta T (µs)	750
PIV Exposure (µs)	10375

The processing of PIV images is started by using the rotation option in the post processing suite, which rotates the image $+90^{o}$ to the correct position. The cross-correlation technique is used to process the images and that can be broken down into many steps as follows: generation of grids, masking spots, performing the correlation, location of peaks and, finally, performing vector validation and conditioning. The parameters which are used to processing the PIV images are presented in Table 5 with more explanation (TSI Coorporation (TM) 2008; Raffel et al. 1998).

Table 5 Setting up of PIV Parameters for Processing

Grid Engine	Recursive Nyquist Grid	Use this plugin to increase accuracy or obtain higher spatial resolution.
Spot Mask Engine	Gaussian Mask	Use this condition (weight function) to give more value to the pixel's centre and less to the edges of the pixels
Correlation Engine	Fast Fourier Transform (FFT)	The correlation is compute using a FFT and the spots must be squared and spot A must be has the same size as the spot B.
Peak Engine	Gaussian Peak	It locates the correlation peak with sub-pixel accuracy by fitting a Gaussian curve to the highest pixel and its four nearest neighbors.
Vector Validation (Post-processing)	1-Local Validation (Median)	It is widely used and the velocity vectors are the median value of all values of all vectors in the neighborhood.
	2-Global Validation (Standard Deviation Range)	The range of valid velocities is defined by multiply of standard deviation and is centred at the mean velocity.
Vector Conditioning	Filling Holes (Recursive Filling)	The filling procedure sorts the holes by the number of valid neighbors found initially.

The size of the interrogation window was set to 32× 32 pixels, and a 50 % window overlap was used to increase the number of vectors. Considering the 1600×1200 pixel resolution of the images, an array of 99× 74 velocity vectors, which was oriented vertically, was generated from each image pair (TSI Coorporation(TM) 2008). The spatially mean velocity, <U>, will be calculated at each captured frame by using the following correlation:

$$< U > = \frac{\sum_{i=1}^{i=N}(<U_i>)}{N}$$

(4.1)

Where:

<U> is the spatial mean velocity (m/s), N is the total velocity vectors = 7326 for each frame

$<U_i >$ is the local velocity $= \sqrt[2]{u_i^2 + v_i^2}$

$u_i \ and \ v_i$ are the axial and vertical velocity components respectively.

Chapter 5

5 Results and Discussion

5.1 Introduction

In this chapter, virological aerosol sampling, mid-turbinate swab results, hot wire probe (H.W.A) and particle image velocimetry (PIV) measurements will be presented, analyzed and discussed for each technique. The results from the winter 2016-17 flu season, encompass 9 participants who were recruited when they were presumed ill. Experiments were conducted for two separate visits; trials were run when the participant was sick, and they returned for a convalescent visit. Moreover, the results from trials conducted in summer 2013, which are for 12 healthy individuals, will be used in this chapter, as well as the results from winter 2014, which includes 5 sick participants and 3 convalesced participants.

5.2 Virological analysis and MTS Results

The target of this study was to recruit 50 participants. Several challenges were met while recruiting and the goal was not met. Recruitment via self-referral might have resulted in more participants, but could have resulted in participants who would not have had respiratory illness.

5.2.1 The results of WeCoF study of winter 2014:

From January 9th to March 1st seven students were referred to WeCoF study recruiters by the Western Student Health Service (WSHS) doctors of whom five agreed to participate. The five participants recruited yielded three participants who tested positive for respiratory viruses. The three etiologic agents found were corona virus (CoV) NL63, influenza A (H1N1) and respiratory syncytial virus (RSV). Viral RNA was extracted

from open-faced cassettes and analyzed using droplet digital PCR. All results were negative except one from the influenza-infected participant, where 0.163 copies/µL of vRNA were recovered from the filter located at 1m.

5.2.2 The results of WeCoF study of winter 2017:

From January 14th to March 30th, 2017 a total of nine participants were recruited from Western Student Health Service (WSHS) during the flu season. The present study resulted 4 out of 9 participants having an illness determined from MTS results, which is considered an overall good yield with a limited number of flu cases. Usually in clinical studies, the biological sample analysis is performed blinded to avoid any bias, and therefore the results presented are without the participant identification number. The four etiologic agents found were corona virus (CoV) NL63, (CoV) OC43, influenza A (H3N2) and respiratory syncytial virus (RSV). Although the MTS yielded a super positive result, the Polymerase Chain Reaction (PCR) data for the filter air samples of the flu A H3N2 for the participant at 0.5 and 1 m were all negative. All Ribonucleic acid (RNA) was extracted using the *MagMax* bead kit. Table 5.1 summarizes the PCR data and MTS result of influenza A H3N2 case.

Table 6 PCR and MTS data flu A H3N2 patient

Sample	CT*	quantity (copies/well)*	quantity (copies/ml)	log10/ml
MTS	20.64	172775.98	10366558.8	7.02
PTFE 0.5m	Undetermined	n/a	n/a	n/a
PTFE 1m	Undetermined	n/a	n/a	n/a

*Where:

 CT: is cycle threshold, or the cycle at which the sample is detected by the machine.

Copies/well: The flu RNA copies/well is extrapolated from a standard curve which was incorporated into the assay (the flu A standard for 10E6 RNA copies has a CT of 20).

5.3   H.W.A. Results

The hot wire probe, which was calibrated by the developed facilities within 10% uncertainty, provides results for 9 participants. Three voluntarily coughs from each participant were collected when they were presumed ill and after they recovered. Data was collected for 27 coughs in each category.

5.3.1   Time history of cough velocity

A typical sample of the best set of coughs is used to compare the time history for three coughs expelled from the same (a) sick and (b) convalescent participant. (Fig. 31: participant no 952). The participant was asked to produce a series of three coughs with the same strength for each, but the results showed that in the sick case the participant produced a peak instantaneous velocity at 0.9, 0.7 and 1.5 m/s for coughs 1, 2, 3, respectively. The same participant was asked to produce three coughs of similar strength after recovering from illness. The participant produced three coughs with a higher peak velocity of 2.1, 2.3 and 2.3 m/s for coughs 1, 2, 3, respectively. The comparison of the 6 coughs for both cases shows that the strength of the velocity field for convalescent coughs is higher than that of the sick coughs. The time history of the instantaneous velocity field depicts the flow as a non-stationary phenomenon. For more informative

comparisons, the results are presented in terms of moving average velocity instead of the instantaneous velocity, in both cases as illustrated in section 3.6. Fig. 32 shows the comparison of the time history of the first cough for the same participant. The peak coughs velocities of the sick case are 0.6, 0.53, and 1.1 m/s, respectively, while for the convalescent case are 1.49, 1.5 and 1.65 m/s. There is a consistent ratio between u_p-instantaneous to u_p-moving average for all 6 coughs in the order of 1.4 (+/- 10%).

For a more generalized comparison, the moving average velocity is normalized by using the correlations presented in section 3.6. Figure 33 shows the comparison of normalized velocity for three coughs for the same participant in each case.
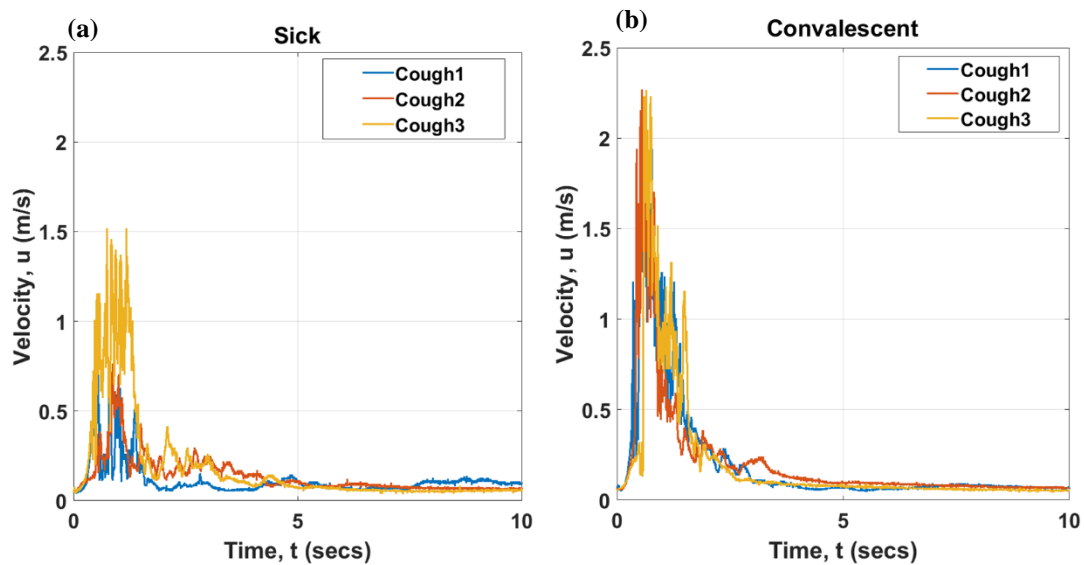
Figure 31 The time history of three coughs of participant no 952 for (a) sick and (b) convalescent
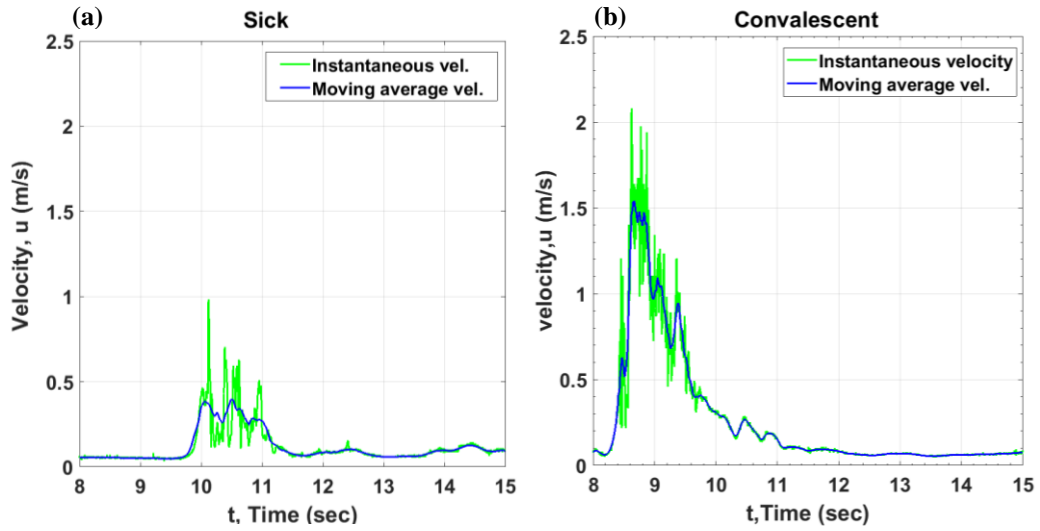
Figure 32 The time history of moving average velocity and instantaneous velocity for (a) sick and (b) convalescent

$$U= \frac{u(t)-u_s}{u_p-u_s}$$

$$\tau = \frac{t_i - t_s}{t_p - t_s}$$
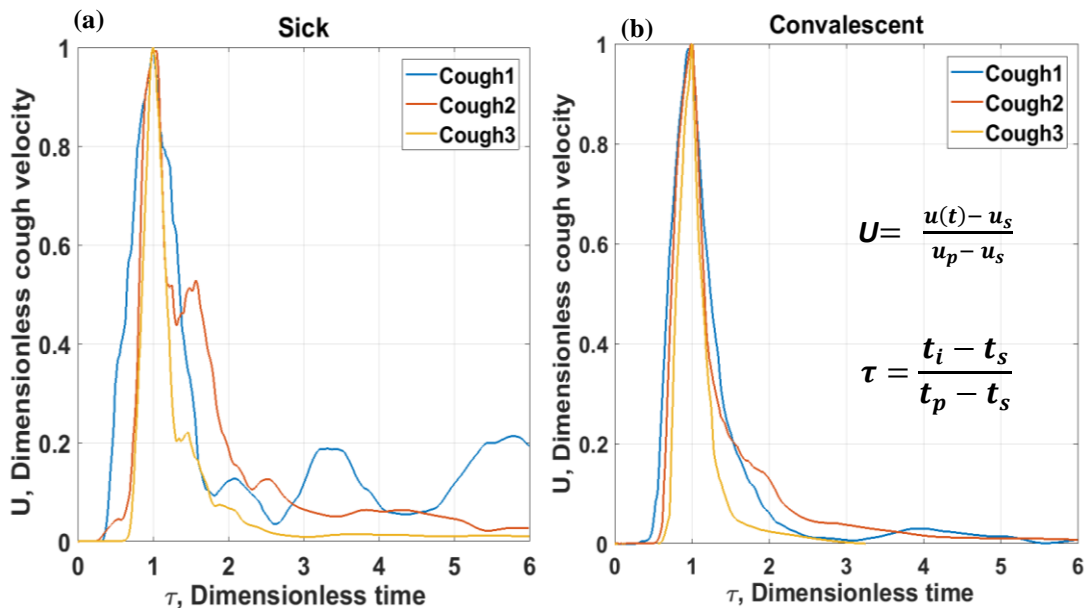
Figure 33 Normalized three cough's velocities for (a) sick and (b) convalescent case

Participant (952)

The comparison of the time history for the sick and convalescent cases provides a good insight to the flow behavior of a transient coughing process at a specific point. For these 6 coughs, it is clear from the following comparison that the sick coughs are weaker than convalescent coughs. The moving average velocity gave a good estimation for cough velocities in both cases compared to instantaneous velocities because this approach removed the short time scale variations. The normalized velocities comparison showed that the sick coughs do not collapse very well and the sick coughs took a longer time to terminate.

5.3.2   Variability of peak cough velocity

The measured peak moving average velocity is sorted from the weaker cough to the strongest one to compare the variability of peak cough velocity. Figure 34 presents the variability of max velocity measurements (m/s) for all trials for sick and convalescent period. For sick coughs, trials 26 and 27 showed abnormal peak values,
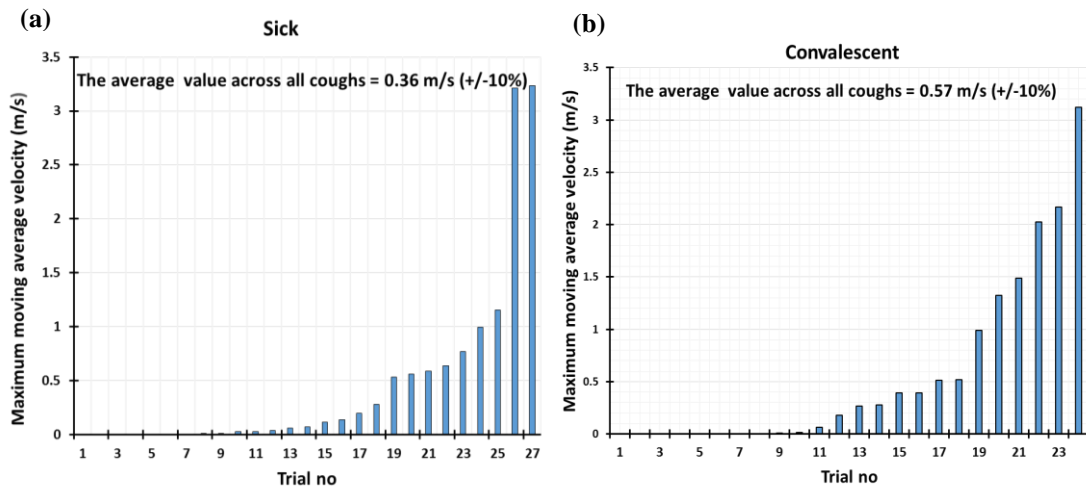
Figure 34 Variability of peak moving average velocity for all participants

so both are excluded for analysis in the present study. Whilst comparing the RMS of the peak cough velocity, the general trend of variability of the average values across all sick coughs (($u_{P-average}$) =0.36 m/s) is lower than average of all convalescent coughs (($u_{P-average}$) =0.57 m/s). The nine weaker coughs, which have u_P value ≤ 0.1 m/s, are excluded from both sick and convalescent cases, and the normalized moving average velocities are compared to understand the general behavior of all coughs in both cases. Figure 35 shows normalized velocities of all convalescent & sick coughs. The comparison of normalized velocity profiles between the two cases shows that the sick coughs take a long interval to terminate because the sick coughs have velocities lower than that of the convalescent coughs. All data of dimensionless time history from both cases are lumped together to find the general trend by using 5th order Gaussian equation.

$$U = \frac{u_{(t)} - u_S}{u_p - u_S}$$

$$\tau = \frac{t_i - t_s}{t_p - t_s}$$
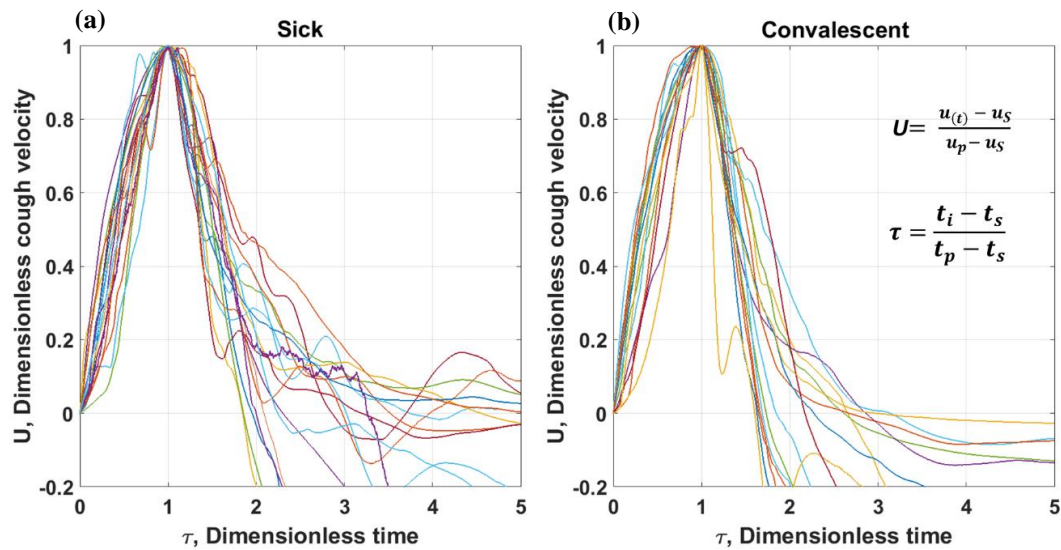
Figure 35 Normalized velocities of all (a) sick & (b) convalescent coughs

Figure 36 shows the general trend of time history of all coughs from sick and convalescent cases. The R^2, which is a statistical indication of how close the data are to the fitted Gaussian equation, gives a value of 0.84 which is considered as high variability of the response data.
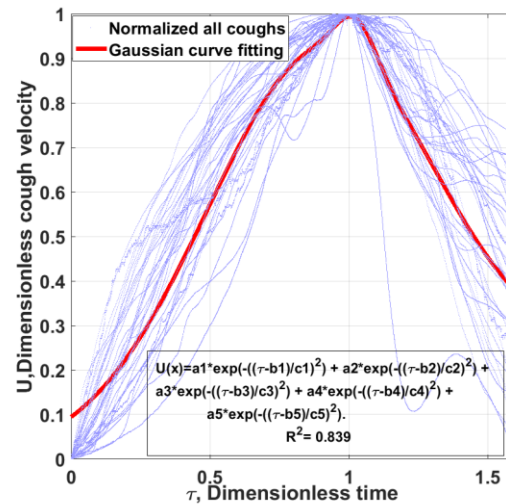
Figure 36 General trend of all normalized velocities for all both of sick & convalescent coughs

To investigate the dimensionless time history of both sick and convalescent cases, the curve fitting is implemented by using the Gaussian 5th order fit equation in the interval ($0 < \tau < 1.6$). Figure 37 (a) and (b) presents the general trend of dimensionless time history for both cases and it can be observed that the coefficient of determination (R^2) is slightly different for sick and convalescent cases (89% for sick, 80% for convalescent).
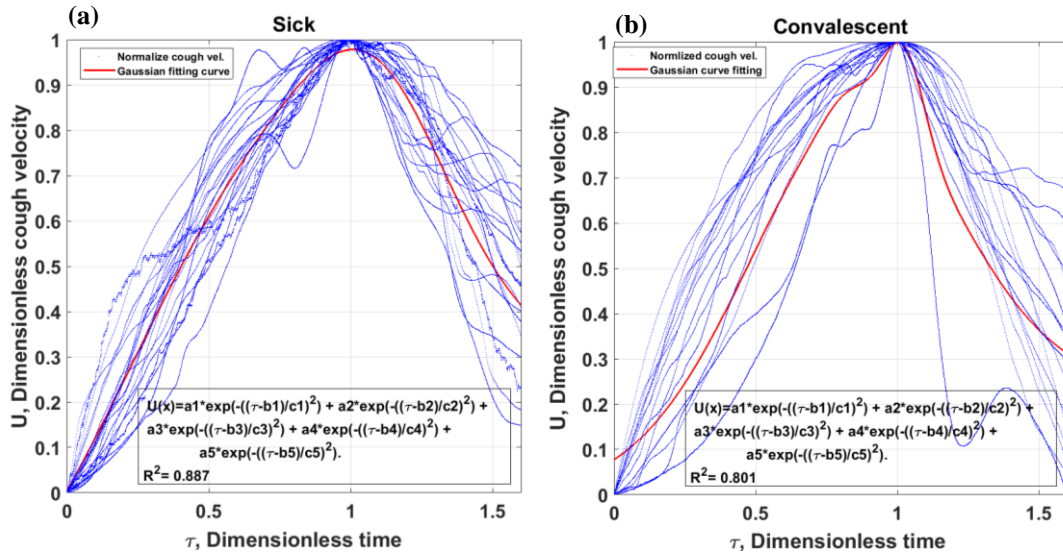
Figure 37 General trend of all normalized velocities for all (a) sick & (b) convalescent coughs

The accumulative frequency of all coughs which are sick or convalescent is calculated by using eqn. 5.1.

$$u_{p,c} = \frac{\sum_{i=1}^{i=c} U_{p,i}}{c} \tag{5.1}$$

Where:

u$_p$ is the peak of moving average

c =1: n and (n is the number of the highest value of u$_p$)

Figure 38 illustrates the variation of the cumulative frequency of the peak moving average velocity for sick and convalescent coughs. There is no variation substantially in low velocity regime, but remarkable difference is observed in the high velocity regime between sick and convalescent coughs.
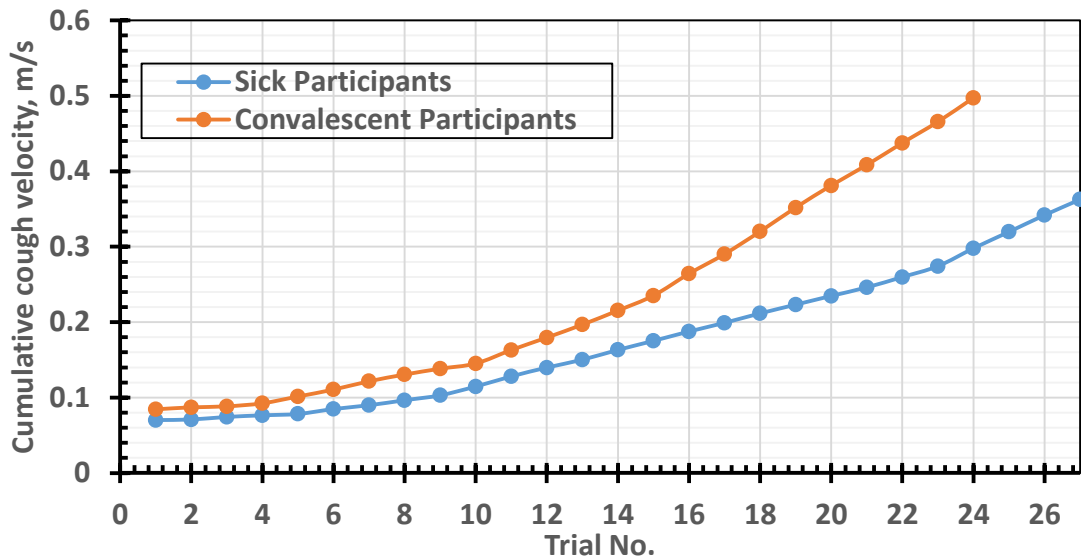
Figure 38 Cumulative Chart of peak moving average velocity for all sick and convalescent coughs

The percentage difference of the cumulative averaging cough velocity between sick and convalescent coughs is roughly 16% for the first cough sample and 45% for the last sample (24). Ultimately, the general trend of variability for sick coughs does not vary substantially from convalescent coughs. For a more generalized comparison, the normalized velocities show a long cough period for sick coughs that which could be explained by weaker velocity magnitudes for sick coughs. Although the distribution of convalescent coughs missed three coughs from one participant, a slight difference is observed between the ensemble average of sick and convalescent coughs. The ensemble average of 24 convalescent coughs is 0.57 m/s while for sick coughs is 0.36 m/s across of 27 coughs.
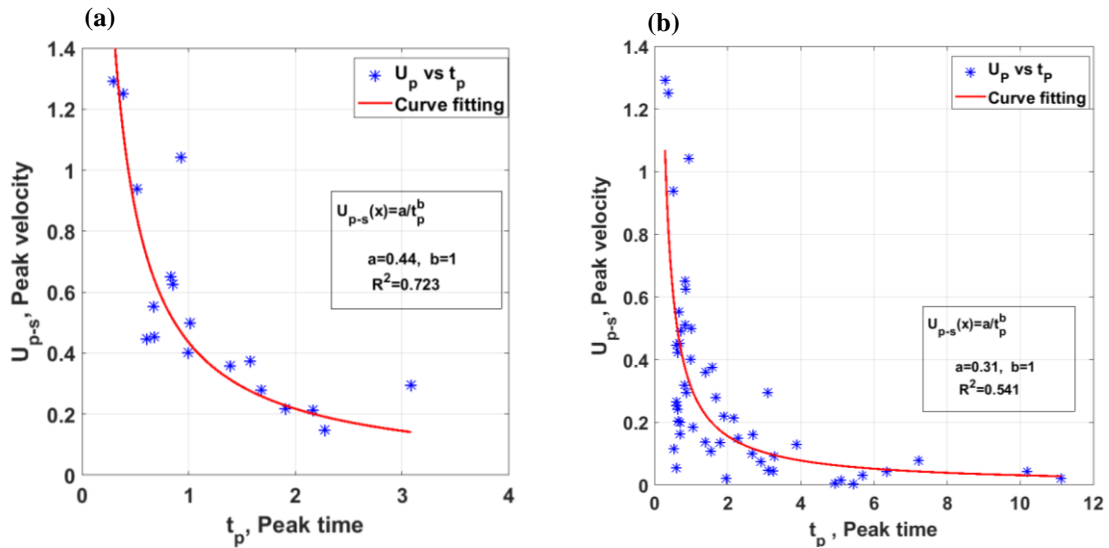
Figure 39 The general trend of Peak coughs velocity of all coughs, (a) for the best 7 coughs for each case and (b) for all 51 coughs from both cases as sick and convalescent

The peak velocity of the cough is plotted verses the peak time in Fig. 39; the peak velocity is calculated from equation 5.2 as follows:

$$Up\text{-}s = u_p\text{-}u_s \tag{5.2}$$

Where u_p and u_s are the moving average velocity at the start and peak points as described in Fig.25. To leave the weaker coughs out of the present analysis, the best seven coughs, which have a peak velocity ≥ 0.20 m/s, are selected from each case. It is clear from Fig.39 (a) that the peak velocity is inversely proportional to the time and the peak cough interval ranges between 0.5 s to 3 s for most of the strong coughs. In Fig. 39 (b), it is noticed that a large variation of the peak cough velocity exists among the participants, and the peak cough interval is also extended to 11s for very weak coughs. This clearly does not fit the data very well.

5.3.3. Coughs Turbulent Intensity

The turbulent intensity for each cough is calculated by using eqn. 5.3 for sick and convalescent case (Savory 2015).

$$I_u = \frac{(u'_{rms}) \, of \, cough \, period}{U_{p-s}}$$

(5.3)

Where:

u'_{rms} is the root mean square of fluctuation velocity.

$\mathbf{U_{p-s}}$ is the moving average velocity from min to max value of cough velocity.

An accumulative chart for turbulent intensity is created by a similar technique to the one used in the previous subsection. Fig.40 illustrates the accumulative turbulent intensity for sick and convalescent coughs have values mostly in the range of $3 - 6\%$ for both cases. The comparison showed that the sick participant produces larger accumulative average compared to the convalescent participant, excluding the first three convalescent coughs. These are higher than the sick participants, because these three convalescent coughs have average velocity smaller than the sick coughs. The power spectral density (PSD) of the cough velocity fluctuations represents the distribution of energy in the turbulent mean flow. To characterize the spectral energy produced by sick and convalescent coughs, the Welch's power spectral density method is employed in a Matlab script (Appendix F-(a)). Figure 41 shows a comparison of the power spectral density function between the sick and convalescent cough (1st sample of both cases) obtained from participant 952. A -5/3 slope of the spectra is observed, which confirms the Kolmogorov decay law. It is clear that the convalescent cough has a higher peak frequency compared to the sick cough, but

it is difficult to propose any general trend from this sort of comparison between the power spectrum energy of the first cough sample in sick and convalescent case.
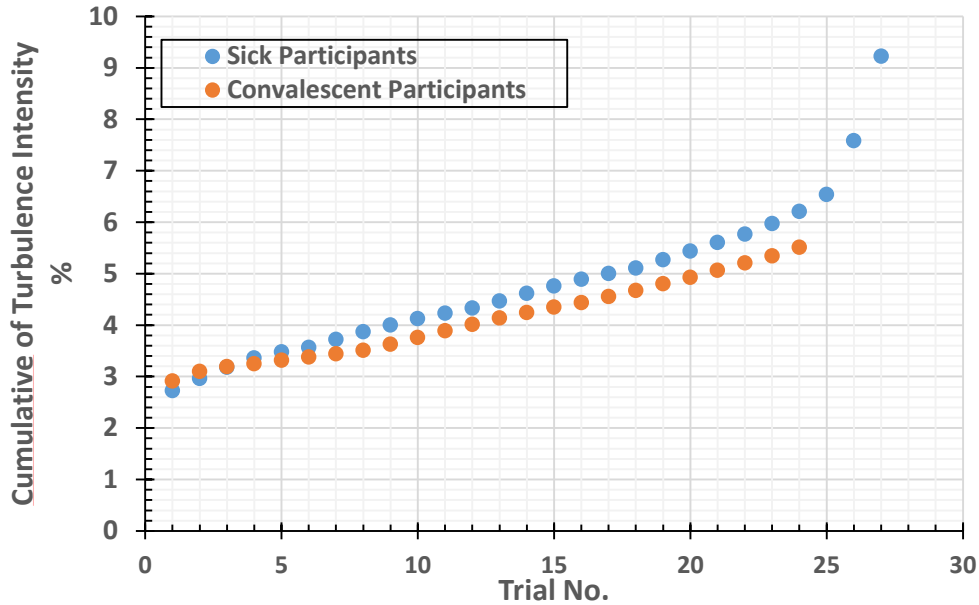
Figure 40 Cumulative chart of turbulent intensity for all sick and convalescent coughs

(a)   (b)
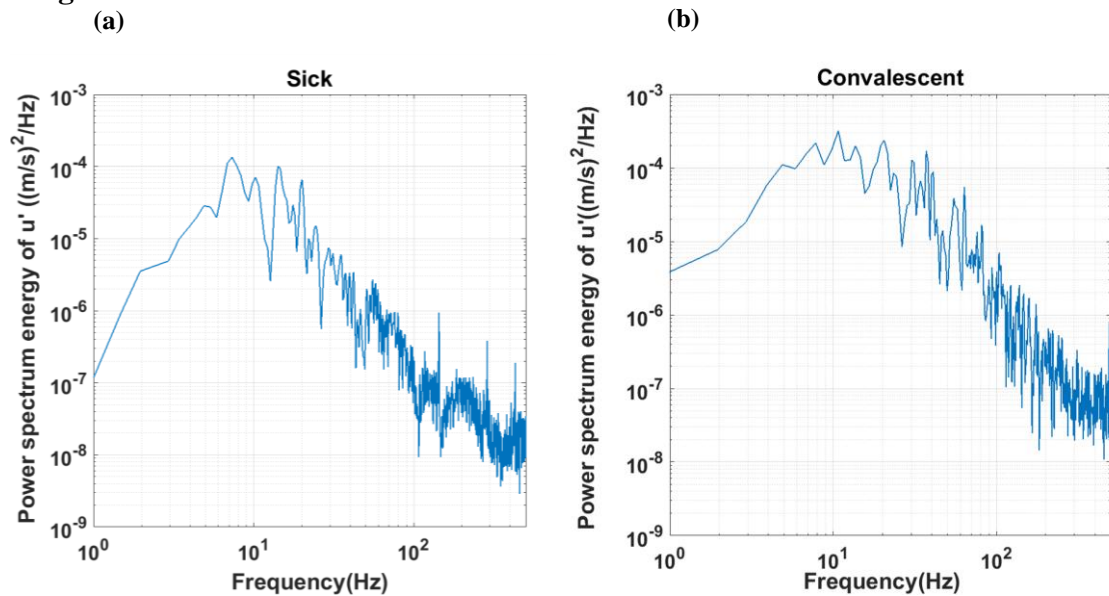
Figure 41 Power spectral density of the first sick and convalescent cough for participant 952

For this reason, the power spectral energy for all coughs of participant 952 was plotted in Fig. 43 to compare and extract any trend for these coughs.
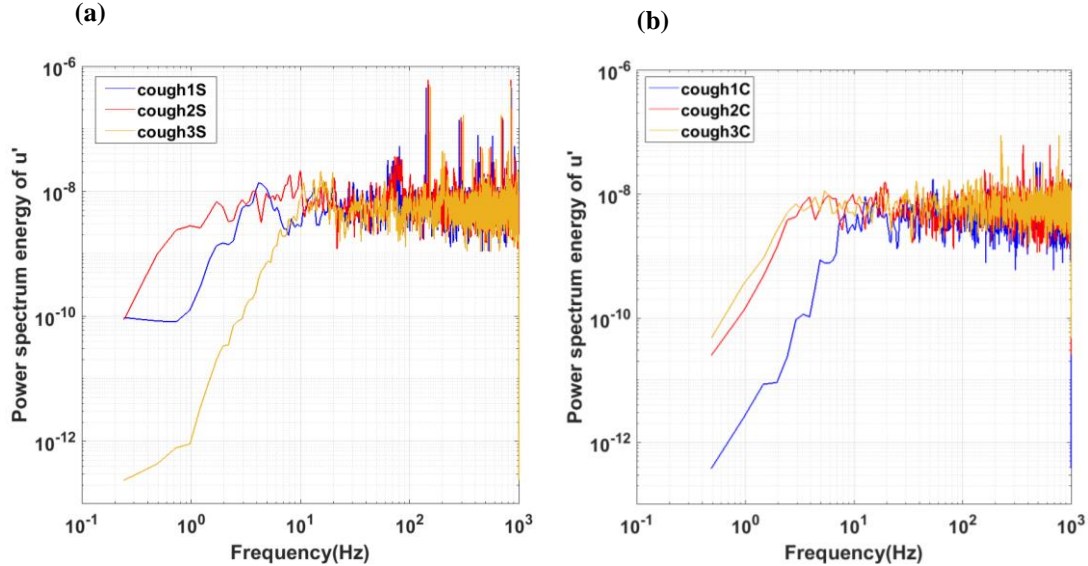
Figure 42 Power spectral density of no flow period for all coughs (a) sick and (b) convalescent cases

To quantify the noise level in the power spectral density (PSD) of all coughs for both sick and convalescent cases, a PSD function of all coughs during no flow period is plotted for each sick and convalescent case of participant 952. From Fig. 42, it is seen that any signal $\leq 10^{-8}$ is purely noise, so the power spectrum should end with a lower limit of 10^{-8} $(m/s)^2/Hz$. Since no power spectra have any turbulent energy above the noise level at higher frequencies, the frequency that can be resolved in the spectrum will be half of the sampling rate, i.e. 500 Hz as presented in Fig. 43. The power spectral density information will be utilized later to compute the turbulence intensity. From Fig. 43, it is clear from this pictorial comparison of the power spectral density (PSD) for all 6 sick and convalescent coughs (participant 952), the behavior of power spectral for each cough is not similar due to different flow conditions of each single cough.
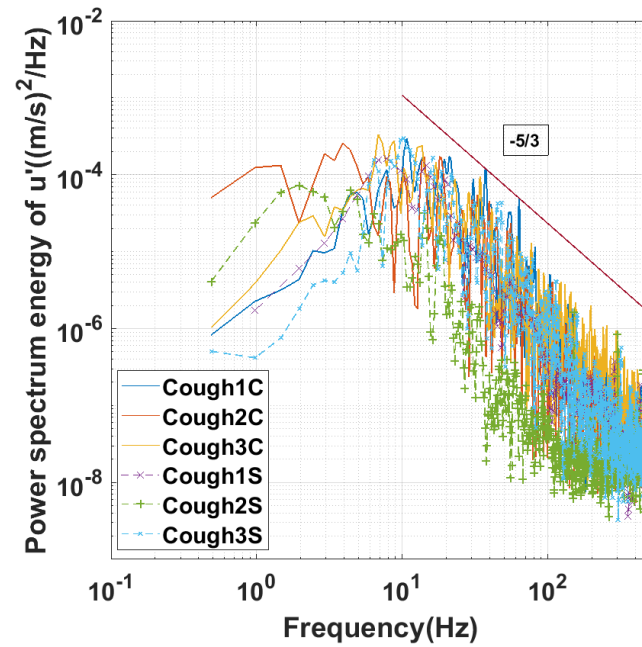
Figure 43 Power spectral density of all coughs from participant 952
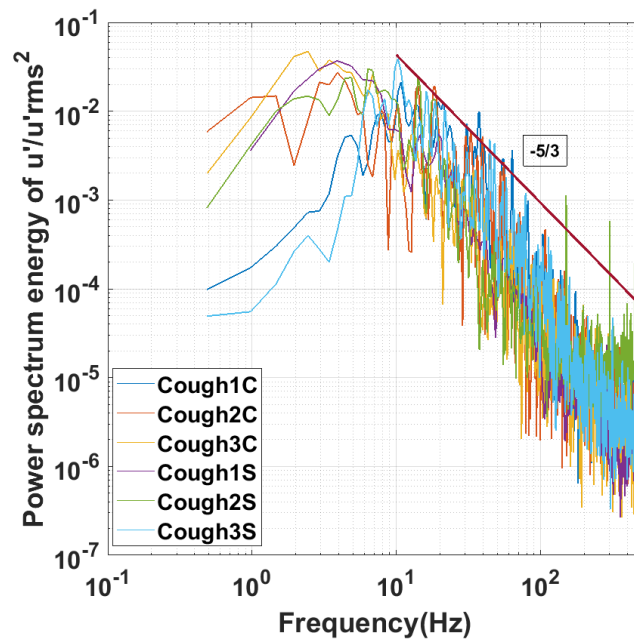
Figure 44 Power spectral density per u'$_{rms}^2$ of all coughs from participant 952

Fig.44 illustrates the normalized power spectrum energy of all convalescent and sick coughs. The curves are normalized by u'^2_{rms}, and this comparison shows that the results of all coughs decay according to -5/3 law. The areas under the curves are roughly equal to 0.5. The turbulence intensity of sick coughs (average I_u = 7 %) is slightly higher than convalescent coughs (average I_u = 6%) as present in table 7. Turbulent intensity is calculated by using eqn. 5.3 and by integrating the area under the spectrum curve by using the trapz function in Matlab given by eq. (5.4)

$$A=0.5* u'^2_{rms} \tag{5.4}$$

The results show a slight difference between sick coughs (the average of Iu from trapz function 11%) and convalescent coughs (the average of Iu from trapz function 6%) computed by two methods. The low frequency showed differences for all coughs compared to high frequency regions which are similar. These differences in low frequencies regions of all coughs may be imputed to large-scale variations due to the initial cough angle, the mouth opening area and movement by the subject during the cough, as well as any initial ambient air movement in the cough chamber.

Table 7 Turbulent fluctuation velocities and turbulent intensities of all coughs

	u'$_{rms}$	u'$_{rms}$(tpz)	$\bar{U}$	$\bar{U}nf$	I_u (mv)	I_u(tpz)
cough-1C	0.08	0.09	1.49	0.06	5.34	5.80
cough-2C	0.08	0.07	1.43	0.06	5.70	5.10
cough-3C	0.16	0.13	1.58	0.06	7.30	8.11
cough-1S	0.06	.08	0.47	0.05	11.63	16.17
cough-2S	0.03	.04	0.49	0.05	5.71	8.01
cough-3S	0.07	.09	1.14	0.05	6.20	8.19

Where:

u'$_{rms}$ is the fluctuation velocity of moving average values

u'$_{rms}$ (tpz) is the fluctuation velocity from integrated of the spectra curve

$\bar{U}$ is the mean of moving average velocity

I_u (mv) is turbulent intensity of moving average values

I_u (tpz) is turbulent intensity of integrated of the spectra curve

Since the measurements were done at a fixed point in space, an estimate of the autocorrelation function will be considered in this study. The autocorrelation represents the correlation between two variables at different points in time, t. The autocorrelation is always computed between the same variable; the velocity fluctuations u_i. The autocorrelation relates the velocity at time t to the same velocity at time $t + \Delta t$ as presented in equation (5.5).

$$R\ (\tau) = R\ (r\Delta t) = \frac{1}{\overline{u^2}} \frac{1}{N-r} \sum_{n=1}^{N-r} u_n u_{n+r} \qquad (5.5)$$

Where: R is the autocorrelation, r = 0, 1, 2, 3, …., N. (N is the maximum lag number).

Fig. 45 shows the time interval from 0 to 0.1, which presents the initial portion of the autocorrelation.
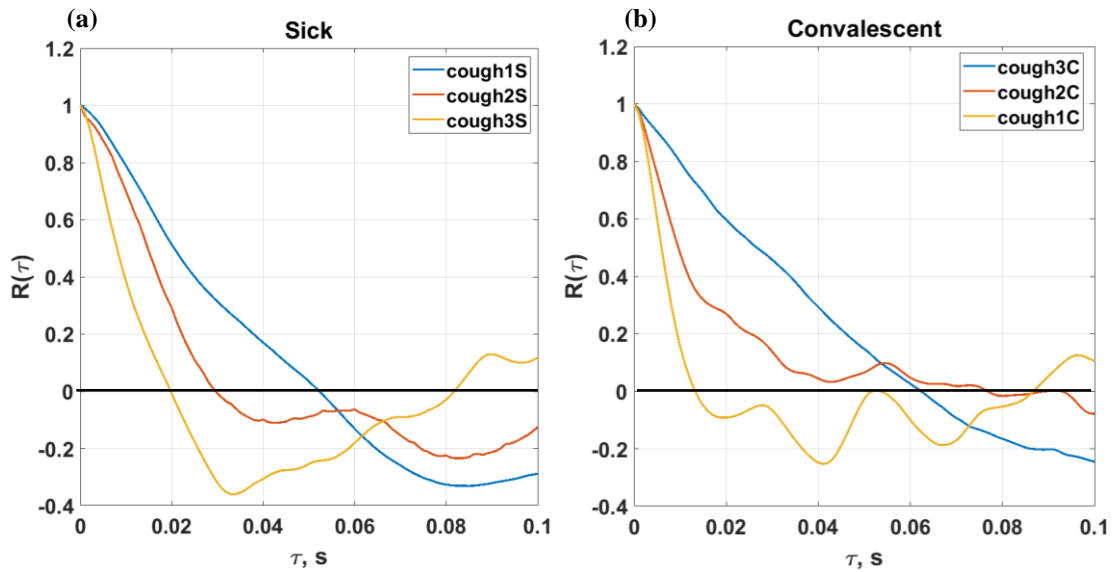
Figure 45 Autocorrelation for interval from 0 to 0.1s

Table 8 Results of computing the time scales and length scales of the flow

	cough1S	cough2S	cough3S	cough1C	cough2C	cough3C
Integral length scale, L (mm)	4.1	0.6	0.28	4.60	11.00	22.10
Integral time scale, T_E (s)	0.023	0.0022	0.0005	0.0062	0.0153	0.028

Figure 45 shows that the auto correlation reaches its first zero value roughly at 0.02, 0.03, 0.052 seconds, for the three sick coughs respectively, and 0.015, 0.078, 0.062 second for the three convalescent coughs. The area under each curve is the integral time scale of

residual turbulence, T_E. The integral time scale was computed by using the numerical approximation of the second derivative of the autocorrelation, given by equation 5.6 (Savory 2015):

$$T_E = \frac{\tau}{\sqrt{1-R(\tau)}} \qquad \text{as} \quad \tau \longrightarrow 0 \tag{5.6}$$

Where:

R is the autocorrelation, τ is the time lag, $\tau = r\,\Delta t$.

From Fig. 45, an estimation of the integral time scale can be done by integrating the area under the autocorrelation curve bounded by time equals zero and the time at which the first zero autocorrelation takes place. This time scale, which is calculated using eqn. 5.6, will be used to compute the length scales as described in eqns. 5.7 (Savory 2015),

$$L \approx \bar{U}\, T_E \tag{5.7}$$

Where:

L is the integral length scale, $\bar{U}$ is the local mean velocity ($\bar{U} = 0.5\text{x}\ (u_p - u_s)$), T_E is the integral time scale. The integral time scale was found using trapezoidal role. The results of time and length scales are listed above in Table 5.3.

5.4   Particle Image Velocimetry (PIV) Measurements

Particle image velocimetry (PIV) techniques were used for measuring the two-dimensional velocity fields in a vertical plane (see Fig. 16). The field of view was positioned within the FLUGIE chamber at 1 m downstream from the cough inlet chamber. The PIV measurements were conducted in this study by using a double pulsed Nd: YAG crystal laser of power 120 mJ per pulse to generate a laser sheet of 532 nm wavelength at 15 kHz with two CCD cameras (see Fig. 10). In this section, results from Western Cold and Flu (WeCoF) aerosol studies, which were conducted by PIV technique, will also be presented.

5.4.1   Results of summer 2013 WeCoF Aerosol Study

The far field aerodynamics of human coughs, which was produced by the healthy subjects, had been studied in FLUGIE chamber using the prior mentioned Nd: YAG laser system with one 4 MP CCD camera. A cohort of 12 healthy individuals had been carried out to quantify the strengths of their coughs 1 m away from the mouth (Savory et al. 2014). The velocity fields associated with 36 coughs from 12 healthy young adults (9 males and 3 females ages 20 to 32) were quantified by the PIV (Savory et al. 2014) measurement techniques. The time histories of spatially averaged velocity <U> values for all 29 coughs of the participants are presented in the figure 46. Seven coughs out of 36, have a peak cough velocity less than 0.1 m/s, and are excluded from this comparison. It is seen that, in all cases, the cough velocity through the field of view, (174.8 mm x 233.1 mm), is clearly defined with initial rapid increase of cough velocity followed by a slower decay. The study showed that, the limitation on the PIV window size and variable physical traits of the study participants, had considerable variation in location and

strength of each cough, with some coughs missing most of the imaged field of view entirely (Savory et al. 2014).
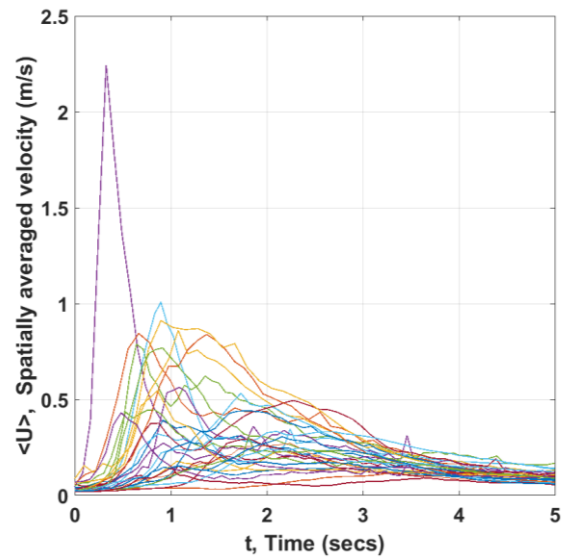
Figure 46 Time histories of all 29 coughs from 9 males and 3 females (Summer 2013)
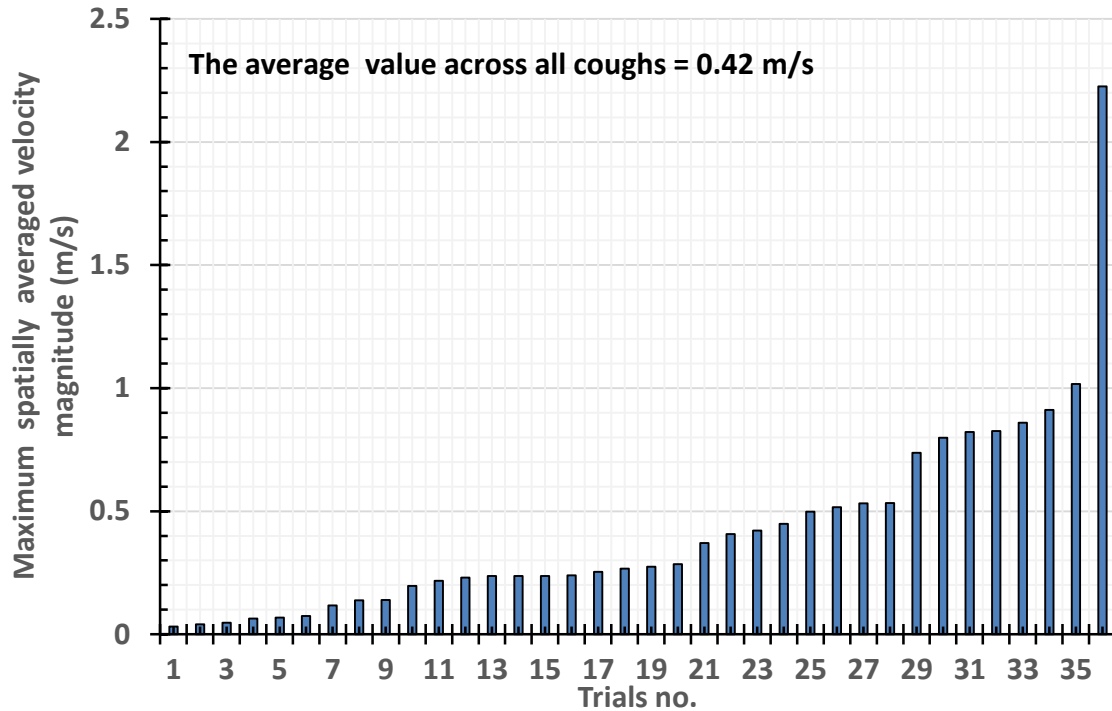
Figure 47 The peak, spatially-averaged velocity magnitudes across all 36 coughs

The variability of maximum spatially averaged velocity magnitudes across all 36 trials are presented here in Fig.47. The average value of all 36 coughs at 1m downstream is 0.42 m/s, which reflects significant air motion of the cough at that location from the source. To make an observation for the general trend of all coughs, the time histories of all 29 coughs are normalized as described in section 3.5. The normalized cough velocities of all coughs are plotted in Fig.48 (a) against dimensionless time (τ). To describe the general characteristics of all measured cough velocities, a third order Gaussian curve fitting analysis was performed in MATLAB to obtain the regression trend of these coughs up to (τ) = 1.6 as shown in Fig. 48(b). The coefficient of determination was $R^2 =$ 78%.
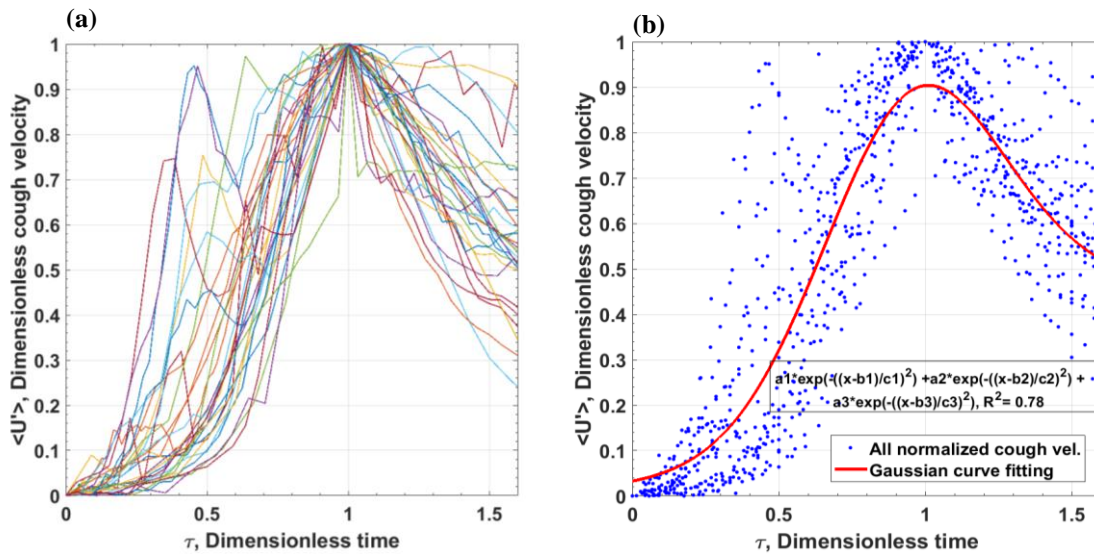
Figure 48 Normalized cough velocities (a) and the Gaussian curve fitting (b) for all 29 coughs (Summer 2013)

5.4.2   Results of winter 2014 WeCoF Aerosol Study

In the flu season of winter 2014, a total of five participants agreed to participate in WeCoF aerosol study, and a similar set up of FLUGIE of WeCoF 2013 was used. Two out of five participants did not return for convalescent visits, which produced 24 coughs in total, 3 coughs from each participant from a single visit. A typical time history of 7 sick coughs, which have a peak velocity greater than 0.1 m/s, is presented here in Fig. 49 (a) and for 7 convalescent coughs in Fig 49 (b). The mean of the peak sick coughs is 0.33 m/s, while 0.22 m/s is the mean of peak convalescent coughs.
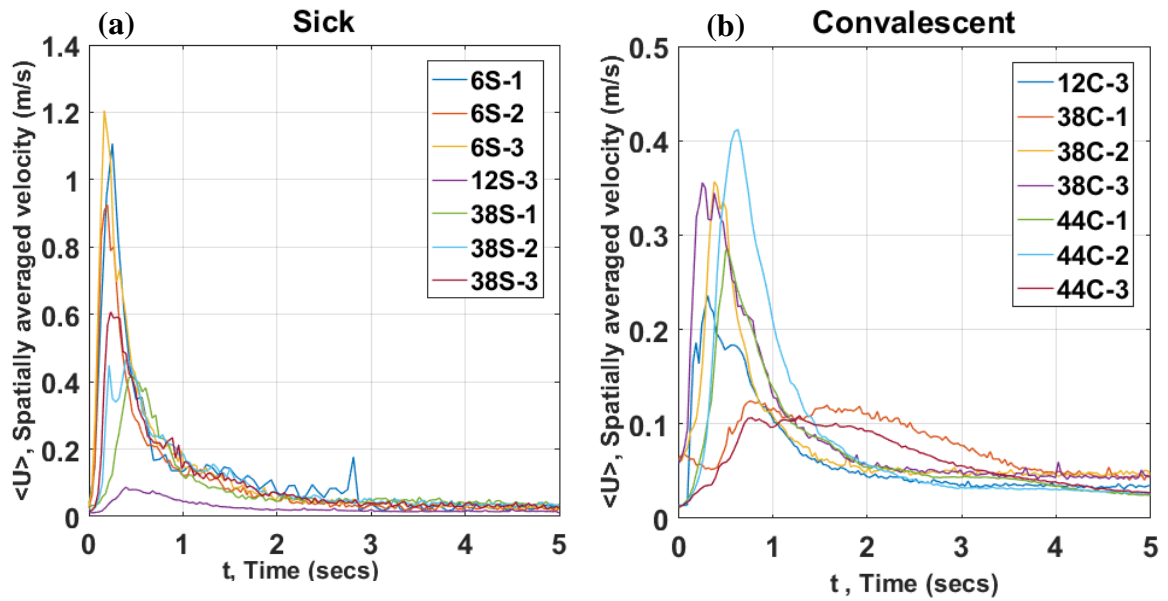
Figure 49 The time history of 7 sick coughs (a) and 7 convalescent coughs (b),

(Winter 2014)

The variability of the spatially averaged peak velocity in Fig 50 ranged between 0.02 to 1.2 m/s. The average value across all 24 coughs is 0.34 m/s. The time histories of all these 14 coughs are shown in Fig. 51. To perform the regression analysis for all cough flows, normalization of all 14 coughs is done using MATLAB as described in section 3.5 (see Fig. 52 (a)).
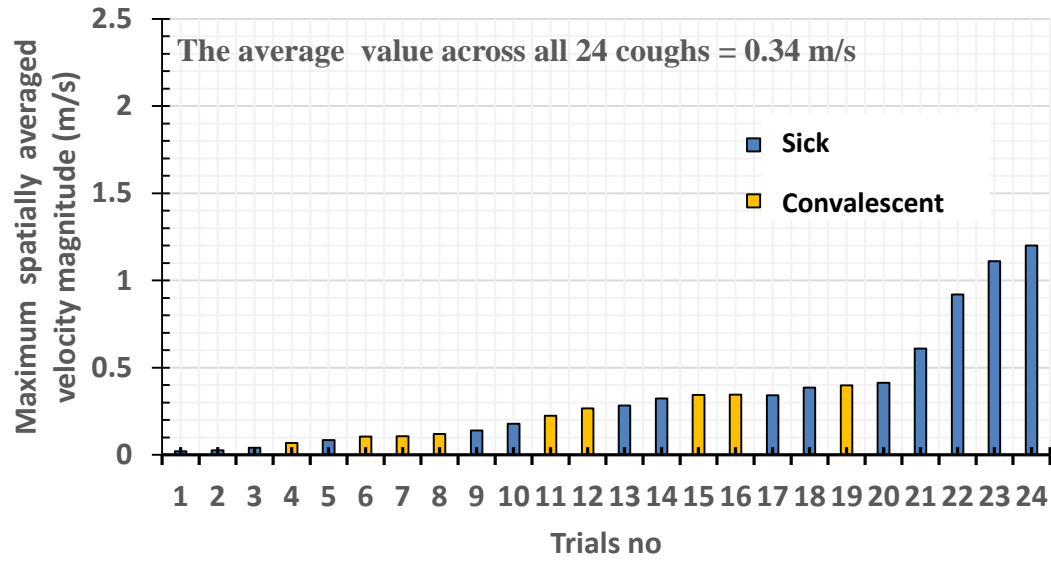
Figure 50 The peak, spatially-averaged velocity magnitudes across all coughs (Winter 2014)
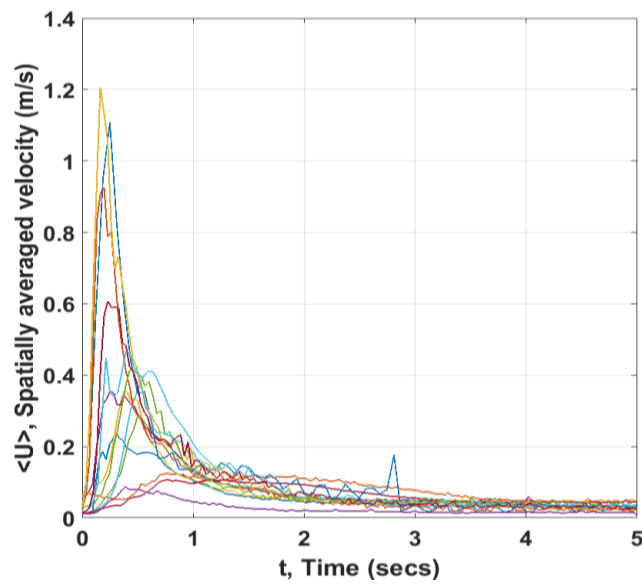
Figure 51 The time history of all coughs (Winter 2014)
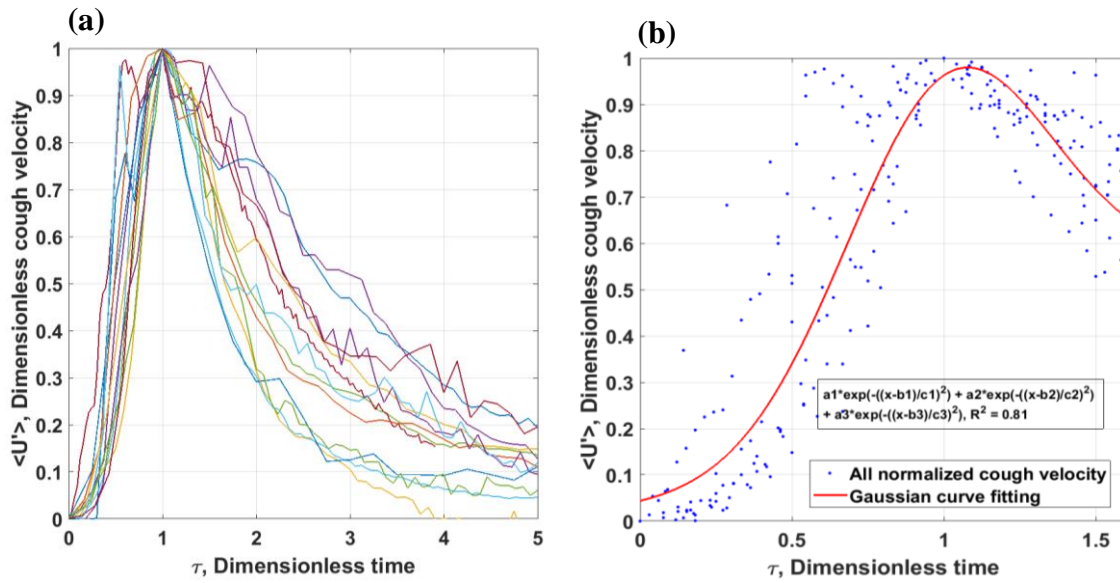
Figure 52 Normalized of all 14 coughs velocity (a) and Gaussian curve fitting (b)

The general trend for all normalizing coughs was generated by fitting a third order Gaussian curve with coefficient of determination of $R^2 = 81\%$ as illustrated in Fig. 52 (b). An instantaneous vector field of the third cough of participant 38 is presented in Fig. 53. The peak period of the cough velocity took about 2 seconds to disperse. The green vectors which were generated and validated by Insight3G processing represent the cough flow field and yellow vectors represent the interpolated vectors. From Fig. 53, it can be observed that, though the used camera captures majority of the flow field, a significate part of the cough was missed from the field of view of the used camera. This can be considered as a major limitation for 174.8 x 233.1 mm field of view of the used camera.
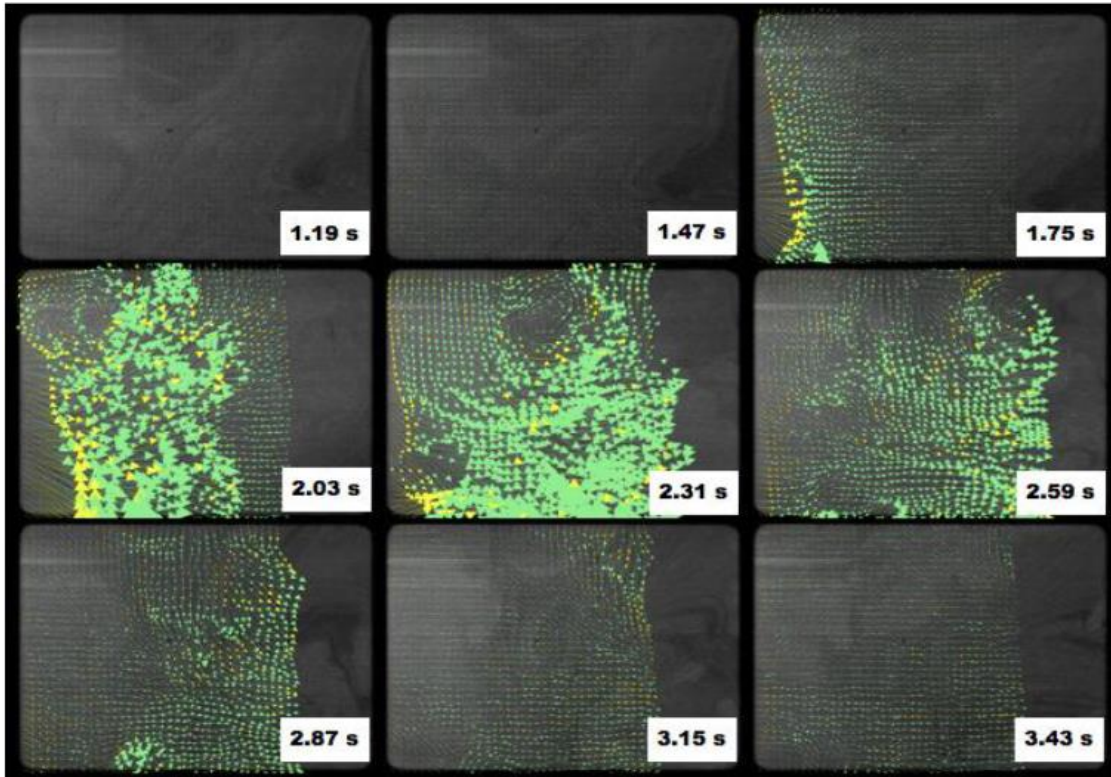
Figure 53 Time history of an instantaneous vector field through field of view

obtained during participant 38 sick's cough (no. 1),

(Lin et al. 2014 (with author's premission))

5.4.3   Results of winter 2017 WeCoF Aerosol Study

To expand our field of view, two cameras were used. This yielded 140.73×336.3 mm

field of view, which is considered as an overall good extent of space to cover the cough

flow field at 1 m downstream from the cough inlet of the FLUGIE chamber. The field of

view has been increased in this study, compared with the previous studies, to view a

wider range of flow dynamics of the coughs. In winter season of 2017, the recruitment

procedure took place in the period between January 14th and March 30th. Nine students

had agreed to participate in this study and all of them participated in the experimental

measurements twice, first when they were sick and after they recuperated. Although the

PIV system was calibrated before the recruitment procedure for PIV measurements, the data captured by the PIV system were affected by unexpected change of a set frequency. Therefore, all the data from the winter 2017 PIV study are not considered for measurement analysis in this thesis.

5.4.4   Results of summer 2017 WeCoF Aerosol Study

In summer 2017 season, according to the recommendations from the previous WeCoF studies, two cameras were used to generate field of view of cough velocity at 1 m downstream of the cough source to let each camera capture majority or minority of the cough depending on the initial boundary conditions of the cough. For example, Fig. 54 shows the time history of spatially averaged velocity of a trial cough during calibration process. The lower camera captured majority of the cough flow as shown in Fig. 54 (a), while some of the cough was captured by the upper camera as in (b). Matlab script was written (Appendix F- (b)) to generate one field of view from two cameras as shown in Fig 54, which presents the time history of cough trial during the calibration steps.
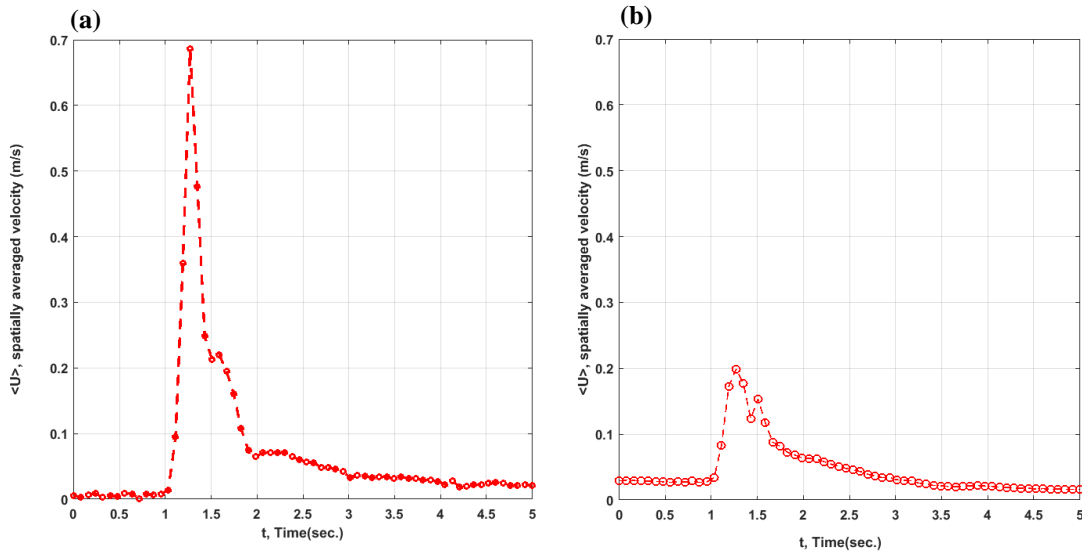
Figure 54 Time history of cough velocity captured (a) lower and (b) upper camera.
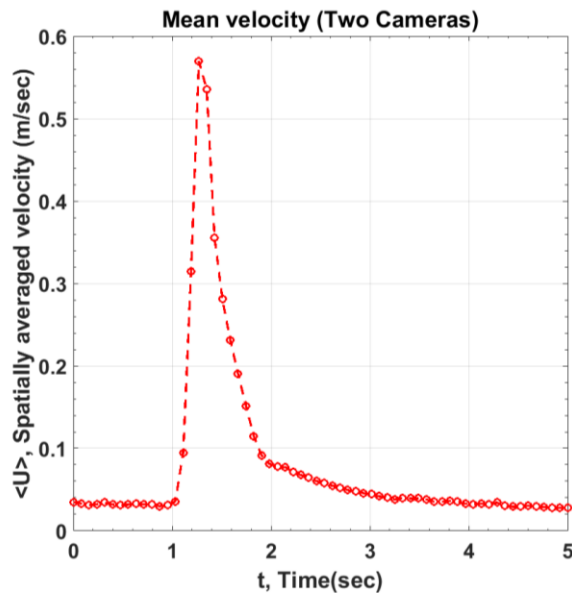
Figure 55 Time history of cough velocity within the generated field of view

In this season, we aimed to recruit a cohort of 25 healthy individuals. Eleven participants conducted the WeCoF measurements before the lower camera started malfunctioning. The results from 3 participants showed good quality coughs from both the used cameras and those results were used in this analysis. To analyze the healthy cough flow from the

present measurements, a typical cough no. 2 of participant 221, with a peak spatial averaged velocity profile around 0.8 m/s, was selected. Figure 56 shows the time history of spatially averaged velocity for a whole field of view captured by two cameras. It is seen that the cough peak period lasted for almost 2 seconds (0.5-2.5 secs) with peak velocity of 0.89 m/s at 0.73 sec. To investigate the time history of the cough velocity in the shared area between the two cameras, one point was selected to present the time history in Y- direction at vector 37. Figure 57 presents the time history at the captured frame number 11 and point (37, 99) within the vector field of both cameras. It is clear that the time history of the velocity magnitude at the shared area shows good agreement.
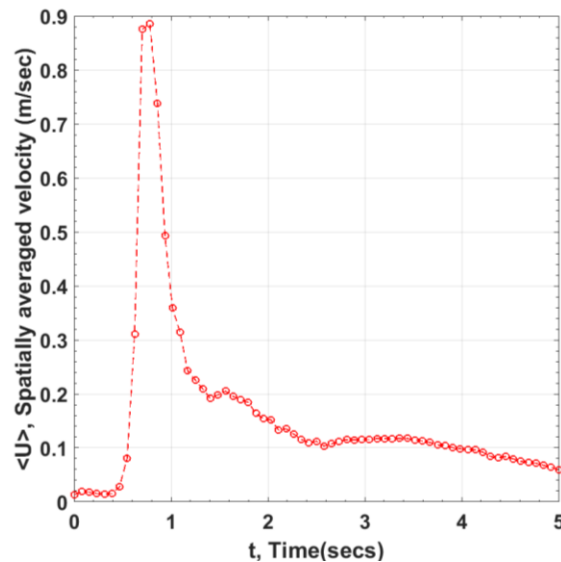
Figure 56 Time history of a whole field of view for cough no. 2, participant -221
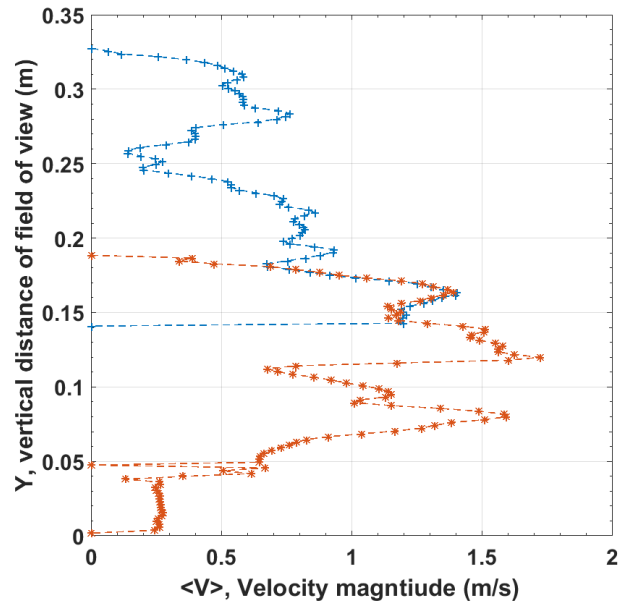
Figure 57 The time history of the instantaneous velocity to check the shared area
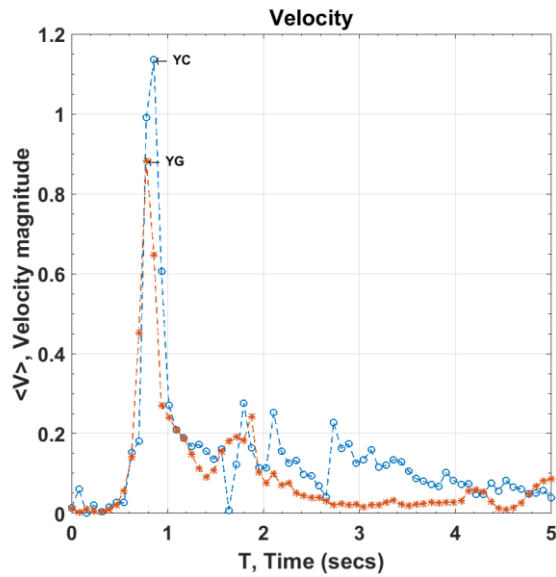
Figure 58 Time history of cough velocity at two points C and G participant-221, cough no.2

Fig. 58 illustrates the time history of the velocity magnitude at the first point (G) at HWA position (0.0847 m, 0.0664 m), and the second point (C) at the centreline (0.0847 m,

0.2864 m) as described in Fig. 16. The time history of cough velocity at HWA point (Y_G) provides an instantaneous peak velocity of 0.83 m/s at 0.8 sec with a peak period of almost 2 seconds. The time history at centreline point (Y_C) shows a high peak with higher value of 1.1 m/s at 0.85 s in the cough peak period. In order to make observation for the whole flow field captured by both cameras, a sequence of velocity contours is shown in Fig. 59. The lower right corner of field of view, which shows spots with high velocities, is effected by camera malfunction. Moreover, from the successive images of velocity contours, it can be inferred that the majority of cough flow falls in the region field between the two points G and C which is equal to 0.22 m.
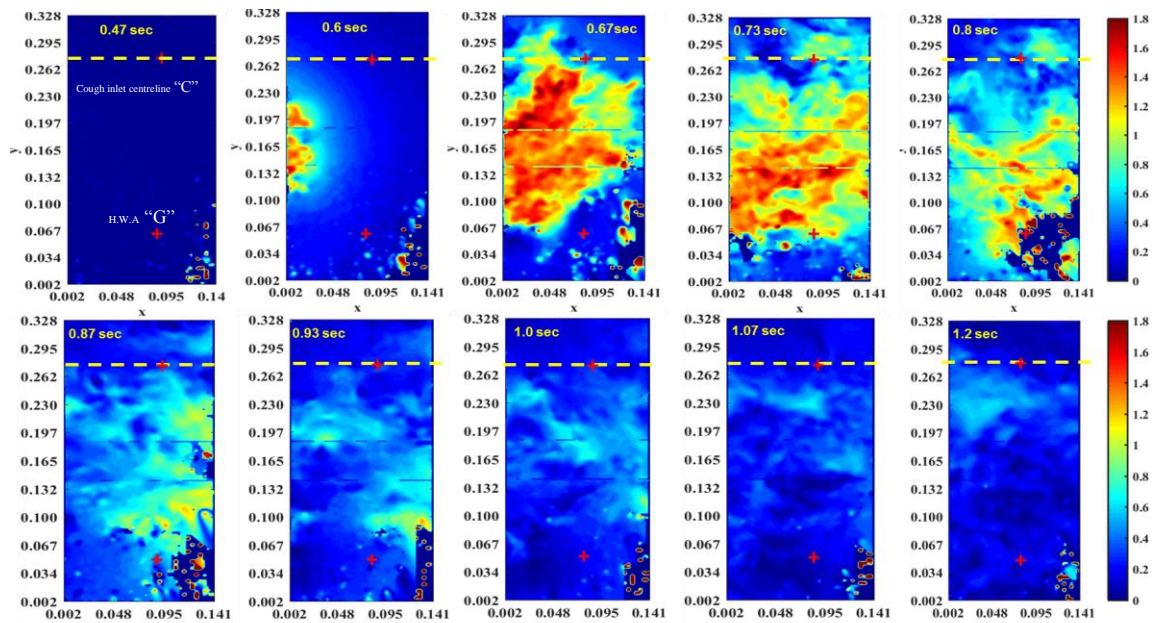
Figure 59 Time history of instantaneous velocity contour field through field of view obtained from healthy participant-221, cough (no. 2)

The variability of the maximum spatially averaged velocity of the 6 coughs from this study ranges between 0.23 to 1.02 m/s as shown in Fig. 60. The average value across all 6 good coughs is 0.6 m/s. The time history of spatially averaged cough velocity for all 6

good coughs is presented in Fig. 61. It is clearly seen that, in all suitably defined 6 coughs, an initial rapid increase of cough velocities is observed as expected, followed by a gradual decay. There is, however, a significant variation of spatially averaged velocity among coughs from the same participant, and also between participants.

To investigate this variation, regression analysis was performed by normalizing all velocities as shown in Fig. 62 (a). The curve fitting by using Gaussian third order function was performed, with the coefficient of determination calculated as $R^2 = 74\%$ (illustrated in Figs 62 (b).
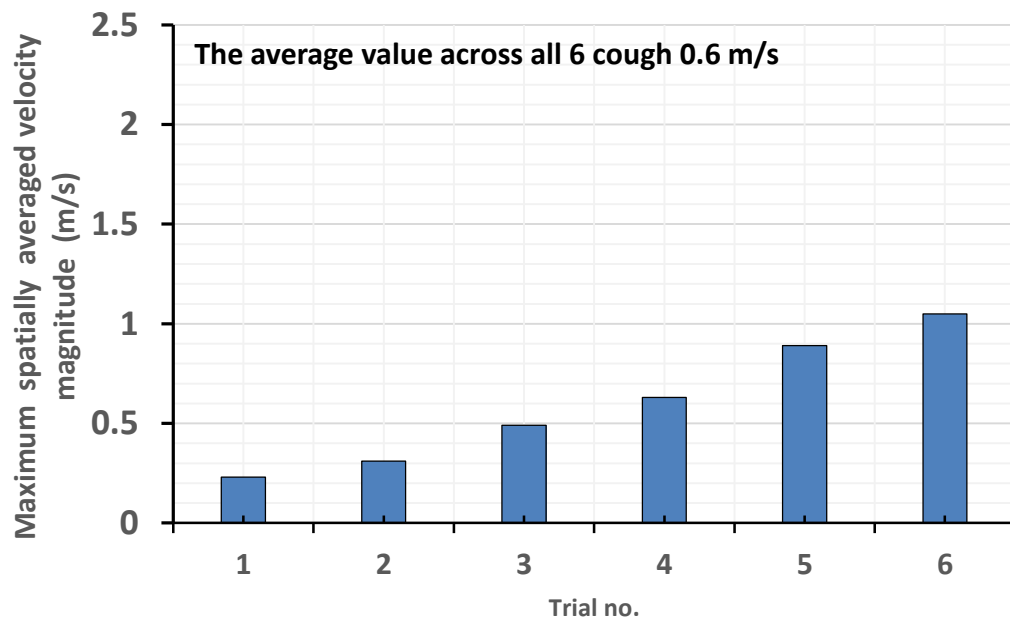
Figure 60 The peak, spatially-averaged velocity magnitudes across all 6 coughs

(Summer 2017)
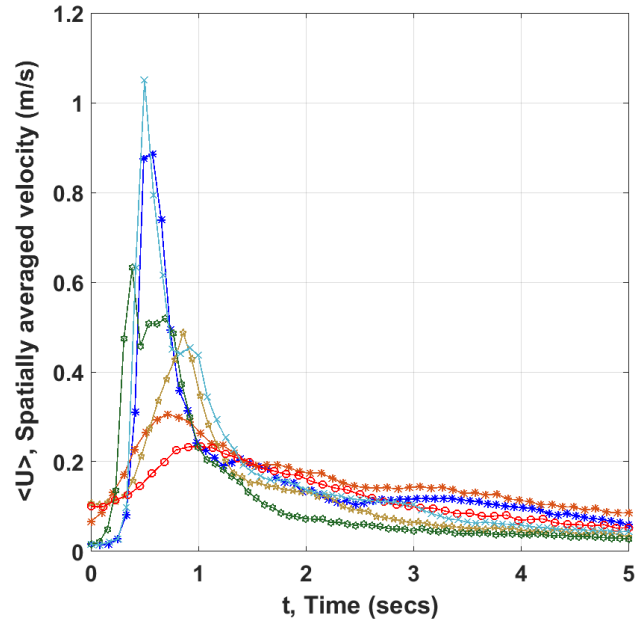
Figure 61 Time history of all 6 coughs from participants 221, 880, and 950

(Summer 2017)
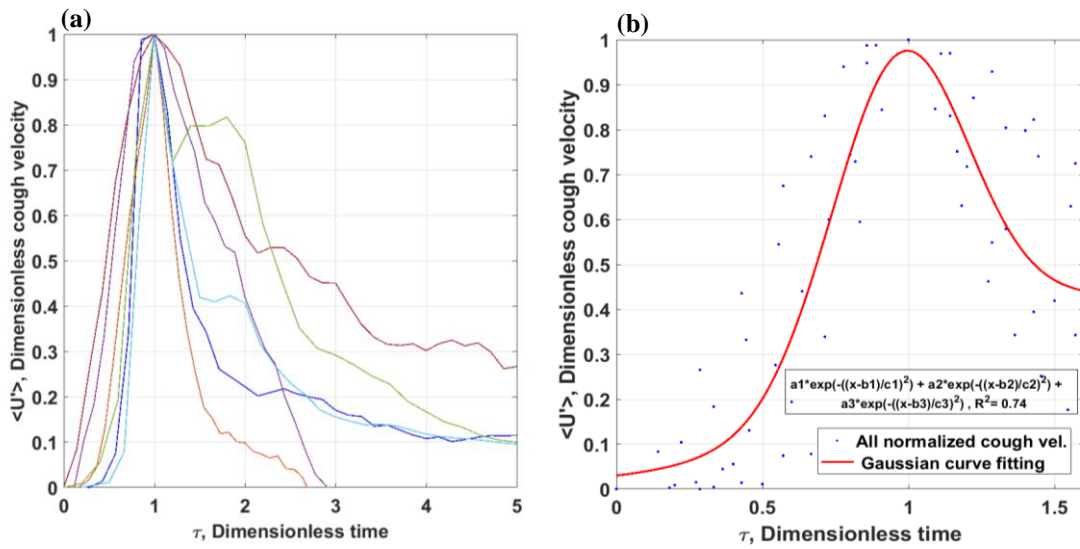
Figure 62 Normalized of all coughs velocity (a) and Gaussian curve fitting (b)

5.4.5 The PIV results of all WeCoF studies

In order to make a comprehensive analysis for all the data, which were measured by used PIV technique, the time history of all 49 coughs (Fig. 63) obtained from sick, convalescent and healthy participants, are compared in this analysis. Around three quarters of the coughs have maximum spatially averaged velocities less than 0.50 m/s and the highest peak velocity is at 2.25 m/s. To make total regression analysis for all data, all cough velocities were normalized as described in section 3.5 and presented in Fig 64 (a). The curve fitting by using a Gaussian, third order equation was performed with the help of MATLAB software, and the coefficient of determination was found to be $R^2 = 74.1\%$ for all coughs (Fig. 64 (b)).
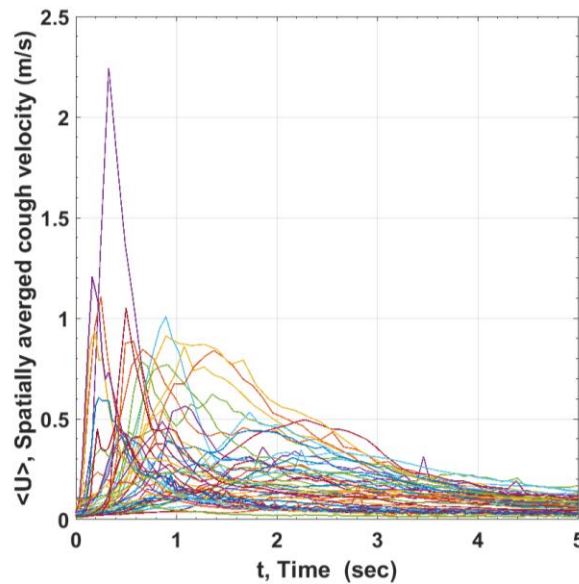
Figure 63 The time history of all 49 coughs measured by PIV during WeCoF studies
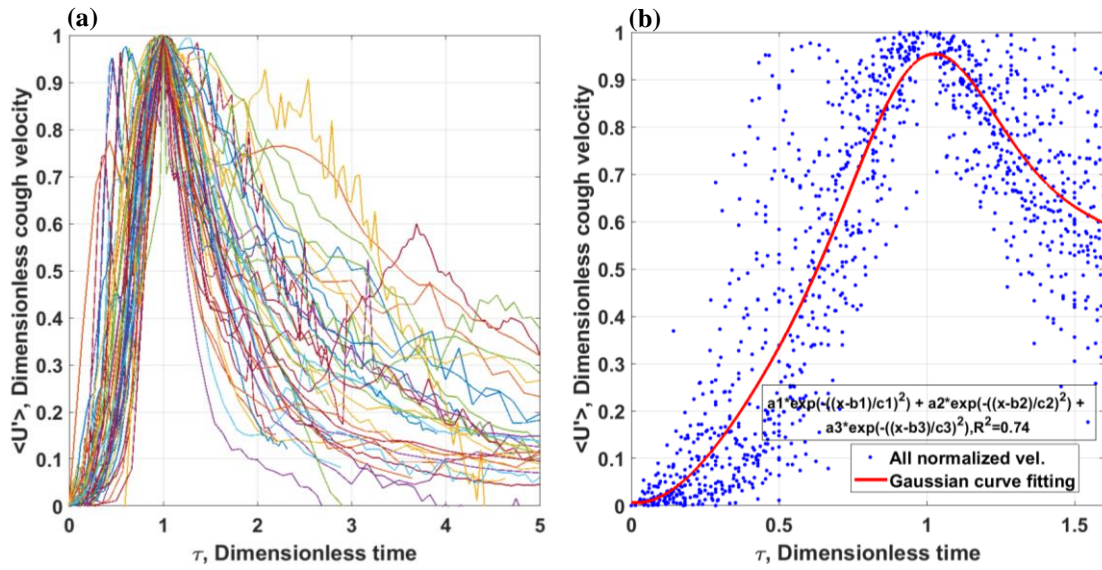
Figure 64 Normalized of all coughs velocity (a) and Gaussian curve fitting (b) for all 49 coughs measured by PIV during WeCoF studies.

Chapter 6

6 Conclusion and Recommendations for Future Work

This study is considered as a part of the Western cold and flu aerosol (WeCoF) studies, which started back in summer 2013. The aim of the present study is to provide experimental statistics of coughs from sick, convalescent, and presumed healthy individuals to identify the factors responsible for the transmission of airborne disease at a distance 1 m away from the source of the cough. This distance has been considered the safe distance between healthy individuals and sick patients. In this chapter the results from aerosol sampling, mid turbinate swab (MTS) analysis, hot wire anemometer (HWA) and particle velocimetry (PIV) measurements are concluded respectively. Moreover, recommendations for future work are provided.

6.1 Conclusion

6.1.1 Virological analysis and MTS Results

In the present study, the MTS results showed that 4 out of 9 participants had an illness. Good results were yielded, considering the limited number of flu cases. The four etiologic agents were corona virus (CoV) NL63, (CoV) OC43, Influenza A (H3N2) and Respiratory syncytial virus (RSV). The PCR data of Influenza A (H3N2) case, which were extracted from both PTFE membrane filters at 0.50 m and 1.00 m, were negative in all cases. Moreover, the PCR data analysis confirmed that an H3N2 case produced a super-positive MTS result. In fact, the residue of TiO_2 particles on the FLUGIE interior surfaces, which were used as tracking particles of the used PIV system, might have reduced the ability to obtain Virological samples by surface sampling (Lin et al. 2014). As mentioned in section 4.2, each PTFE filter was connected to constant air flow sampling pump, which drew air at a flow rate of 4000 +/- 40 mL/min. The sampled air volume was equivalent to 0.07% of the FLUGIE volume for each sampling pump. Based on the preliminary results from the LES model (Bi et al 2017), droplets size in order of 1.00 μm will remain suspended up to 3 seconds at distance of 1.00 m downstream of the cough source, while the larger droplet sizes will have a rapid drop in their speed in the

near region (less than 0.5 m). These results, as expected from the literature, confirmed that the largest droplet could be collected at a distance lower than the cough centreline in the near field region (X < 0.50 m), whereas the fine droplets could be collected around the cough centreline in far field region (X >0.50 m).

6.1.2   HWA measurements

In winter 2014 study, a single-wire HWA probe was placed outside the PIV field of view at greater than one metre distance from the cougher (Lin et al. 2014). The probe, which was used in this study, was not calibrated, and it was used as an additional check that whether a transient flow was indeed produced in the PIV imaged region. The voltage output from this probe showed an intermittent variation of the cough airflow. The study concluded that for coughs produced during illness, the peak of the signal was prominent and lasted approximately for five seconds. For coughs after convalescence, the peak signal was more gradual with a lesser peak voltage and a longer duration approaching ten seconds.

In the present study, a HWA sensor, which is the basic tool for turbulence measurements, was used to study the dynamics of the cough flow and characterize the turbulence properties of cough with 10% uncertainty. Measurements were taken both at the centreline location of 1.00 m downstream from the cough source and also at 0.22 m lower than the centreline. 27 coughs are analyzed from the sick participants and 24 coughs from their convalescent visits. In general, the sick coughs showed a weaker cough velocity when compared to convalescent coughs, but with higher turbulence intensity. The average value of maximum moving average velocity across all coughs is equal to 0.36 m/s for sick participants and 0.5 m/s when they are convalescent. The peak air velocities produced by the sick participants took a longer time to decay when compared with convalescent coughs. The ensemble average of peak mean velocity across all 51 trials is equal to 0.43 m/s. The turbulence intensity for participants with acute respiratory infections ranged between 3 to 9 %, while it ranged between 3 to 6 % on their convalescent visits. A typical sample out of the lot was selected to compare the differences between sick and convalescent coughs. As a typical example, participant 952 showed high cough velocity magnitudes when the participant recuperated, when

compared to the sick condition. The turbulence intensity obtained was slightly higher in sick case with an average of 7.85 % compared to 6.30 % in the convalescent case. The integral length scales estimated from the residual turbulence of 6 coughs were 8.4 mm. In order to quantify the distribution of turbulent energy, the power spectral density was presented for 6 coughs. The comparison between the spectra for all coughs showed a peak value in the range of 5 – 10 Hz; and a universal slope of -5/3 (Kolmogorov decay law) was also achieved.

6.1.3   PIV measurements

A modified setup of two cameras was used in the present study to extend the field of view and cover a large part of the cough at 1 m downstream the source. An unanticipated change in the set frequency of the used PIV system affected all the data captured during winter 2017 flu season. The results from summer 2017 season, where we aimed to recruit 25 healthy participants before the lower camera started malfunctioning interrupting the measurements, provided an overall 6 good quality coughs from 3 healthy participants. The ensemble average of the spatially peak averaged velocities across all these 6 coughs were 0.58 m/s. The two-camera set up was able to capture most of the full-scale flow fields of the cough as evident from the vectors and velocity contours. The results from winter 2014 provided us with 24 cough samples from 5 sick participants during their first and return visit, excluding 2 participants who did not return. The ensemble average of the spatially peak average velocity was equal to 0.29 m/s, with the sick coughs having an average of 0.33 m/s while for the 9 convalescent coughs it was 0.22 m/s. The summer 2013 study showed an ensemble average of 0.51 m/s from 36 coughs of 12 healthy individuals. These results showed a marked variation of air motion which were caused by coughs from sick, convalescent, and healthy subjects at 1.00 m downstream of the cough inlet.

To conclude, this study mainly focused on characterizing the flow dynamics of a human cough in the far field region of (1.00 m downstream). Cough velocities were measured when the subjects were sick, convalescent, and healthy. This is considered as the main key contribution from this study. These findings will be used to validate a LES numerical model which is presently under development and showing promising results (Bi et al

2017). In addition to this, the LES model will also be used to investigate the spatial distribution of expiratory aerosols, penetration of viral droplets to the ambient environment, and how far and for how long will they be suspended in the air by the cough jet flow. The numerical study is expected to cover the technical aspects that are missed in the experimental work.

Compared to the previous WeCoF studies, when non-calibrated probe was used in out the PIV view field, a calibrated HWA probe was used in the present study to measure the flow and characterize the turbulence at specific point. Moreover, two cameras were used to cover a wider field of view (140.73 mm x 336.3 mm) compared with the previous PIV studies. Although a limited number of participants agreed to participate in this study, strong evidence suggests that there is no single unique characteristic shape for cough velocity profile, but a general trend was noticed and it could be used to help validate the CFD models.

Within the context of the limited no of subjects studied (42 sick coughs, 33 convalescent coughs and 42 healthy coughs), a tentative conclusion about the statistically different characteristics of cough aerodynamics (i.e. cough's velocity, turbulence intensity, and length scale) from the sick, convalescent and healthy participants, were obtained during this study. Significant air motion was noticed at 1.00 m downstream of the source with slight difference among three categories. It is anticipated that as the database is enlarged it will likely be possible to make greater definitive statements concerning differences among coughs from sick, convalescent and healthy subjects, as well as the capability of viral droplets to penetrate to $x = 1$ m

6.2   Recommendations and Future Work

• For a statistically significant cohort, more participants are required, to come up with final recommendations for thesis objectives, to conclude important points for implementing precaution of any measures in the future to mitigate the spread of any disease during epidemics.

• Measurements should be taken with more sick participants to define an envelope of cough profiles, 1 m downstream, and there is a need to announce about the study early in on-campus multimedia and social media in parallel with recruiting from student health service at the University of Western Ontario (SHSW).

• A separate group of measurements with a limited number of trials should be taken in the near field region to compare the profiles with literature and the numerical model.

• Periodic and short calibration process should be conducted for PIV system and HWA probe to confirm the accuracy of the measurement from the used tools.

• Further study is required to quantify the viral content of the aerosols produced during the three coughs of each participant within the FLUGIE chamber by relocating the PTFE positions and using greater sampled air volume devices.

All of these points are important for implementing precaution any measures in the future for mitigation during epidemics. Moreover, the experimental data and analysis, which will continue through to the end of 2018, will be linked to validate the CFD model based on Large Eddy Simulation (LES). This numerical work is expected to aid the challenges of the experimental work in determining the cough aerodynamics and droplet transport in a realistic three-dimensional domain.

References

Afshari, A., Azadi, S., Ebeling, T., Badeau, A., Goldsmith, W. T., Weber, K. C., & Frazer, D. G. (2002). " Evaluation of cough using Digital Particle Image velocimetry". In Engineering in Medicine and Biology, 2002. *24th Annual Conference and the Annual Fall Meeting of the Biomedical Engineering Society EMBS/BMES Conference,* 2002. Proceedings of the Second Joint (Vol. 2, pp. 975-976). IEEE.

Aliabadi, A. A., Rogak, S. N., Bartlett, K. H., & Green, S. I. (2011). " Preventing airborne disease transmission: review of methods for ventilation design in health care facilities*". Advances in preventive medicine*, 2011.

Bohm, G., & Zech, G. (2010)." Introduction to statistics and data analysis for physicists*"* (Vol. 1). *DESY*.

Booth, T. F., Kournikakis, B., Bastien, N., Ho, J., Kobasa, D., Stadnyk, L., ... & Mederski, B. (2005). " Detection of airborne severe acute respiratory syndrome (SARS) coronavirus and environmental contamination in SARS outbreak units*". The Journal of infectious diseases*, 191(9), 1472-1477.

Bourouiba, L., Dehandschoewercker, E., & Bush, J. W. (2014). *"* Violent expiratory events: on coughing and sneezing*". Journal of Fluid Mechanics*, 745, 537-563.

Bruun, H. H. (1995). " Hot wire anemometry : Principles and signal analysis*". Oxford ; Oxford Unversity Press.*

Kumar, A., Zarychanski, R., Pinto, R., Cook, D. J., Marshall, J., Lacroix, J., ... & Turgeon, A. F. (2009). "Critically ill patients with 2009 influenza A (H1N1) infection in Canada*". Jama, 302(17)*, 1872-1879.

Cao, X., Liu, J., & Jiang, N. (2014)." An overview of the applications of Particle Image

Velocimetry for indoor airflow field measurement*". In Proceedings of the 8th *International Symposium on Heating, Ventilation and Air Conditioning* (pp. 223-231). *Springer*, Berlin, Heidelberg.

Cao, X., Liu, J., Jiang, N., & Chen, Q. (2014). " Particle image velocimetry measurement of indoor airflow field: A review of the technologies and applications*". Energy and Buildings*, 69, 367-380

Chao, C. Y. H., Wan, M. P., Morawska, L., Johnson, G. R., Ristovski, Z. D., Hargreaves, Mengersen, M., Corbett,S., Li,Y., Xie, X. & Katoshevski, D. (2009). " Characteriz---ation of expiration air jets and droplet size distributions immediately at the mouth opening*". Journal of Aerosol Science*, 40(2), 122-133.

Cowen, E. A., & Monismith, S. G. (1997). "A hybrid digital particle tracking velocimetry technique". *Experiments in fluids*, 22(3), 199-211.

Deller, B., Stolarsky,G.,Tietjen,L., and Lewison,D.(2008). " Preventing the Transmission of Avian or Pandemic Influenza in Health Care Facilities with Limited Resources." 1st Edtion. Baltimore,Maryland,USA: *Jhpiego*.

Duguid, J. P. (1946). " The size and the duration of air-carriage of respiratory droplets and droplet-nuclei". *Epidemiology & Infection*, 44(6), 471-479.

Elatar, A. (2013). " Channel Flow Behaviour During Mixed Convection At Low." *Electronic Ph.D. Thesis*, Electronic Ph.D. Thesis, School of Graduate and Postdoctoral Studies, University of Western Ontario, London, Ontario

Savory, E.(2015). " Mechanism and Theory of Turbulent Flow." *(MME9715) Grad course notes*, University of Wsernt Ontario - London, Ontario.

Bozzuto, G., Ruggieri, P., & Molinari, A. (2010). " Molecular aspects of tumor cell migration and invasion. Annali dell'Istituto superiore di sanitÃ, 46(1), 66-80.

Government of Canada, Public Health Agency of Canada. (2006). " Canadian Pandemic Influenza Preparedness: Planning Guidance for the Health Sector - Influenza - Public Health Agency of Canada." *http://www.phac-aspc.gc.ca/cpip-pclcpi/report-rapport-2015-eng.php#a1*.

Gupta, J. K., Lin, C. H., & Chen, Q. (2009). "Flow dynamics and characterization of a cough". *Indoor air*, 19(6), 517-525.

Holmes, N. S., & Morawska, L. (2006). "A review of dispersion modelling and its application to the dispersion of particles: an overview of different dispersion models available". *Atmospheric environment*, 40(30), 5902-5928.

Coleman, H. W., & Steele, W. G. (2009). " Experimentation, validation, and uncertainty analysis for engineers". *John Wiley & Sons*.

Jensen, P. A., & Schafer, M. P. (1998). " Sampling and characterization of bioaerosols". *NIOSH manual of analytical methods*, 1(15), 82-112.

Jørgensen, F. E. (2002)" How to measure turbulence with hot-wire anemometers: a practical guide". *Dantec dynamics*, Publication no.: 9040U6151.

Kähler, C. J., Scharnowski, S., & Cierpka, C. (2012). " On the resolution limit of digital particle image velocimetry". *Experiments in fluids*, 52(6), 1629-1639.

Kinnamer, M.(2007). " Infection Control for Health Care Providers". 2nd Ed. ,pp79-85: *Thomson Delmar Learning*.

Knibbs, L. D., Johnson, G. R., Kidd, T. J., Cheney, J., Grimwood, K., Kattenbelt, J. A., ... & Wood, M. E. (2014). " Viability of Pseudomonas aeruginosa in cough aerosols generated by persons with cystic fibrosis". *Thorax*, thoraxjnl-2014.

Durst, F. (2008). " Fluid mechanics: an introduction to the theory of fluid flows".

Springer Science & Business Media. ISBN: 9783540713425(2008).

Kwon, S. B., Park, J., Jang, J., Cho, Y., Park, D. S., Kim, C., Bae,G. & Jang, A. (2012). "Study on the initial velocity distribution of exhaled air from coughing and speaking". *Chemosphere*, 87(11), 1260-1264.

Li, A., Qin, E., Xin, B., Wang, G., & Wang, J. (2010). " Experimental analysis on the air distribution of powerhouse of Hohhot hydropower station with 2D-PIV". *Energy Conversion and Management*, 51(1), 33-41.

Lin, W., Naik, U., Cuthbertson, L.R., Savory, E., and Mubareka, S.,(2014). "Pulsed UV Light Decontamination of Virus-Laden Airstreams." *Final Report for Topnotch Building Maintenance*, no.1. October: 1–49.

Lowen, A. C., Steel, J., Mubareka, S., & Palese, P. (2008). " High temperature (30 C) blocks aerosol but not contact transmission of influenza virus". *Journal of virology,* 82(11), 5650-5652.

Lowen, A. C., Mubareka, S., Steel, J., & Palese, P. (2007)." Influenza virus transmission is dependent on relative humidity and temperature". *PLoS pathogens*, 3(10), e151.

Memarzadeh, F. (2013)." Literature Review: Room Ventilation and Airborne Disease Transmission". *ASHE*.

Morawska, L. (2006)." Droplet fate in indoor environments, or can we prevent the spread of infection?". *Indoor air*, 16(5), 335-347.

Mubareka, S., Lowen, A. C., Steel, J., Coates, A. L., García-Sastre, A., & Palese, P. (2009). " Transmission of influenza virus via aerosols and fomites in the guinea pig model". *The Journal of infectious diseases*, 199(6), 858-865.

NCIRD. "Avian Influenza A Virus Infections in Humans | Avian Influenza (Flu)." *www.cdc.gov*, *Centers for Disease Control and Prevention*, 15 Feb. 2016, 3:15 p.m., www.cdc.gov/flu/avianflu/avian-in-humans.htm

Nishimura, H., Sakata, S., & Kaga, A. (2013)." A new methodology for studying dynamics of aerosol particles in sneeze and cough using a digital high-vision, high-speed video system and vector analyses". *PloS one*, 8(11), e80244.

Shinya, K., Ebina, M., Yamada, S., Ono, M., Kasai, N., & Kawaoka, Y. (2006)." Avian flu: influenza virus receptors in the human airway". *Nature*, 440(7083), 435-436.

Prasad, A. K., Adrian, R. J., Landreth, C. C., & Offutt, P. W. (1992)." Effect of resolution on the speed and accuracy of particle image velocimetry interrogation". *Experiments in Fluids*, 13(2), 105-116.

Raffel, M., Willert, C. E., Wereley, S., & Kompenhans, J. (2013). Particle image velocimetry: a practical guide. Springer.

Bi,R., Ali, S., Savory, E., Zhang, C. (2017). "Computational Fluid Dynamics Modeling of Human Coughs." In CFD 2017, 1–10. Windsor- Ontario- *CANADA: CFD SOCIETY OF CANADA*.

Marple, S. L., & Marple, S. L. (1987)." Digital spectral analysis: with applications" (Vol. 5). *Englewood Cliffs, NJ*: Prentice-Hall.

Savory, E., Lin, W. E., Blackman, K., Roberto, M. C., Cuthbertson, L. R., Scott, J. A., & Mubareka, S. (2014). Western Cold and Flu (WeCoF) aerosol study–preliminary results. BMC research notes, 7(1), 563.

Shah, U., Zhu, J., Zhang, C., & Nother, J. H. (2006). " Numerical investigation of coarse powder and air flow in an electrostatic powder coating process". *Powder technology*, 164(1), 22-32.

Stamhuis, E. J. (2006). " Basics and principles of particle image velocimetry (PIV) for mapping biogenic and biologically relevant flows". *Aquatic Ecology*, 40(4), 463-479.

Sze To, G. N., Wan, M. P., Chao, C. Y. H., Wei, F., Yu, S. C. T., & Kwan, J. K. C. (2008)." A methodology for estimating airborne virus exposures in indoor

environments using the spatial distribution of expiratory aerosols and virus viability characteristics". *Indoor air*, 18(5), 425-438.

Tang, J. W., Li, Y., Eames, I., Chan, P. K. S., & Ridgway, G. L. (2006)." Factors involved in the aerosol transmission of infection and control of ventilation in healthcare premises". *Journal of Hospital Infection*, 64(2), 100-114.

Tang, J. W., Noakes, C. J., Nielsen, P. V., Eames, I., Nicolle, A., Li, Y., & Settles, G. S. (2011)." Observing and quantifying airflows in the infection control of aerosol-and airborne-transmitted diseases: an overview of approaches". *Journal of Hospital Infection*, 77(3), 213-222.

Tang, J. W., Liebner, T. J., Craven, B. A., & Settles, G. S. (2009)." A schlieren optical study of the human cough with and without wearing masks for aerosol infection control". *Journal of the Royal Society Interface*, rsif20090295.

Khadivi, T.(2012). " Experimental and Numerical Study of Flow Structures Associated With Low Aspect Ratio Elliptical Cavities." *Electronic Ph.D. Thesis*, School of Graduate and Postdoctoral Studies, University of Western Ontario, London, Ontario

Hashemi Tari, P. (2012). " Near-Wake Flow Dynamics of a Horizontal Axis Wind Turbine." Electronic Ph.D. Thesis, School of Graduate and Postdoctoral Studies, University of Western Ontario, London, Ontario

Tellier, R. (2006)." Review of aerosol transmission of influenza A virus". *Emerging infectious diseases*, 12(11), 1657.

Tellier, R. (2009)." Aerosol transmission of influenza A virus: a review of new studies". *Journal of the Royal Society Interface*, rsif20090302.

Tropea, C., & Yarin, A. L. (2007)." Springer handbook of experimental fluid mechanics" (Vol. 1). *Springer Science & Business Media*.

TSI Coorporation (TM). 2004. "Installing the Model 610034 LASER PULSE Synchronizer Installing the Model 610034 LASER P ULSE Synchronizer". *TSI*

Incorporated Manuel.

TSI Coorporation(TM). 2008. " Data Acquisition, Analysis, and Display Software Platform User's Guide". *TSI Incorporated User's Guide.*

Van Hoeven, N., Pappas, C., Belser, J. A., Maines, T. R., Zeng, H., García-Sastre, A., ... & Tumpey, T. M. (2009)." Human HA and polymerase subunit PB2 proteins confer transmission of an avian influenza virus through the air". *Proceedings of the National Academy of Sciences*, 106(9), 3366-3371.

VanSciver, M., Miller, S., & Hertzberg, J. (2011)." Particle image velocimetry of human cough". *Aerosol Science and Technology*, 45(3), 415-422.

Verreault, D., Moineau, S., & Duchaine, C. (2008)." Methods for sampling of airborne viruses". *Microbiology and Molecular Biology Reviews*, 72(3), 413-444.

Wei, J., & Li, Y. (2015)." Enhanced spread of expiratory droplets by turbulence in a cough jet". *Building and Environment*, 93, 86-96.

Wei, J., & Li, Y. (2017)." Human Cough as a Two-Stage Jet and Its Role in Particle Transport". *PloS one*, 12(1), e0169235.

Westerweel, J. (1997)." Fundamentals of digital particle image velocimetry". *Measurement science and technology*, 8(12), 1379.

White, F. M. (2010)." Fluid mechanics", *WCB. 7th Ed*. McGraw-Hill New York 862.

World Health Organization (WHO) (2006). "Infection control standard precautions in health care." *Health-care facility recommendations for standard precautions.* [*http://www.who.int/csr/resources/publications/EPR_AM2_E7.pdf?ua=1*]. Geneva, Switzerland: World Health Organization .

Xie, X., Li, Y., Chwang, A. T. Y., Ho, P. L., & Seto, W. H. (2007)." How far droplets can move in indoor environments–revisiting the Wells evaporation–falling curve". *Indoor air*, 17(3), 211-225.

Yan, W., Zhang, Y., Sun, Y., & Li, D. (2009)." Experimental and CFD study of unsteady airborne pollutant transport within an aircraft cabin mock-up". *Building and Environment*, 44(1), 34-43.

Yang, S., Lee, G. W., Chen, C. M., Wu, C. C., & Yu, K. P. (2007)." The size and concentration of droplets generated by coughing in human subjects". *Journal of Aerosol Medicine*, 20(4), 484-494.

Yang, W., Elankumaran, S., & Marr, L. C. (2011)." Concentrations and size distributions of airborne influenza A viruses measured indoors at a health centre, a day-care centre and on aeroplanes". *Journal of the Royal Society Interface*, rsif20100686.

Yue, Z., & Malmström, T. G. (1998)." A simple method for low-speed hot-wire anemometer calibration". *Measurement Science and Technology*, 9(9), 1506.

Zayas, G., Chiang, M. C., Wong, E., MacDonald, F., Lange, C. F., Senthilselvan, A., & King, M. (2012)." Cough aerosol in healthy participants: fundamental knowledge to optimize droplet-spread infectious respiratory disease management". *BMC pulmonary medicine*, 12(1), 11.

Zhu, S., Yang, J. H., & Kato, S. (2006)." Investigation into Airborne Transport Characteristics of Airflow Due to Coughing in a Stagnant Indoor Environment". *ASHRAE transactions*, 112(1).

Zhu, S., Kato, S., & Yang, J. H. (2006)." Study on transport characteristics of saliva droplets produced by coughing in a calm indoor environment". *Building and environment*, 41(12), 1691-1702..

Appendix (A) Previous literature on Aerodynamic Characteristics and Droplet Size Distribution

Table 9 Previous literature on Aerodynamic Characteristics of Coughing Jet Flow

Authors, References Year	Method, Technology	Subjects	Field (Region)	Results
Gupta.et al. (2009)	Moderate speed photography120 Hz (Smoke)	12 Females 13 Males	Near field (near mouth)	Mean angles $\Theta_1=40\pm4$, $\Theta_2=15\pm5$, average mouth opening area 4.00 ± 0.95 cm^2 & 3.37 ± 1.4 cm^2 for male and females, The study measured medical parameters such as CPFR,PVT,CEV.
Tang et al (2009)	Schlieren Video Records (Smoke)	6 Males 4 Females	Near field (near mouth)	Cough considered as classical incompressible turbulent jet with spread angle 23.9^o, 2 litres or so far expelled each cough with average max. velocity 8 m/sec.
Nishimura et al (2013)	Digital high-vision High-speed video and vector analysis	One healthy subject	84 cm from the mouth	Cough velocity at near region greater than 5 m/sec and decreased after 0.05 sec.

Kown et al (2012)	PIV (oil)	26 Subjects	Near field(initial velocity immediately at the mouth)	Cough velocity and spread angles respectively Males=15.3m/s,38° Females=10.6m/s, 32°
Bourouiba et al (2014)	High speed camera	1 subject	70 cm from the mouth	Turbulent multiphase puffs & self-similar leading to increase of its size and decrease its mean speed with distance from source., d=10μm will fall at distance of 0.08mm at speed 3mm/s.
Zhu et al (2006)	PIV (flour)	3 healthy students	Near field (near mouth)	6.7mg of saliva was expelled with 22 m/sec and average velocity11.2 m/sec. Indoor flow field, flow filed weakened & gravity affected transport process of droplets
Chao et al (2009)	PIV (oil mist) Interferometric	Healthy 3 males ,9 females	Near field 10-60 mm from the mouth	Air velocity of coughing Male=13.2 m/sec, Female=10.2m Average max. velocity=11.7 m/sec
VanScriver et al (2011)	PIV (theatrical fog)	10 males 19 females	Within chamber of (25*15)	Cough velocity ranged from 1.5 m/sec-28.8m/sec overall average max cough velocity 10.2 m/sec, no correlation found between sex & weight expanded linearly initially constant at distance from the mouth

| Afshari et al (2002) | PIV (oil droplets) | Cough simulator | Within chamber of dimension (4'*4'*8') | PIV makes possible to undertake detailed analysis of cough flow pattern in an enclosed space. |
| Savory et al. (2014) | PIV (TiO3) | Healthy students 3 Females 9 Male | Far field 1 m | Significant motion & average air velocity of 0.5 m/sec, velocity profiles have no single characteristic shape for cough. |

Table 10 Previous Literature on Droplet Size Distribution of respiratory activities and concentrations

Authors, References & Date	Method, Technology	Subjects	Field (Region)	Results
Xie et al (2007)	Theoretical Simple Physical model	-	Up to 2 m	Examined for free-falling droplets when the relative humidity of the indoor air environment was 0%, 50%, 70%, and 90%,and found that "large droplets" were larger than 125, 100, 85, and 60 μm, respectively. The study found that expelled large droplets were carried more than 2 m away at a velocity of 10 m/s.
Yang, S. et al (2007)	Aerodynamic particle sizer (APS) and scanning mobility particle sizer (SMPS)	54 healthy	Near the mouth	Studied effects of age and gender on droplet and airborne distribution sizes. Total average size distribution of the droplet nuclei was 0.58–5.42 μm, and 82% of droplet nuclei in the range of 0.74–2.12 μm, the size distribution of coughed droplets peaked at approximately 1 μm, 2 μm, and 8 μm. At a low relative humidity, more droplets and droplet nuclei could remain suspended in the air
Lowen et. al. (2007)	Mammalian model	Hartley strain guinea pigs	-	Large droplets and/or droplet nuclei were enhanced at low temperature (5°C) and high temperature (30°C) interrupted airborne transmission at all values of RH. At 20° C, transmission was highly efficient at an RH of 20 and 35 %, low at 50 %, efficient again at 65 % and absent at 80 %

Mubareka, S. (2009)	Mammalian model	Guinea pig model	80 or 107 cm	The study showed that different influenza strains differ considerably in their capacity for aerosol transmission
Van Hoeven, N.(2009)	Ferret model	Genetic determinants that confer the transmission phenotype	-	Not all influenza strains are capable of 'airborne transmission', by which they meant large droplets and/or aerosols, as their experimental set-up did not allow for the distinction.
Yang, W. et al (2011)	Filter extracts	Health centre, a day-care facility and onboard aeroplanes	16 samples	8 out 16 collected samples contained influenza (A) viruses by the concentration ranged from 5800 to 37000 genome copies per m^3. On average, 64% of viruses-laden particles were found to be associated with particles smaller than 2.5μm, which can remain as airborne for prolonged time
Chao, et al (2009)	Interferometric Mie Imaging (IMI)	Healthy 8 males 3 females	close proximity to the mouth	The results estimated that 950-2100 droplets were expelled per cough. The study found that the droplet concentration ranged from 2.4-5.2 per cm^3 for each cough
Zayas et al., (2012)	Laser diffraction system in the open bench	45 healthy non-smokers	close proximity to the mouth	Droplets ranging from 0.1 - 900 μm in size were generated by voluntary coughs. Droplets of less than one micron size represent 97% of the total number

Appendix (B): Pressure transducer final calibration

Table 11 Pressure transducer final calibration (Manufacture's Datasheet)

```
                    O M E G A D Y N E    I N C.
               An Affiliate of Omega Engineering, Inc.

                        PRESSURE TRANSDUCER
                        FINAL CALIBRATION

                   0.00 -        1.00 PSIG
                   Excitation   24.000 Vdc

         Job: R6735                        Serial: 436108
       Model: PX409-001G5V-EH           Tested By: KSM
        Date: 6/22/2016        Temperature Range: -17 to +85 C
  Calibrated:      0.00 -     1.00 PSIG      Specfile: PX409V5<=1GEH

          Pressure    Unit Data
            PSIG         Vdc
        ----------    ----------
            0.00        0.011
            0.50        2.512
            1.00        5.018
            0.50        2.512
            0.00        0.011

  Balance          0.011    Vdc
  Sensitivity      5.007    Vdc


          ELECTRICAL LEAKAGE: PASS
  PRESSURE CONNECTION/FITTING: 1/4-18 NPT Male
  ELECTRICAL WIRING/CONNECTOR: Integral Cable 4-Cond
                               BLACK = - EXCITATION
                               WHITE = + OUTPUT
                               GREEN =  N/C
                               RED   = + EXCITATION

      This Calibration was performed using Instruments and Standards that are
      traceable to the United States National Institute of Standards Technology.
    S/N          Description            Range           Reference    Cal Cert
  801         PPC3  2.2 PSIG AUTO  0 -       1.00 PSIG   C-1952       C-1952
  0           2.2                  Unit Under Test       0            0

  Q.A. Representative :                          Date: 6/22/2016


  This transducer is tested to & meets published specifications. After final
  calibration our products are stored in a controlled stock room & considered in
  bonded storage. Depending on environment & severity of use factory calibration
  is recommended every one to three years after initial service installation date.
```

Appendix (C)

C-1 : HWA Error calculations

The following subsection provides the uncertainty of a single velocity sample which is acquired by a CTA anemometer with a single-sensor probe. The relative standard uncertainty u(y$_i$) is a function of the standard deviation of the input variance (Coleman 2009):

$$u(y_i) = \frac{1}{y_i} * s * [\frac{\Delta x}{k_i}]$$ (C-1)

Where:

$S = \frac{\partial y_i}{\partial x_i}$ is the sensitivity factor, k_i is the coverage factor related to the distribution of the input variance (Gaussian, rectangular etc.).

In general, a Gaussian error distribution is assumed and the highest confidence level, which is normally required, is achieved by multiplying the standard uncertainty with the coverage factor k=2. The total relative expanded uncertainty then becomes (Coleman 2009):

$$U \text{ (tot)} = 2*\sqrt{(u(y_i)^2)}$$ (C-2)

The uncertainty of CTA anemometer measurements is a combination of the calibration equipment, instrumentation, and experimental conditions.

C-1.1 The Uncertainty of the Calibration Equipment

The major source of uncertainty comes from the calibration when it is performed with a dedicated calibrator such as that used in the present work. The uncertainty is computed by using the root sum squared R.S.S. method on equation C-3 that recall (Coleman 2009; Jørgensen 2002),

$$U_{th} = 2 * \frac{A_t}{A_p} * \frac{dh}{dt} * \left(1 - \frac{r^2}{R^2}\right) \qquad (C\text{-}3)$$

Let us consider $\frac{dh}{dt} = S$ and rewrite eqn. (C-1)

$$U_{th} = 2 * \frac{A_t}{A_p} * S * \left(1 - \frac{r^2}{R^2}\right) \qquad (C\text{-}4)$$

Δ_u can be obtained From R.S.S. method then

$$\Delta_u = \left[\left(\frac{\partial u_{th}}{\partial S} * \Delta_s\right)^2 + 0\right]^{1/2} \qquad (C\text{-}5)$$

where:

Δ_u is the uncertainty in the final measured result (U_{th}) due to the uncertainties in each S.

Δ_s is the uncertainty of the measured result (S) which equals to 0.00035.

Equation C-5 may be rearranged to yield:

$$\Delta_u = \sqrt{\left(\frac{\partial U_{th}}{\partial S} * \Delta_s\right)^2} = \frac{\partial U_{th}}{\partial S} * \Delta_s \qquad (C\text{-}6)$$

Differentiating eqn. C-2 with respect to S and substituting in eqn. C-6 yields:

$$\Delta_u = 2 * \frac{A_t}{A_p} * \left(1 - \frac{r^2}{R^2}\right) * \Delta_s \qquad\qquad (C-7)$$

where:

r- The probe position from the pipe centre = 0.001075 m

R − The pipe radius =0.00925m

A_t − Water tank cross section area, R_t = 0.1507m

A_p- Pipe cross section area

C-1.2 A/D board resolution

The resolution uncertainty, which is related to data acquisition, is stochastic with a square distribution and it is relative standard uncertainty can be expressed as (Jørgensen 2002; Coleman 2009):

$$(\Delta_{res}) = \frac{1}{\sqrt{3}} * \frac{1}{U} * \frac{E_{AD}}{2^a} * \frac{\partial U}{\partial E} \qquad\qquad (C-8)$$

Where:

U the air velocity, E_{AD} is the A/D board input range (3V), n is its resolution in bits (a=12)

$\frac{\partial U}{\partial E}$ is the slope (sensitivity factor) of the inverse calibration curve.

From king's law $E^2 = B * U^n$, then

$$U = \left(\frac{E^2 - A}{B}\right)^{\frac{1}{n}} \tag{C-9}$$

Differentiating eqn. (C-9) yields:

$$\frac{\partial U}{\partial E} = \frac{1}{n} * \left(\frac{E^2 - A}{B}\right)^{\frac{1-n}{n}} * \frac{2E}{B} \tag{C-10}$$

Substitute eqn. C-8 to C-10 and rearrange eqn. C-10 will yield:

$$(\Delta_{res}) = \frac{1}{\sqrt{3}} * \frac{1}{U} * \frac{E_{AD}}{2^a} * \frac{1}{n} * \left(\frac{E^2 - A}{B}\right)^{\frac{1-n}{n}} * \frac{2E}{B} \tag{C-11}$$

where:

A and B are King's law coefficients and from the calibration process they typically have values 1.5719 and 0.6081, respectively, and so accordingly   E =1.36 v.

C-1.3   Uncertainties of experimental conditions

The uncertainties related to experimental conditions include probe positioning, temperature variations, and ambient pressure variations. In following subsections these uncertainties are presented (Jørgensen 2002; Coleman 2009).

C-1.3a Probe Positioning

This is related to the probe alignment in the experimental setup after calibration, and can be calculated by this expression (Jørgensen 2002):

$$\Delta_{pos} = \frac{1}{\sqrt{3}} * (1 - cos\theta) \tag{C-12}$$

In general, the probe can be positioned with an uncertainty of $\Delta\theta = \pm 1°$, (Jørgensen 2002).

C-1.3b Temperature Variation

This is considered as systematic error produced from the calibration to experiment or during an experiment. It caused a stochastic uncertainty when a changes in temperature changes the sensor over-temperature. The relative standard uncertainty can be expressed as (Coleman 2009):

$$\Delta_{temp}= \frac{1}{\sqrt{3}} * \frac{1}{U} * \frac{1}{T_w-T_o} * \left(\frac{A}{B} * U^{-0.5} + 1\right) \qquad (C\text{-}13)$$

Where T_w is the sensor temperature= 300°C, T_0 the ambient reference temperature =20.1°C, and the uncertainty due to changes in air density with temperature alone can be calculated from the following correlation (Coleman 2009):

$$\Delta_{\rho,temp.}= \frac{1}{\sqrt{3}} * \frac{\Delta T}{273} \qquad (C\text{-}14)$$

Where: ΔT is the difference between the ambient reference temperature and the temperature during the measurement.

C-1.3c Ambient pressure variations

This contributes as a stochastic uncertainty because the ambient pressure variations influence the density and, hence, the calculated velocity and can be expressed as (Hugh W. Coleman 2009):

$$\Delta_{\rho,P}= \frac{1}{\sqrt{3}} * \frac{\Delta P}{P_\circ+\Delta P} \qquad (C\text{-}15)$$

Where: ΔP is the pressure drop, P_o is the ambient pressure.

C-2: PIV Error Calculations

In particle image velocimetry measurements as in any an experimental measurements the main source of errors comes from two components. The first component systematic error, also known as bias error, which comes from which is caused by many aspects of the measurement technique and equipment. The second component is the random error, which is come by the statistical variation of the measured quantities (Khadive, 2012.; Tari, 2012.; Elatar, 2013.). These errors can be combined and regrouped in terms of error due to velocity gradient, the seeding particles diameter, out of plane motion of particles, peak-locking bias error, and finally the interpolation of velocity vectors (Cowen and Monismith 1997).

The error due to each of these parameters has been investigated and the total measurement error has been calculated accordingly.

C-2.1 The velocity gradient error:

The raw PIV data were used to compute the largest mean velocity in pixel/pixel. The Matlab code (Appendix F-b) used to calculate the velocity gradients which are:

$\frac{\partial u}{\partial y} = 0.000374$, and $\frac{\partial v}{\partial x} = 0.00042$ (pixel/pixel)

Using figure 5(e) (Cowen and Monismith 1997), the error associated with velocity gradient are computed for RMS error and were found to be approximately:

$\varepsilon_u = 0.0045$ pixel and $\varepsilon_v = 0.005$ pixel.

C-2.2 The error due to seeding particles diameter:

In the present study and as mentioned in section 3.2.3, the maximum diameter for seeding particles equal to 0.47μm which means less than micron. According to the calibration process the particle diameter in image size will equal 0.004 pixel. However, the error associated to the particle diameter cannot be resolved by using figure 5(a) (Cowen and Monismith 1997), where the smallest size of particles is 0.06 pixel. Prasad (Prasad et al. 1992) provided in his work a good estimation of the increasing in uncertainty due to particle diameter. Figure 13 (Prasad et al. 1992) present the variation of bias and random errors with the ratio of bias and random error s with the ratio of ratio of pixels per particles ($d\tau/d_{pix}$). The pixel spacing of the used PowerView2MP cameras is 7.4 micron and the absolute size of the particle image is 0.004 pixel. Then $d\tau/d_{pix} = 0.054$. The particle image error from Fig.13 (Prasad et al. 1992) equal to 0.01 pixel.

C-2.3 The interpolation error:

In the PIV measurements, it is required to interpolate the randomly located data grid in order to calculate turbulent statistics (Cowen and Monismith 1997; Taravat Khadive, 2012.). Figure 5f (Cowen and Monismith 1997) shown the results for the dynamic range sensitivity tests are unaffected. In Fig.5f, only the RMS error shown since the mean results are unaffected. From Fig5f, it is clear that the error due to interpolation is almost constant with 0.08 pixel (Cowen and Monismith 1997).

C-2.4 The error due to out of the plane:

The out of plane particle error is estimated by computing the maximum in plane displacements (Tari, 2012.). The thickness of the laser sheet in the present work is 1.34 mm in the measured area, which according to the calibration coefficients equals to 11.48 pixel. The largest in plane displacement in this work (participant 221- cough2) is 4.8 pixel, which is less than the laser sheet thickness. Assuming that the out of plane pixel displacement is less than the in plane displacement (Khadive, 2012.; Tari, 2012.;

Elatar,2013.), it can be inferred that the estimated error due to out of plane motion of the particles is negligible in the current scenario.

C-2.5 Peak locking bias error:

Peak locking bias error is defined as the particle displacements towards integer pixel values, which is a result of both the choice of sub-pixel fit estimator, and under- resolved optical sampling of the particle images (Khadive, 2012.; Kähler, Scharnowski, and Cierpka 2012). The RMS velocity and Reynolds stress are sensitive to peak locking, however, the mean velocity profiles are insensitive to this effect (Kähler et al 2012). Despite the various proposed sub fit estimators, Westerweel has shown that sub-pixel estimation is capable of reducing the effect of peak locking significantly compared to other method (Westerweel 1997). In the present work, Insight 3G PIV software, is used to process the captured data, implements a Gaussian sub-pixel estimator for the correlation peak. Therefore, the peak-locking error has been assumed to be negligible (Khadive, 2012.).

Appendix (D) Approved Documents

ROMEO - Researcher Portal

General Info

FileNo: 108945
Title: Characterization of influenza virus laden infectious bioaerosols (Western Cold and Flu or WeCoF Aerosol Study)
Start Date: 21/02/2017
End Date: 21/02/2018
Keywords: Influenza, cough, bioaerosol, transmission, particle image velocimetry, air sampling, respiratory virus, particle generation

Project Members

Principal Investigator

Prefix: Dr.
Last Name: Savory
First Name: Eric
Affiliation: Engineering\Mechanical & Materials Engineering
Rank: Professor
Gender: Male
Email:
Phone1:
Phone2:
Fax:
Mailing Address:

Institution: Western University
Country: Canada
Comments:

Common Questions

1. Registration Information

#	Question	Answer
1.1	Do you confirm that you have read the above information and that based on that information you are completing the correct form?	Yes

2.2	Please provide a clear statement of the purpose and objectives of this project (one page maximum).	The novelty of the proposed research lies in the fact that the fluid dynamics of the jet aerosols produced by coughing will be examined concurrently with the biological processes associated with virus droplet formation and transmission, using human subjects when they are naturally infected by influenza virus and, again, when they return to health. Newer generations of air samplers have the capacity to retain viral particles which may be detected by molecular methods and in some cases, growth in cell culture. This approach contrasts with previous fluid dynamic studies that have either used artificial aerosol sources or only healthy subjects. The primary objective of this study is to gather data on infectious bioaerosols generated by participants with influenza-like illness (ILI) and presumed viral upper respiratory tract infection (URTI). Specifically, we will generate flow velocity measurements during quiet breathing and expulsion events such as coughing to create cough envelopes during acute and convalescent phases of illness. Secondary objectives include air sampling for infectious virus and viral nucleic acid during acute illness and particle enumeration during acute and convalescent phases of illness. We also need to

		compare the cough fluid dynamics against those from a healthy cohort of recruited subjects for reference. Correlation of cough envelope characteristics, viral shedding, and particle generation will be made with participant gender, symptoms (type, duration), co-infection of respiratory viruses, influenza vaccination status and medication (including antiviral) use. We hypothesize that given the anticipated flow rates from expulsion events such as coughs, viral particles will be identified in the field beyond the commonly quoted 3 or even 6 feet. In order to achieve a statistically significant database and to determine an envelope of cough flow fields it is planned to recruit up to 50 sick and 50 healthy participants over the entire study period, encompassing two flu seasons (2016/7 and 2017/8), due to the inherent variability in the structure of each individual cough.

Attachments

Description	File Name	Version Date
	108945 Savory post.pdf	30/01/2017
	Response to REB recommendations_30 Jan 2017.docx	30/01/2017
	108945_Revised 30 Jan 2017_Clean.docx	30/01/2017
	Letter of information 2017_Revised 30 Jan 2017_Clean.docx	30/01/2017
Consent Form	Consent Form 2017_Revised 30 Jan 2017_Clean.docx	30/01/2017
Initial Approval Notice	DOC022217-0003.pdf	22/02/2017

Unique identifier | **DD/MM/201_**

WeCoF Aerosol Study Participant Eligibility Form

1. Is your age between 18 and 35 years old inclusive?
   - ☐ Yes
   - ☐ No

2. In the past 48 hours have you experienced
   - Fever
       - ☐ Yes
       - ☐ No
   - Cough
       - ☐ Yes
       - ☐ No
   - Sore throat
       - ☐ Yes
       - ☐ No

3. Do any of the following apply to you?
   - ☐ Yes
   - ☐ No

- **Pregnant**
- **Recent asthma or puffer use**
- **Smoker (smoked any amount in the last month)**
- **Untreated HIV**
- **Organ or bone marrow transplant**
- **Hematological malignancy**
- **Receiving chemotherapy**
- **On steroids or other immunosuppressant(s)**
- **Autoimmune disease**
- **Congenital heart disease**
- **Cystic fibrosis**

Document Version Date: 18/1/17

Western Engineering

Project Title: Characterization of influenza virus laden infectious bioaerosols (Western Cold and Flu or WeCoF Aerosol Study)

Principal Investigator: Dr. Eric Savory, PhD, Department of Mechanical and Materials Engineering.

Letter of Information

1. **Invitation to Participate**

   You are being invited to participate in this research study about the aerosols produced by people with colds or the flu when they cough or sneeze because you are experiencing these symptoms.

2. **Purpose of the Letter**

   The purpose of this letter is to provide you with information required for you to make an informed decision regarding participation in this research.

3. **Purpose of this Study**

   The purpose of this study is to understand the nature of the aerosols produced by people with colds or the flu when they cough or sneeze. This is important to understand how these types of infections are transmitted.

4. **Inclusion Criteria**

   Individuals who are between the ages of 18 and 35, inclusive, and have experienced fever and cough and/or sore throat are eligible to participate in this study during illness and after recovery. Individuals who are between the ages of 18 and 35, inclusive, and are not experiencing fever and cough and/or sore throat are eligible to participate in this study as part of a healthy participant control group.

5. **Exclusion Criteria**

   Individuals who are immunocompromised, pregnant, smokers, or have underlying heart or lung conditions are not eligible to participate in this study.

6. **Study Procedures**

   If you agree to participate, you will be asked to complete a brief eligibility form and sign a consent form. You do not waive any legal rights by signing this consent form.

You will then be asked to self-collect a nose swab which will be used to identify the cold or flu virus you have. You will be requested to cough in a box where we can measure the aerosols you produce. We will also sample the air you exhale. We will ask you to return within a month to repeat these measurements after you have recuperated. If you have influenza symptoms is anticipated that the entire task will take 2 hours: just over an hour for the first visit and approximately 45 minutes for the second visit. If you are participating as a healthy subject your single visit will last approximately 45 minutes. The task(s) will be conducted in Room 308 in the Thompson Engineering Building. There will be a maximum total of fifty healthy and fifty unwell participants.

7. **Possible Risks and Harms**

The possible risks and harms to you include a very small risk of eye damage due to the laser used to produce a thin light-sheet inside the box which will be used to determine the airflow velocities in your coughs . You will be seated outside the box but you will also be provided with protective goggles to further mitigate this risk. Also, the box you will cough into contains particles to seed the air so we can see your cough. This will not pose a risk to you if it is not inhaled in large quantities.

8. **Possible Benefits**

You may not directly benefit from participating in this study but information gathered may provide benefits to society as a whole which include a more profound understanding on how colds and flu are transmitted from one person to another, leading to new ways to prevent the spread of these infections.

9. **Compensation**

You will be compensated $75.00 for participation in this study, $50.00 for the first visit during your illness and $25.00 for the follow-up visit when you have recuperated from your illness. If you do not complete the entire study you will still be compensated by $50.00 for the first visit to our laboratory.

If you are only participating as a healthy volunteer, you will receive $25.00 for completing a single visit to our laboratory.

10. **Voluntary Participation**

Participation in this study is voluntary. You may refuse to participate, refuse to answer any questions or withdraw from the study at any time with no effect on

Western Engineering

your future care. You may, at any time, request the withdrawal from the study database any data and/or biological samples taken during your participation in this study. The electronic data will be permanently deleted, paper-based data shredded and the samples destroyed. Note that if your request is made after the results from the study have been published it will not be possible to modify those results to reflect the removal of your data from the database.

11. Confidentiality

All data collected will remain confidential and accessible only to the investigators of this study. Your research records will be stored in the following manner: locked in a cabinet in a secure office. If the results are published, your name will not be used. If you choose to withdraw from this study, your data will be removed and destroyed from our database. Representatives of Western University Health Sciences Research Ethics Board may contact you or require access to your study-related records to monitor the conduct of the research. If we find information we are required by law to disclose, we cannot guarantee confidentiality.

12. Contacts for Further Information

If you require any further information regarding this research project or your participation in the study you may contact **Dr. Eric Savory**,

If you have any questions about your rights as a research participant or the conduct of this study, you may contact The Office of Research Ethics

13. Publication

If the results of the study are published, your name will not be used. If you would like to receive a copy of any potential study results, please provide your name and contact number on a piece of paper separate from the Consent Form.

This letter is yours to keep for future reference.

Western Engineering

Consent Form

Project Title: Characterization of influenza virus laden infectious bioaerosols (Western Cold and Flu or WeCoF Aerosol Study)

Study Investigator's Name: Dr. Eric Savory, PhD, Department of Mechanical and Materials Engineering. Tel

I have read the Letter of Information, have had the nature of the study explained to me and I agree to participate. All questions have been answered to my satisfaction. I understand that I do not waive any legal rights by signing this consent form.

Participant's Name (please print): _____

Participant's Signature: _____

Date: _____

Person Obtaining Informed Consent (please print): _____

Signature: _____

Date: _____

Version Date: 30/01/17
Participant Initials___

Appendix (E): FLUGIE Procedures

Install the virus sampling cassettes

- Put on gloves and N95 mask. **Do not touch virus sampling cassettes with bare hands or breathe on them.**

- Note the two rings where the tape around the cassette circumference can be cut open

- Take two cassettes, a cutting tool and a ziplock bag. Enter box. Attach cassettes to hanging tubes as follows:

  1. Pull the green plug out of cassette and place the plug in the ziplock bag
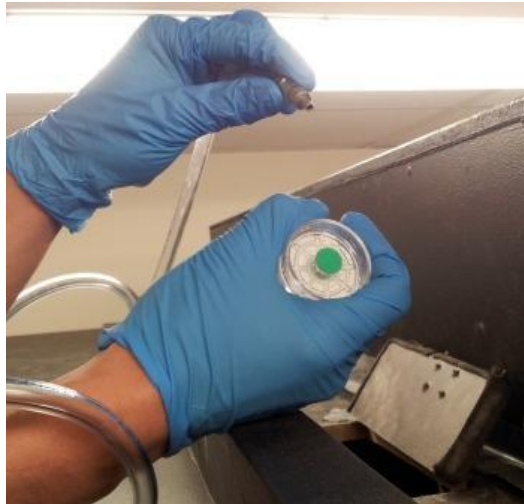
  2. Attach the fitting at the end of the hanging tube to the cassette port where the green plug was attached.
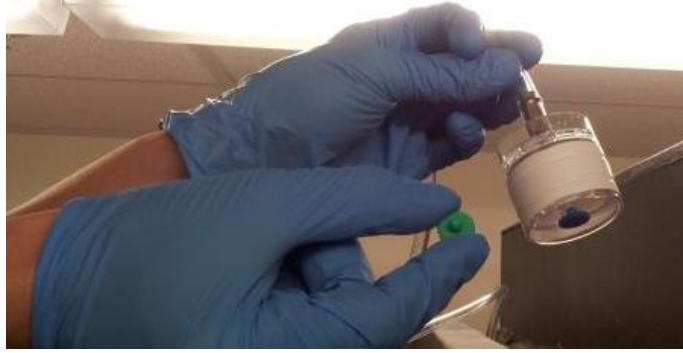
3. Using the cassette opener, cut the tape around the ring closest to the blue plug. Remove and place the cassette end with the blue plug in the ziplock bag. **The sampling surface in the cassette is now exposed so be careful not to contaminate it by touch or breath.**

4. Check each tube is hanging over a white hook and string at the box roof. This step ensures the cassette will be at the correct distance from the cough inlet and on the box centreline.

5. Verify that the cassettes are in the cough path.
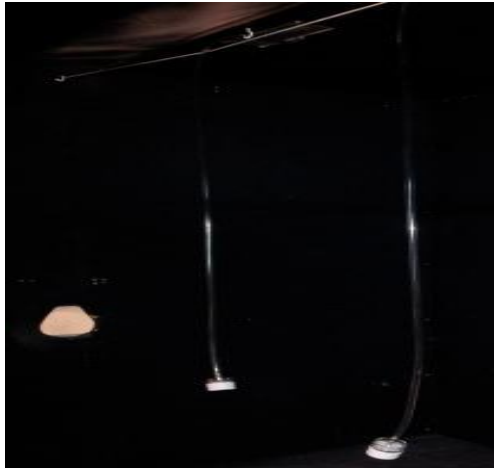
PIV pre-prep before the study participant arrives

- Check box is at 1 m position (duct tape marker on floor)

- Put on laser safety goggles.

- On the two laser units, turn key right to the 'ON' position. Turn flash lamp knob to min power.

- On the laser units, hold 'STANDBY' button for one second and release. Lasers should be humming now. Turn flash lamp knob to max power.

- Turn on synchronizer by pressing power switch (front face, upper right corner).

- Plug camera into power mains. Remove lens cap.

- Start Insight3G on PIV computer. Right-click desired data folder to save to in the Experiment Tree and set current run. Click 2nd tab at lower left and verify settings:

Mode: PIV, Exposure: Synchronized, Capture: Sequence, Laser A: Low, Laser B: Low, $\Delta t = 750$ us.

Other pre-prep

- Clean window on box floor. Shut and lock the door. Dispose of waste in an orange bio-waste bag.
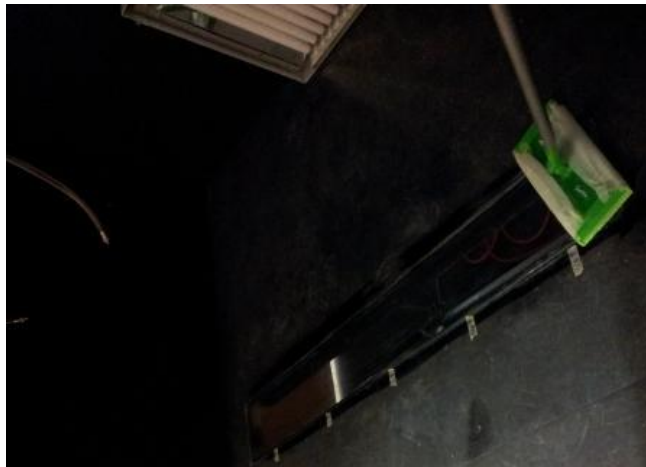
- Turn hallway laser warning sign on (switch is in interior lab room on the wall to your left upon entry)

- Take $50 from the safe and place with a receipt into an accessible drawer

- Put on official study name badge (keep on top of safe/yellow cabinet)

Greet the study participant

- Collect a completed consent form

- Note the participant identifier number.

Conduct virus sampling and cassette recovery

- Seat the participant at the cough inlet

- Remove inlet cover (white plastic) from screw. Wipe the inlet surfaces with Virox.

- Adjust seat height such that chin rests comfortably on the cough inlet bottom.
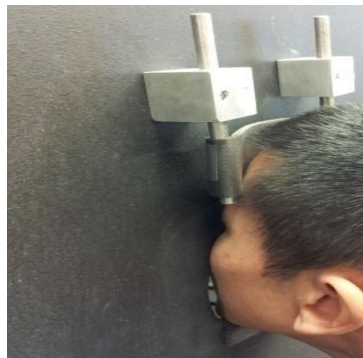
- Adjust forehead rest by unlocking screws (move rods up/down and lock screws).
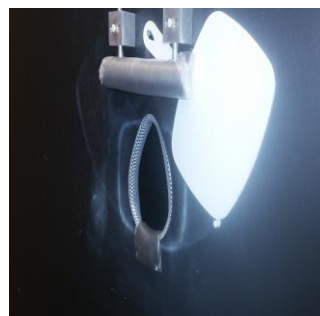
- With participant in coughing posture, view their head in profile to ensure head angle is such that the cough will be emitted horizontally.

- Replace inlet cover on screw.

- Give coughing instructions: Turn head to side and away from inlet, inhale deeply and naturally, and open inlet cover by rotating and holding it to one side. Rest chin on lower padding on inlet cutout and forehead on upper padded band. Cough straight forward (not up or down) with the hot-wire sensor as a target. Close inlet cover.

- Turn on the two air sampling pumps with small screwdriver.
- Turn on hot-wire sensor by plugging into power bar.
- Ask participant if ready to cough. If yes, press Run arrow in 'HWA_Acq.vi' program to start the hot-wire recording (**30 sec to collect a cough**).
- Rename HWA datafile with Participant ID # and Cough #.
- Repeat and collect data for three coughs.
- Two minutes after the last cough, turn off the two air sampling pumps.
- Open roof flap and pull up the cassette. Replace the blue cap end onto the cassette, remove the cassette from tube and replace the green cap. Sanitize the cassette exterior and tubing with Virox wipe. **Note cassette location (0.5 m or 1.0 m)!** Place a new cassette on the tubing, place over hook and string, and lower into box. Close and lock roof flap. Repeat for second cassette.
- **Label the cassettes with participant identifier number, location (0.5 or 1.0 m)** Store cassettes in fridge.

Conduct MT swabbing

- Remove swab kit from the lab fridge with correct participant ID # and open it with the participant.
- Ensure instructions are fully understood:
  1. Insert in nose up to measured point
  2. Twirl around
  3. Place in tube
  4. Snap off upper portion

- Ask the participant to perform the MT swab in the washroom or lab

- Ensure participant identifier number is on the tube

- Place tube in fridge (**max 24 hrs**.)

Conduct flow measurements

- Equip all eyes present in the laboratory with laser safety goggles

- Explain laser safety essentials

- Turn on TiO2 seeding from Pitt3 aerosol generator

  o Attach power plug for acoustic speaker to the mains socket

  o Ensure valve is fully shut to start (red handle as shown in photo)

  o Attach hose coupling to the 40 psi air line at the workbench

  o Pull yellow cap on regulator down to unlock the pressure adjustment knob

  o Slowly turn yellow cap right to increase pressure to around 2 psi

  o Fully open valve (turn red handle 90° right)

- Lock lab door to hallway and shut interior lab door. Shut lights in lab.
- When light sheet is full of particles (~ 1 minute of seeding), fully shut the valve (red handle as shown in photo). Wait for uniform particle distribution (~ 2 minutes).

Initial seeding distribution   *Uniform seeding distribution*
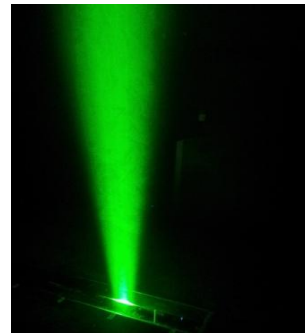
Measure the coughs

- Seat the participant (wearing laser goggles) at the cough inlet
- Remind the participant of the coughing instructions and not to inhale dust from inside the box when the inlet cover is open:
    - Turn head to side and away from inlet
    - Inhale deeply and naturally

- o Open inlet cover by rotating on screw and holding to one side
- o Chin on lower padding on inlet cutout and forehead on upper padding
- o Cough straight forward (not up or down) with the hot-wire sensor as a visual aid for target height.
- o Close inlet cover

- Ask participant if ready to cough. If yes, press Run arrow in 'HWA_Acq.vi' program to start the hot-wire recording (**30 sec to collect a cough**). Press the 'Capture' button in Insight3G to start the first PIV recording.

- Observe particle motion visually inside the box.

- Note any visual observations of the cough motion (e.g. too high, too low) and advise the participant.

- Note start and end frame numbers in Insight3G for each cough. Press 'Save RAM images' button. Ensure previous frame numbers are not saved over (click folder button by 'Capture: Sequence' dropdown menu).

- Rename text file output from HWA (i.e. Participant273-Cough1, Participant273-Cough2, and Participant273-Cough3).

- Repeat for a total of three coughs from the study participant.

- **Unplug hot-wire from power bar.**

Discharge study participant

- Complete both halves of the compensation receipt
- Give $50 and the appropriate half of the receipt page to the participant.
- **Keep the researcher half of the receipt.**
- Upon request, give participant identifier number and Dr. Mubareka's contact info. for MT swab result.

Put the virus samples in -80 °C freezer

- Put on gloves and mask. Prepare access to orange biohazard bag.
- Get tweezers, storage tubes (CA330C 3ml of UTM-RT with glass beads).

- Mark two storage tubes with the participant identifier and location number.
- Get the two cassette samples from fridge.
    1. Cut tape around the ring closest to the green plug and open the cassette at this ring for the cassette sample at 0.5 m.
    2. Discard the cassette half without the membrane (blue plug) into biohazard bag.
    3. Using tweezers carefully separate the membrane from the cassette.
    4. Insert the membrane into a storage tube such that the exposed side is towards inside of the tube.
    5. Fasten the storage tube cap
    6. Discard cassette half in the orange biohazard bag
    7. The tube should be shaken for 10 sec by a vortex shaker and then stored.
- Get the MT swab from the fridge.
- **Verify membranes and swab labels have same participant identifier number.**
- Attach label with following info: 'Prof. Savory, TEB 308, sealed membranes and swab with influenza virus, Participant #'
- Wipe down the zip lock bag and your gloves with Virox.
    - **Keep bio-samples in TEB 308 fridge if all else fails (max 24 hr.) and inform Prof. Savory.**
    - Verify freezer temperature from external display is at -80 °C.
    - Limit the time that their freezer is open to < 30 seconds.
    - Fill out the user log on the freezer door.
- Update record keeping of Participant # samples in -80 freezer.
- Use Vac. machine, insert hose into box and suck for 15+ minutes to evacuate TiO_2.

<u>Post-lab tasks</u>

- Use Virox wipes to clean any surfaces touched by the participant (e.g. cough inlet, inlet cover, forehead rest, chair, lab door handles, fridge door handle, and workbench).

- Press 'Off' button on synchronizer. Press 'STOP' button on laser units. Turnkey on laser unit to off. Turn switch on back of laser units to off. Unplug PIV camera from power. Verify hot-wire is unplugged. Disconnect Pitt3 hose from 40 psi air-line. Turn off hallway laser warning sign. **Do not shut down PCs or power bar.**

- Leave eligibility form, consent form and receipt in locked box for Prof Savory.

- Copy data to external hard drive and analysis PC.

  - Take orange bio-waste bag to autoclave for decontamination and disposal (When it is partially filled (after 5 participants))

Appendix (F): Matlab Codes

F-(a) Hot Wire Anemometer data processing

```matlab
%                       Western University
%                     Faculty of Engineering
%                Mechanical and Material Department
%               Hot Wire Anemometer data processing
%                         Winter- 2017
%*********************************************************
***************
clc
clear
close all
% Import data files
dataMatrix3=importdata('952-3.txt');
dataMatrix2=importdata('952-2.txt');
dataMatrix1=importdata('952-1.txt');

%Recognize of cough's data file

t1=dataMatrix1(:,1);
E1=dataMatrix1(:,2);
%
t2=dataMatrix2(:,1);
E2=dataMatrix2(:,2);
%
t3=dataMatrix3(:,1);
E3=dataMatrix3(:,2);


%%Extracting data based on range

i1=1; % initial counter
iend=30000; % last counter

t1=t1(i1:iend);
E1=E1(i1:iend);
%
t2=t2(i1:iend);
E2=E2(i1:iend);
%
t3=t3(i1:iend);
E3=E3(i1:iend);
```

```matlab
jump=1;
% converts the voltage reading to the velocity according to
the polynomial eqn.

% 1st cough
t1=t1(1:jump:end);
E1=E1(1:jump:end);
U1 = 2.70515928e+00*E1.^4 - 9.13660081e-09*E1.^3 -
8.50447972e+00*E1.^2 - 2.01192272e-08*E1 + 6.68409586e+00;
%2nd cough

t2=t2(1:jump:end);
E2=E2(1:jump:end);
U2 = 2.70515928e+00*E2.^4 - 9.13660081e-09*E2.^3 -
8.50447972e+00*E2.^2 - 2.01192272e-08*E2 + 6.68409586e+00;
%3th cough
t3=t3(1:jump:end);
E3=E3(1:jump:end);
U3 = 2.70515928e+00*E3.^4 - 9.13660081e-09*E3.^3 -
8.50447972e+00*E3.^2 - 2.01192272e-08*E3 + 6.68409586e+00;

%****************** 1st cough*********************
%window size
k1=299;
UM1=movmean(U1,k1);
UMAX1=max(UM1);
UMIN1=min(UM1);
figure
plot(t1,U1,'g')
title('Move averaging of 1st cough data ')
xlabel('Time(Sec)')
ylabel('Velocity (m/sec)')
grid on
hold on
plot(t1,UM1,'B')
grid on
hold on

 UF1=U1-UM1;
% figure
% plot(t1,UF1,'b')
% grid on

%************ Turbulent Intensity Iu1*************
%*********************cough1***************************
```

```matlab
figure
plot(t1,U1)
[tmin1,Umin1] = ginput(1);
[tmax1,Umax1] = ginput(1);
close
%%%Finding indices corresponding to tmin1 and tmax1
difftmin1=abs(tmin1-t1);
itmin1=find(difftmin1==min(difftmin1));
itpeak1=find(UM1==max(UM1))

difftmax1=abs(tmax1-t1);
itmax1=find(difftmax1==min(difftmax1));

UFrms1=rms(UF1(itmin1:itmax1));
%Intensity Array for the cough period
Iu1=UFrms1./UM1(itmin1:itmax1)*100;
%Intensity at the cough peak velocity
PUM1=max(UM1)-min(UM1);
IuPV1=(UFrms1./(PUM1))*100;
TKE1=(3/2)*max(UF1)^2;
% USUP1=UM1(itmin1:itpeak1);
% tStP1=t1(itmin1:itpeak1);

%%%% power spectrum of Cough %%%%
%
%   Pwelch Transform
[pxxUF1,fUF1] =
pwelch(UF1(itmin1:itmax1),[],[],[],1000,'twosided');...
    ...%power density fuction(Welich)

ArUcvPSC1=trapz(fUF1,pxxUF1);% area under the curve before
normalization
pxxUF1PUF1=pxxUF1/(ArUcvPSC1*2);% normalization of power
spectrum u'
ArUcvPSCNorm1=trapz(fUF1,pxxUF1PUF1);% area under the curve
...
...after normalization

UFNF1=UF1(1:itmin1);
[pxxUFNF1,fUFNF1] =
pwelch(UFNF1(1:itmin1),[],[],[],1000,'twosided');...
    ...%power density fuction(Welich)
tNF1=t1(1:itmin1);
UrmsNF1=sqrt(mean(UFNF1.^2));
freqNF1= 1000; %1/t1(itmin1)-t1(1)
PSNF1=((UrmsNF1)/(freqNF1));
%UF unfiltered function
```

```matlab
% new figure
figure
loglog(fUF1,pxxUF1);
title('Power spectrum of 1st cough data ')
xlabel('frequncy(Hz)')
ylabel('Power spectrum energy of velocity flacutation ')
hold on
grid on
box on

%Area under curve to get u'^2
IuCurve1=sqrt(2.*(trapz(fUF1,pxxUF1)))/(max(UM1)-
min(UM1))*100;
ufsq1=trapz(fUF1,pxxUF1);
ufrmsps1=sqrt(2.*(ufsq1));
PUM1NF=mean(UM1(1:itmin1));
IucurvNF1=sqrt(2.*(trapz(fUFNF1,pxxUFNF1)))/PUM1NF*100;
ufsqNF1= trapz(fUFNF1,pxxUFNF1);

%%% Independence check for normalized power spectrum
%
for i=itmin1: itmax1
 UFrmsCheck1(i-itmin1+1)=rms(UF1(itmin1:i));
 end
SampleNo1=1:length(UFrmsCheck1);
figure
plot(SampleNo1,UFrmsCheck1)
%
%***********************************************************
%******************** 2nd  cogh*************************
%window size
k2=199;
UM2=movmean(U2,k2);
UMAX2=max(UM2);
UMIN2=min(UM2);
figure
plot(t2,U2,'g')
title('Move averaging of 2nd cough data ')
xlabel('Time(Sec)')
ylabel('Velocity (m/sec)')
grid on
hold on
plot(t2,UM2,'b')
grid on
hold on
UF2=U2-UM2;
% figure
```

```matlab
% plot(t2,UF2,'b')
% grid on

%*********** Turbulent Intensity Iu2*********************
%********************cough2****************************
figure
plot(t2,U2)
[tmin2,Umin2] = ginput(1);
[tmax2,Umax2] = ginput(1);
close
%%%Finding indices corresponding to tmin1 and tmax1
difftmin2=abs(tmin2-t2);
itmin2=find(difftmin2==min(difftmin2));

difftmax2=abs(tmax2-t2);
itmax2=find(difftmax2==min(difftmax2));

UFrms2=rms(UF2(itmin2:itmax2));
%Intensity Array for the cough period
Iu2=UFrms2./UM2(itmin2:itmax2)*100;
%Intensity at the cough peak velocity
PUM2=max(UM2)-min(UM2);
IuPV2=(UFrms2./(PUM2))*100;
TKE2=(3/2)*max(UF2)^2


%%%% power spectrum of Cough %%%%
%
% Transform
[pxxUF2,fUF2] =
pwelch(UF2(itmin2:itmax2),[],[],[],1000,'twosided');...
    ...%power density fuction(Welich)

ArUcvPSC2=trapz(fUF2,pxxUF2);% area under the curve before
normalization
pxxUF2PUF2=pxxUF2/(ArUcvPSC2*2);% normalization of power
spectrum u'
ArUcvPSCNorm2=trapz(fUF2,pxxUF2PUF2);%...
...area under the curve after normalization

UFNF2=UF2(1:itmin2);
[pxxUFNF2,fUFNF2] =
pwelch(UFNF2(1:itmin2),[],[],[],1000,'twosided');...
    ...%power density fuction(Welich)
tNF2=t2(1:itmin2);
UrmsNF2=sqrt(mean(UFNF2.^2));
freqNF2= 1000 %1/t1(itmin1)-t1(1))
```

```matlab
PSNF2=((UrmsNF2)/(freqNF2));
%UF unfiltered function
% new figure
figure
loglog(fUF2,pxxUF2)
title('Power spectrum of 2nd cough data ')
xlabel('frequncy(Hz)')
ylabel('Power spectrum energy of velocity flacutation ')
hold on
grid on
box on


%Area under under curve to get u'^2
IuCurve2=sqrt(2.*(trapz(fUF2,pxxUF2)))/(max(UM2)-
min(UM2))*100;
ufsq2=trapz(fUF2,pxxUF2);
ufrmsps2=sqrt(2.*(ufsq2));
PUM2NF=mean(UM2(1:itmin2));
IucurvNF2=sqrt(2.*(trapz(fUFNF2,pxxUFNF2)))/PUM2NF*100;
ufsqNF2= trapz(fUFNF2,pxxUFNF2);

%%% Independence check for normalized power spectrum
%
for i=itmin2: itmax2
 UFrmsCheck2(i-itmin2+1)=rms(UF2(itmin2:i));
 end
SampleNo2=1:length(UFrmsCheck2);
figure
plot(SampleNo2,UFrmsCheck2)
%

%**********************************************************
%***************** 3th cough ****************
%window size
k3=101;
UM3=movmean(U3,k3);
UMAX3=max(UM3);
UMIN3=min(UM3);
figure
plot(t3,U3,'g')
title('Move averaging of 3th cough data ')
xlabel('Time(Sec)')
ylabel('Velocity (m/sec)')
grid on
hold on
plot(t3,UM3,'b')
```

```matlab
grid on
hold on
UF3=U3-UM3;
% figure
% plot(t3,UF3,'b')
% grid on
% hold on


%************ Turbulent Intensity Iu3 ********************

%*********************cough3***************************
figure
plot(t3,U3)
[tmin3,Umin3] = ginput(1);
[tmax3,Umax3] = ginput(1);
close
%%%Finding indices corresponding to tmin1 and tmax1
difftmin3=abs(tmin3-t3);
itmin3=find(difftmin3==min(difftmin3));

difftmax3=abs(tmax3-t3);
itmax3=find(difftmax3==min(difftmax3));

UFrms3=rms(UF3(itmin3:itmax3));
%Intensity Array for the cough period
Iu3=UFrms3./UM3(itmin3:itmax3)*100;
%Intensity at the cough peak velocity
PUM3= max(UM3)-min(UM3);
IuPV3=(UFrms3./(PUM3))*100;
TKE3=(3/2)*max(UF3)^2;

%%%% power spectrum of Cough %%%%
%
% Transform
[pxxUF3,fUF3] =
pwelch(UF3(itmin3:itmax3),[],[],[],1000,'twosided');...
    ...%power density fuction(PWelich)

ArUcvPSC3=trapz(fUF3,pxxUF3);% area under the curve before
normalization
pxxUF3PUF3=pxxUF3/(ArUcvPSC3*2);% normalization of power
spectrum u'
ArUcvPSCNorm3=trapz(fUF3,pxxUF3PUF3);%...
...area under the curve after normalization

UFNF3=UF3(1:itmin3);
```

```matlab
[pxxUFNF3,fUFNF3] =
pwelch(UFNF3(1:itmin3),[],[],[],1000,'twosided');%...
...power density fuction(Welich)
tNF3=t3(1:itmin3)
UrmsNF3=sqrt(mean(UFNF3.^2))
freqNF3= 1000 %1/t1(itmin1)-t1(1))
PSNF3=((UrmsNF3)/(freqNF3))
%UF unfiltered function
% new figure
figure
loglog(fUF3,pxxUF3)
title('Power spectrum of 3th cough data ')
xlabel('frequncy(Hz)')
ylabel('Power spectrum energy of velocity flacutation ')
hold on
grid on
box on

%Area under under curve to get u'^2
IuCurve3=sqrt(2.*(trapz(fUF3,pxxUF3)))/(max(UM3)-
min(UM3))*100;
ufsq3=trapz(fUF3,pxxUF3);
ufrmsps3=sqrt(2.*(ufsq3));
PUM3NF=mean(UM3(1:itmin3));
IucurvNF3=sqrt(2.*(trapz(fUFNF3,pxxUFNF3)))/PUM3NF*100;
ufsqNF3= trapz(fUFNF3,pxxUFNF3);

%%% Independence check for normalized power spectrum
%
for i=itmin3: itmax3
 UFrmsCheck3(i-itmin3+1)=rms(UF3(itmin3:i));
 end
SampleNo3=1:length(UFrmsCheck3);
figure
plot(SampleNo3,UFrmsCheck3)
%
%%%%%%%%%%Autocorrelation function%%%%%%%%%%%%

time_interval=1/1000;
lag_time=1;
max_lag=lag_time/time_interval;
Ucough3=U3(itmin1:itmax1);
UFcough3=UF3(itmin1:itmax1);
UMcough3=UM3(itmin1:itmax1);

for r=1:max_lag+1
    Rtau3(r)=0;
```

```matlab
    for n=1:(length(Ucough3)-r)
        Rtau3(r)=Rtau3(r)+1/mean( UFcough3.^2
)/(length(Ucough3)-r-1)*...
            UFcough3(n)*UFcough3(n+r-1);
    end
    tau3(r)=(r-1)*time_interval;
end
figure;
plot(tau3,Rtau3)
hold on
xlabel('\tau3, s');ylabel('R(\tau3)');grid;
title('Autocorrelation function3');

% Integral length scale and Taylor micro length scale
for r0=1:max_lag
    if Rtau3(r0)*Rtau3(r0+1)<=0
        break
    end
end
tau03=tau3(r0);   %First tau at which Rtau=0
time_scale3=0;
for j=1:r0

time_scale3=time_scale3+(Rtau3(j)+Rtau3(j+1))*time_interval
…/2;
end
length_scale3=time_scale3*(max(UM3)-min(UM3))*0.5; %...
    ...Integral length scale in m
Taylor_time3=tau3(2)/sqrt(1-Rtau3(2));
Taylor_length_longitudinal3=Taylor_time3*(max(UM3)-
min(UM3));% ...
    ...%Taylor longitudinal length scale in m
Taylor_length_transverse3=Taylor_length_longitudinal3/sqrt(
2); %
...Taylor transverse length scale in m

%%%%%%%%%%%Autocorrelation function cough1%%%%%%%%%%%

time_interval=1/1000;
lag_time=1;
max_lag=lag_time/time_interval;
Ucough1=U1(itmin1:itmax1);
UFcough1=UF1(itmin1:itmax1);
UMcough1=UM1(itmin1:itmax1);

for r=1:max_lag+1
    Rtau(r)=0;
```

```matlab
    for n=1:(length(Ucough1)-r)
        Rtau(r)=Rtau(r)+1/mean( UFcough1.^2
)/(length(Ucough1)-r-1)*...
        UFcough1(n)*UFcough1(n+r-1);
    end
    tau(r)=(r-1)*time_interval;
end
figure;
plot(tau,Rtau)
hold on
xlabel('\tau, s');ylabel('R(\tau)');grid;
title('Autocorrelation function1');

%%%%%%%%%%%%% Integral length scale and Taylor micro length
scale %%%%%%%%%%
for r0=1:max_lag
    if Rtau(r0)*Rtau(r0+1)<=0
        break
    end
end
tau0=tau(r0);   %First tau at which Rtau=0
time_scale=0;
for j=1:r0

time_scale=time_scale+(Rtau(j)+Rtau(j+1))*time_interval/2;
end
length_scale=time_scale*(max(UM1)-min(UM1))*0.5;%Integral
length scale in m
Taylor_time=tau(2)/sqrt(1-Rtau(2));
Taylor_length_longitudinal=Taylor_time*(max(UM1)-
min(UM1));...
    ...%Taylor longitudinal length scale in m
Taylor_length_transverse=Taylor_length_longitudinal/sqrt(2)
;...
...%Taylor transverse length scale in m

%%%%%%%%%%%%%Autocorrelation function cough2 %%%%%%%%%%%%%

time_interval=1/1000;
lag_time=1;
max_lag=lag_time/time_interval;
Ucough2=U2(itmin1:itmax1);
UFcough2=UF2(itmin1:itmax1);
UMcough2=UM2(itmin1:itmax1);

for r=1:max_lag+1
    Rtau2(r)=0;
```

```matlab
    for n=1:(length(Ucough2)-r)
        Rtau2(r)=Rtau2(r)+1/mean( UFcough2.^2
)/(length(Ucough2)-r-1)*...
            UFcough2(n)*UFcough2(n+r-1);
    end
    tau2(r)=(r-1)*time_interval;
end
figure;
plot(tau2,Rtau2)
hold on
xlabel('\tau2, s');ylabel('R(\tau2)');grid;
title('Autocorrelation function2');

%%%%%%%%%% Integral length scale and Taylor micro length
scale %%%%%%%%%
for r0=1:max_lag
    if Rtau2(r0)*Rtau2(r0+1)<=0
        break
    end
end
tau02=tau2(r0);   %First tau at which Rtau=0
time_scale2=0;
for j=1:r0

time_scale2=time_scale2+(Rtau2(j)+Rtau2(j+1))*time_interval
/2;
end
length_scale2=time_scale2*(max(UM2)-min(UM2))*0.5;
%Integral length scale in m
Taylor_time2=tau2(2)/sqrt(1-Rtau2(2));
Taylor_length_longitudinal2=Taylor_time2*(max(UM2)-
min(UM2));...
    ...%Taylor longitudinal length scale in m
Taylor_length_transverse2=Taylor_length_longitudinal2/sqrt(
2);...
...%Taylor transverse length scale in m
figure;
plot(tau,Rtau)
hold on
plot(tau2,Rtau2)
plot(tau3,Rtau3)
xlabel('\tau2, s');ylabel('R(\tau2)');grid;
title('Autocorrelation function2');
%************************************************************

%******* characteristics of three coughs flow**************
  figure
```

```matlab
plot(t1,U1,'g')
hold on
plot (t2,U2,'b')
hold on
plot (t3,U3,'r')
hold on
grid on
box on
legend ('Cough1', 'Cough2', 'Cough3');
title('Time Histroy of three coughs ')
xlabel('Time (sec)')
ylabel('Velocity(m/sec) ')
U1max=max(U1);
U2max=max(U2);
U3max=max(U3);

%*************cough normalizing***********************
%*************************cough1************************
ipeak1=find(UM1==max(UM1));
ipeak1=ipeak1(1);% to select the first max element of
array...
...if we have more than one
tpeak1=t1(ipeak1);
USUP1=(max(UM1)-UM1(itmin1))
tStP1=(tpeak1-t1(itmin1))
Unormal1=(UM1-UM1(itmin1))/(max(UM1)-UM1(itmin1));...
    ...%normalize the cough velocity

tnormal1=(t1-t1(itmin1))/(tpeak1-t1(itmin1));...
    ...%normalize the cough time period
%****************************cough2*********************
%
ipeak2=find(UM2==max(UM2));
ipeak2=ipeak2(1);%...
...to select the first max element of array if we have more
than one
tpeak2=t2(ipeak2);
USUP2=(max(UM2)-UM2(itmin2))
tStP2=(tpeak2-t2(itmin2))
Unormal2=(UM2-UM2(itmin2))/(max(UM2)-UM2(itmin2));%...
...normalize the cough velocity

tnormal2=(t2-t2(itmin2))/(tpeak2-t2(itmin2));% ...
...normalize the cough time period
%
%****************************cough3*******************
ipeak3=find(UM3==max(UM3));
```

```matlab
ipeak3=ipeak3(1);%...
...to select the first max element of array if we have more
than one
tpeak3=t3(ipeak3);
USUP3=(max(UM3)-UM3(itmin3))
tStP3=(tpeak3-t3(itmin3))
Unormal3=(UM3-UM3(itmin3))/(max(UM3)-UM3(itmin3));%...
...normalize the cough velocity

tnormal3=(t3-t3(itmin3))/(tpeak3-t3(itmin3));...
    ...% normalize the cough time period

%************** plot three normalize coughs*************
figure
plot(tnormal1,Unormal1)
 xlabel('\tau,(Time dimensionless)')
ylabel('Dimensionless cough velocity of three trials ')
hold on
grid on
box on
plot(tnormal2,Unormal2)
plot(tnormal3,Unormal3)
legend ('Cough1', 'Cough2', 'Cough3');
%***********************************************************
jump=1;
tref1=t1(itmin1:jump:end)-t1(itmin1);
Uref1=U1(itmin1:jump:end);
tref2=t2(itmin2:jump:end)-t2(itmin2);
Uref2=U2(itmin2:jump:end);
tref3=t3(itmin3:jump:end)-t3(itmin3);
Uref3=U3(itmin3:jump:end);
figure
hold on
grid on
box on
plot(tref1,Uref1)
title('refined All three coughs instant');
plot(tref2,Uref2)
plot(tref3,Uref3)
legend ('Cough1', 'Cough2', 'Cough3');
%***********************************************************
%%******** create file of turbulent intensity table
fid=fopen('par-PSCD-952s.txt','w');
fprintf(fid, 'UFrms-of moving average\n');

fprintf(fid, '%f %f %f  \n', [ UFrms1 UFrms2 UFrms3]');
```

```matlab
fprintf(fid, 'Turbulance Intensity Iu\n');

fprintf(fid, '%f %f %f  \n', [ IuPV1 IuPV2 IuPV3]');
fprintf(fid, 'Turbulance Intensity Iu-trapz function\n');
fprintf(fid, '%f %f %f  \n', [ IuCurve1 IuCurve2
IuCurve3]');
fprintf(fid, 'Turbulance Intensity Iu-no flow\n');
fprintf(fid, '%f %f %f  \n', [ IucurvNF1 IucurvNF2
IucurvNF3]');
fprintf(fid, 'UFrms-of trapz function curve\n');

fprintf(fid, '%e %e %e  \n', [ ufrmsps1 ufrmsps2
ufrmsps3]');
fprintf(fid, 'PUM1  PUM2  PUM3\n');
fprintf(fid, '%f %f %f  \n', [ PUM1 PUM2 PUM3]');
fprintf(fid, 'PUM1NF  PUM2NF  PUM3NF\n');
fprintf(fid, '%f %f %f  \n', [ PUM1NF PUM2NF PUM3NF]');
fprintf(fid, 'ArUcvPSC1  ArUcvPSC2  ArUcvPSC3\n');
fprintf(fid, '%f %f %f  \n', [ ArUcvPSC1 ArUcvPSC2
ArUcvPSC3]');
fclose(fid);true
%
fid=fopen('par-PSCh1-952s.txt','w');
fprintf(fid, '%e %e \n', [ pxxUF1 fUF1]');
fclose(fid);true
%
fid=fopen('par-PSCh2-952s.txt','w');
fprintf(fid, '%e %e \n', [ pxxUF2 fUF2]');
fclose(fid);true
%
fid=fopen('par-PSCh3-952s.txt','w');
fprintf(fid, '%e %e \n', [ pxxUF3 fUF3]');
fclose(fid);true
 %create file one for moving average velocity
fid=fopen('participant952s.txt','w');
fprintf(fid, 'TKE\n');

fprintf(fid, '%f %f %f  \n', [ TKE1 TKE2 TKE3]');

fprintf(fid, 'Turbulance Intensity Iu\n');

fprintf(fid, '%f %f %f  \n', [ IuPV1 IuPV2 IuPV3]');
fprintf(fid, 'Maximum averging velocity for three
coughs\n');
fprintf(fid, '%f %f %f  \n', [ max(UM1) max(UM2)
max(UM3)]');
fprintf(fid, '%f %f %f  \n', [ USUP1 USUP2 USUP3]');
```

```matlab
fprintf(fid, '%f %f %f  \n', [ tStP1 tStP2 tStP3]');
fprintf(fid, '%e %e %e %e %e %e \n',...
[ tnormal1 Unormal1  tnormal2 Unormal2 tnormal3
Unormal3]');
fclose(fid);true

% % %***************** Widows size independent ***********
WindowMaxLimit=1000;

for i=1:WindowMaxLimit/2
k1(i)=2*i-1;
UM1=movmean(U1,k1(i));
UF1=U1-UM1;
UFrms1(i)=sqrt(mean(UF1.^2));

end
figure
plot(k1,UFrms1)
legend('cough 1')
xlabel('Window Size')
ylabel('Ufrms^2) ')
% hold on
for i=1:WindowMaxLimit/2
k2(i)=2*i-1;
UM2=movmean(U2,k2(i));
UF2=U2-UM2;
UFrms2(i)=sqrt(mean(UF2.^2));

end
figure
plot(k2,UFrms2)
legend('cough 2')
xlabel('Window Size')
ylabel('Ufrms^2) ')
for i=1:WindowMaxLimit/2
k3(i)=2*i-1;
UM3=movmean(U3,k3(i));
UF3=U3-UM3;
UFrms3(i)=sqrt(mean(UF3.^2));

end
figure
plot(k3,UFrms3)
legend('cough 3')
xlabel('Window Size')
ylabel('Ufrms) ')
```

F-(b) PIV data processing

```
%                      Western University
%                    Faculty of Engineering
%            Mechanical and Material Department
%                      PIV data processing
%                        Summer- 2017
%************************************************************
clear
clc
close all

%%%% input participant and cough numbers
HealthySick='healthy'; % Name of parent folder
Participant='Analysis-221'; % Input the forlder name of the
participant
CoughNo='cough5';    %Input cough number folder name


%%%%% Inputs and conversions
convfacvel =((1.1905e-4*1000000)/750);%...
...This factor was used to convert from Pixel to Physical
unit(m)
convfacdis =1.1905e-4;
NCellX=74;  %Vector field in X direction
NCellY=99; %Vector field in Y direction
IntersectionLength=0.039+0.0104;
CameraHeight=0.1885; % Max Y value from the given data
FrameToCheck=11;
XToCheck=37; % X index varies from 1 to 74

%%%% Reading
cd(char(HealthySick)); %% Change directory...
...It will direct you to the folders of Sick or Healthy
cd (char(Participant)); %% Change directory...
...It will direct you to the folder of the participant
cd (char(CoughNo)); % select the cough number folder
cd 'RH';  % Select the right camera folder

folder=pwd; %pwd means current folder
filetype='*.vec'; …
… % "Insigh3G-PIV platform" output files format

%%% Reading all vec files inside the given cough
f=fullfile(folder,filetype);
```

```matlab
dR=dir(f);

for k=1:numel(dR) %Number of files or frames
  dataR{k}=importdata(fullfile(folder,dR(k).name));
end


cd ..;   %%Back one level
cd LH


folder=pwd; %pwd means current folder
filetype='*.vec';  % "Insigh3G-PIV platform" output files
format
f=fullfile(folder,filetype);
dL=dir(f);

for k=1:numel(dL)
  dataL{k}=importdata(fullfile(folder,dL(k).name));
end

NfigsR=numel(dR); %Number of frames right
tR=0:5/(NfigsR-1):5;

NfigsL=numel(dL); %Number of frames left
tL=0:5/(NfigsL-1):5;


%%% We used the first frame to define x and y since they do
...not change with time

%%% Here, xR is similar to xL and yR is similar to yL
xR=dataR{1,1}.data(:,1)*convfacdis;
yR=dataR{1,1}.data(:,2)*convfacdis;

xL=dataL{1,1}.data(:,1)*convfacdis;
yL=dataL{1,1}.data(:,2)*convfacdis;

for i=1:NfigsR %This will create a matrix for each variable
%with a size of (74*99) x65
% where 74*99 is the total number of data points in one
%frame and 65 is the number of frames
uStakR(:,i)=dataR{1,i}.data(:,3)*convfacvel;
%dataR{1,i}.data(:,3) to read the u velocity from the third
column of the data matrix
vStakR(:,i)=dataR{1,i}.data(:,4)*convfacvel;
```

```
velmagStakR=sqrt(uStakR.^2+vStakR.^2);
velMagMaxR(i)=max(velmagStakR(:,i));
velMagMeanR(i)=mean(velmagStakR(:,i));

uStakL(:,i)=dataL{1,i}.data(:,3)*convfacvel;
vStakL(:,i)=dataL{1,i}.data(:,4)*convfacvel;

velmagStakL=sqrt(uStakL.^2+vStakL.^2);
velMagMaxL(i)=max(velmagStakL(:,i));
velMagMeanL(i)=mean(velmagStakL(:,i));

end


%%%% To calculate the velocity for upper camera in pixels
for uncertainty
for i=1:NfigsL
    %This will create a matrix for each variable with a
size of (74*99) x65
    % where 74*99 is the total number of data points in one
frame and 65 is
    % the number of frames
ibadL=find (dataL{1,i}.data(:,5)<=0);
 uStakLi=dataL{1,i}.data(:,3);
 vStakLi=dataL{1,i}.data(:,4);
 uStakLi(ibadL)=[];
  vStakLi(ibadL)=[];
 uPixelmaxL(i)=max(uStakLi);%dataR{1,i}.data(:,3) to read
the u velocity from the third column of the data matrix
vPixelmaxL(i)=max(vStakLi);

end

%%%% To calculate the velocity for lower camera in pixels
…for uncertainty
for i=1:NfigsR
%This will create a matrix for each variable with a size of
(74*99) x65
% where 74*99 is the total number of data points in one
frame and 65 is
% the number of frames
ibadR=find (dataR{1,i}.data(:,5)<=0);
 uStakRi=dataR{1,i}.data(:,3);
 vStakRi=dataR{1,i}.data(:,4);
 uStakRi(ibadR)=[];
  vStakRi(ibadR)=[];
```

```matlab
  uPixelmaxR(i)=max(uStakRi);  %dataR{1,i}.data(:,3) to read
the u velocity from the third column of the data matrix
 vPixelmaxR(i)=max(vStakRi);

end

%%%%%%%%%%% Combining L and R Shifting Upper camera …
upwards by the difference between height and intersection
length

NfigsR=numel(dR); %Put number of files needed here

yR=dataR{1,1}.data(:,2)*convfacdis+CameraHeight-
IntersectionLength;
%%% {Cell}     (Matrix)

%%%To check shared area consistence


for i=FrameToCheck:FrameToCheck

XR=repmat(xR(1:NCellX)',NCellY,1); %Repeat X vector to form
a matrix of 99*74


        % yR(1: Jump (74): End (7326))
YR=repmat(yR(1:NCellX:NCellX*NCellY),1,NCellX); %Repeat Y
vector to form a matrix of 99*74

% converting the cell to matrix (No repetition in velocity)
VR=vec2mat(velmagStakR(:,i),NCellX);
uR=vec2mat(uStakR(:,i),NCellX);
vR=vec2mat(vStakR(:,i),NCellX);



XL=repmat(xL(1:NCellX)',NCellY,1);
YL=repmat(yL(1:NCellX:NCellX*NCellY),1,NCellX);
VL=vec2mat(velmagStakL(:,i),NCellX);
uL=vec2mat(uStakL(:,i),NCellX);
vL=vec2mat(vStakL(:,i),NCellX);


%%% Shared area indices
[shareiR,sharejR]=find(YR<=CameraHeight);
[shareiL,sharejL]=find(YL>=(CameraHeight-
IntersectionLength));
```

```matlab
%Number of shared rows in both right and left cameras
NshareRowsR=length(shareiR)/NCellX;
NshareRowsL=length(shareiL)/NCellX;

% Extracting shared data for right and left
VshareR=VR(end-NshareRowsR+1:end,:);
ushareR=uR(end-NshareRowsR+1:end,:);
vshareR=vR(end-NshareRowsR+1:end,:);
XshareR=XR(end-NshareRowsR+1:end,:);
YshareR=YR(end-NshareRowsR+1:end,:);


VshareL=VL(1:NshareRowsR,:);
ushareL=uL(1:NshareRowsR,:);
vshareL=vL(1:NshareRowsR,:);
XshareL=XL(1:NshareRowsR,:);
YshareL=YL(1:NshareRowsR,:);

%%%% Take the average of right and left shared velocties
Vshare=0.5*VshareR+0.5*VshareL;
ushare=0.5*ushareR+0.5*ushareL;
vshare=0.5*vshareR+0.5*vshareL;
Xshare=0.5*XshareR+0.5*XshareL;
Yshare=0.5*YshareR+0.5*YshareL;

VpureR=VR(1:end-NshareRowsR,:);
upureR=uR(1:end-NshareRowsR,:);
vpureR=vR(1:end-NshareRowsR,:);
XpureR=XR(1:end-NshareRowsR,:);
YpureR=YR(1:end-NshareRowsR,:);

VpureL=VL(NshareRowsR+1:end,:);
upureL=uL(NshareRowsR+1:end,:);
vpureL=vL(NshareRowsR+1:end,:);
XpureL=XL(NshareRowsR+1:end,:);
YpureL=YL(NshareRowsR+1:end,:);


%%%% Combined data cell array for both cameras at each
frame
Vall{1,i}=[VpureR;Vshare;VpureL]; %Magnitude
uall{1,i}=[upureR;ushare;upureL]; % vel in x
vall{1,i}=[vpureR;vshare;vpureL]; % vel in y
Xall{1,i}=[XpureR;Xshare;XpureL]; % X does not change with
frames but was written for consistency
Yall{1,i}=[YpureR;Yshare;YpureL];
```

```matlab
Vortall{1,i}=curl(Xall{1,i},Yall{1,i},uall{1,i},vall{1,i});

end
figure
plot(VR(:,XToCheck),YR(:,XToCheck),VL(:,XToCheck),YL(:,XToC
heck))
h=xR(2)-xR(1);

for i=1:NfigsR
XR=repmat(xR(1:NCellX)',NCellY,1); %Repeat X vector to form
a matrix of 99*74
% yR(1: Jump (74): End (7326))
YR=repmat(yR(1:NCellX:NCellX*NCellY),1,NCellX); %Repeat Y
vector to form a matrix of 99*74

% converting the cell to matrix (No repetition in velocity)
VR=vec2mat(velmagStakR(:,i),NCellX);
uR=vec2mat(uStakR(:,i),NCellX);
vR=vec2mat(vStakR(:,i),NCellX);
XL=repmat(xL(1:NCellX)',NCellY,1);
YL=repmat(yL(1:NCellX:NCellX*NCellY),1,NCellX);
VL=vec2mat(velmagStakL(:,i),NCellX);
uL=vec2mat(uStakL(:,i),NCellX);
vL=vec2mat(vStakL(:,i),NCellX);
%%% Shared area indices
[shareiR,sharejR]=find(YR<=CameraHeight);
[shareiL,sharejL]=find(YL>=(CameraHeight-
IntersectionLength));

%Number of shared rows in both right and left cameras
NshareRowsR=length(shareiR)/NCellX;
NshareRowsL=length(shareiL)/NCellX;

% Exracting shared data for right and left
VshareR=VR(end-NshareRowsR+1:end,:);
ushareR=uR(end-NshareRowsR+1:end,:);
vshareR=vR(end-NshareRowsR+1:end,:);
XshareR=XR(end-NshareRowsR+1:end,:);
YshareR=YR(end-NshareRowsR+1:end,:);

VshareL=VL(1:NshareRowsR,:);
ushareL=uL(1:NshareRowsR,:);
vshareL=vL(1:NshareRowsR,:);
XshareL=XL(1:NshareRowsR,:);
YshareL=YL(1:NshareRowsR,:);

%%%% Take the average of right and left shared velocties
```

```
Vshare=0.5*VshareR+0.5*VshareL;
ushare=0.5*ushareR+0.5*ushareL;
vshare=0.5*vshareR+0.5*vshareL;
Xshare=0.5*XshareR+0.5*XshareL;
Yshare=0.5*YshareR+0.5*YshareL;

VpureR=VR(1:end-NshareRowsR,:);
upureR=uR(1:end-NshareRowsR,:);
vpureR=vR(1:end-NshareRowsR,:);
XpureR=XR(1:end-NshareRowsR,:);
YpureR=YR(1:end-NshareRowsR,:);

VpureL=VL(NshareRowsR+1:end,:);
upureL=uL(NshareRowsR+1:end,:);
vpureL=vL(NshareRowsR+1:end,:);
XpureL=XL(NshareRowsR+1:end,:);
YpureL=YL(NshareRowsR+1:end,:);


%%%% Combined data cell array for both cameras at each
frame
Vall{1,i}=[VpureR;Vshare;VpureL]; %Magnitude
uall{1,i}=[upureR;ushare;upureL]; % vel in x
vall{1,i}=[vpureR;vshare;vpureL]; % vel in y
Xall{1,i}=[XpureR;Xshare;XpureL]; % X does not change with
frames but was written for consistency
Yall{1,i}=[YpureR;Yshare;YpureL];
%%%%Vorticity vector
Vortall{1,i}=curl(Xall{1,i},Yall{1,i},uall{1,i},vall{1,i});

%%Gradient matrix GX=dV/dX, GY=dV/dY

[GVX,GVY]=gradient(Vall{1,i},h);
[GuX,GuY]=gradient(uall{1,i},h);
[GvX,GvY]=gradient(vall{1,i},h);

DV_DX_SpAvg(i)=mean(mean(GVX))*convfacdis/convfacvel;%%%%
To convert m/m to pixels/pixel
DV_DY_SpAvg(i)=mean(mean(GVY))*convfacdis/convfacvel;%%%%
To convert m/m to pixels/pixel
Du_DX_SpAvg(i)=mean(mean(GuX))*convfacdis/convfacvel;%%%%
To convert m/m to pixels/pixel
Du_DY_SpAvg(i)=mean(mean(GuY))*convfacdis/convfacvel;%%%%
To convert m/m to pixels/pixel
Dv_DX_SpAvg(i)=mean(mean(GvX))*convfacdis/convfacvel;%%%%
To convert m/m to pixels/pixel
```

```matlab
Dv_DY_SpAvg(i)=mean(mean(GvY))*convfacdis/convfacvel;%%%%
To convert m/m to pixels/pixel
end
DV_DX_SpAvgTimeMax=max(DV_DX_SpAvg)
DV_DY_SpAvgTimeMax=max(DV_DY_SpAvg)
Du_DX_SpAvgTimeMax=max(Du_DX_SpAvg)
Du_DY_SpAvgTimeMax=max(Du_DY_SpAvg)
Dv_DX_SpAvgTimeMax=max(Dv_DX_SpAvg)
Dv_DY_SpAvgTimeMax=max(Dv_DY_SpAvg)

%%%%%%%%%%%%%%%%%%%%%%%%%%%%%%%%%%%%%%%%%%%%%%%%%%%%%%%%%%%%%

for i=1:NfigsR
    %%Get the velocity column at each frame
     velmagStakR_i=velmagStakR(:,i);
     velmagStakL_i=velmagStakL(:,i);


        uStakR_i=uStakR(:,i);
    uStakL_i=uStakL(:,i);
    % find bad vectors
 ibadR=find (dataR{1,i}.data(:,5)<=0);
 ibadL=find (dataL{1,i}.data(:,5)<=0);

 %Remove bad vectors from the column at each frame
 velmagStakR_i(ibadR)=[];
 velmagStakL_i(ibadL)=[];
 uStakR_i(ibadR)=[];
 uStakL_i(ibadL)=[];

 %Merging both camera data
 velmagStakAll=[velmagStakR_i;velmagStakL_i];
  uStakAll=[uStakR_i;uStakL_i];

 VallMax(i)=max(velmagStakAll);
  uallMax(i)=max(uStakAll);

 VallMean(i)=mean(velmagStakAll);

VallWeightMean(i)=sum(velmagStakAll.^2)/sum(velmagStakAll);
end

%%% Plotting mean with time

figure
plot(tR,VallMean,'--ro');
title('Mean velocity (Two Cameras)')
xlabel('time(sec.)')
```

```matlab
ylabel('Mean Velocity (m/sec)')
hold on
grid on
box on
ax = gca;
ax.XTick =0:0.2:5;
hold on

%%% Plotting max with time
figure
plot(tR,VallMax,'--ro');
title('Maximum velocity (Two Cameras)')
xlabel('time')
ylabel('Max.Velocity (m/sec.)')
hold on
grid on
box on
ax = gca;
ax.XTick =0:0.2:5;

%%%% *****************Contour Plotting**************

for i=1:NfigsR
figure1=figure;
axes1 =
axes('Parent',figure1,'BoxStyle','full','Layer','top',...
    'FontWeight','bold',...
    'FontSize',12,'FontName','Times New Roman');
box(axes1,'on');
hold(axes1,'on');
[C,h] = contourf(Xall{1,i},Yall{1,i},Vall{1,i});

h.LevelStep=2/100;
h.LineStyle='none';
colormap('jet')


hold on

xlabel('x','FontWeight','bold','Rotation',0,'FontSize',12,'
FontName',...
'Times New Roman');
 ylabel(
'y','FontWeight','bold','Rotation',90,'FontSize',12,'FontNa
me',...
    'Times New Roman');
```

```matlab
  ax = gca;

 intervCountX=10;
     XMIN=min(xL);
     XMAX=max(xR);
     ax.XLim=[XMIN XMAX];
     ax.XTick=XMIN:(XMAX-XMIN)/intervCountX:XMAX;
     ax.XTickLabel=sprintf('%0.3f\n',ax.XTick);

     intervCountY=10;
     YMIN=min(yL);
     YMAX=max(yR);
     ax.YLim=[YMIN YMAX];
     ax.YTick=YMIN:(YMAX-YMIN)/intervCountY:YMAX;
     ax.YTickLabel=sprintf('%0.3f\n',ax.YTick);

     c = colorbar;
    c.LineWidth=1.5;
    title(['Two Cameras' ' ' sprintf('%03d',i)])
  %c.Ticks=0:0.1:0.7;***********************

%c.TickLabels=sprintf('%0.1f\n',c.Ticks);*******************
*****
    caxis([0 1.2])
   %  title(c,'B(\xi,\zeta)', 'Position',[-16.4
429.600005080157 0])*****
%%%This will save the figure as png with format fig1, fig2,
...figN********
saveas(gcf,['Velocity Contour' sprintf('%03d',i) '.png'])
hold on
close
end


%*****************************Vorticity*********************
for i=1:NfigsR
figure2=figure;
axes1 =
axes('Parent',figure2,'BoxStyle','full','Layer','top',...
    'FontWeight','bold',...
    'FontSize',12,'FontName','Times New Roman');
box(axes1,'on');
hold(axes1,'on');
[C,h] = contourf(Xall{1,i},Yall{1,i},Vortall{1,i});
h.LevelStep=2/10;
h.LineStyle='none';
```

```matlab
colormap('jet')
hold on

xlabel('x','FontWeight','bold','Rotation',0,'FontSize',12,'FontName','Times New Roman');
 ylabel(
'y','FontWeight','bold','Rotation',90,'FontSize',12,'FontName','Times New Roman');

  ax = gca;

 intervCountX=10;
     XMIN=min(xL);
     XMAX=max(xR);
     ax.XLim=[XMIN XMAX];
     ax.XTick=XMIN:(XMAX-XMIN)/intervCountX:XMAX;
     ax.XTickLabel=sprintf('%0.3f\n',ax.XTick);

     intervCountY=10;
     YMIN=min(yL);
     YMAX=max(yR);
     ax.YLim=[YMIN YMAX];
     ax.YTick=YMIN:(YMAX-YMIN)/intervCountY:YMAX;
     ax.YTickLabel=sprintf('%0.3f\n',ax.YTick);

     c = colorbar;
    c.LineWidth=1.5;
    caxis([-600 800])
    title(['Two Cameras' ' ' sprintf('%03d',i)])
 saveas(gcf,['Vort and Vector' sprintf('%03d',i) '.png'])
 close
end


%%%******************** Vector Plotting **************
for i=1:NfigsR
  figure
    quiver(Xall{1,i},Yall{1,i},uall{1,i},vall{1,i},3)
    Color='k';
    AutoScaleFactor=20;
    LineWidth=25;
    title(['Two Cameras' ' ' sprintf('%03d',i)])
    saveas(gcf,['Vector' sprintf('%03d',i) '.png'])
    close
end
```

```matlab
%%%*******************PDF*********************************
for i=1:NfigsR
%This is to convert the matrix to a single column for
%easier manipulations
    VallColumnVec=reshape(Vall{1,i},[numel(Vall{1,i}),1]);
    % Data density function
%Input for the interval
IntervalR=0.05;
%Number of intervals
NintervalsR=round((max(VallColumnVec)-
min(VallColumnVec))/IntervalR);
%Minimum instantaneous velocity
UminR=min(VallColumnVec);
for j=1:NintervalsR
  % Finding the indices of samples which lie in every
interval
    NindexR=find((UminR+IntervalR*(j-1))<=VallColumnVec
&VallColumnVec<=(UminR+IntervalR*j));
    %Calculating the number of samples for every interval
    NcountR(j)=length(NindexR);
    %Calculating the instantaneous velocity at the centre of
the interval
    UcR(j)=UminR+(j-1/2)*IntervalR;
end
%Calculating probability density function
NR=length(VallColumnVec); % Number of samples
BUFR=NcountR./NR;%/Interval; %PDF
%Plotting the PDF
figure
bar(UcR,BUFR)
xlabel('U (m/s)')
ylabel('No of sample per bin/Total No of samples')
title(['Two Cameras' ' ' sprintf('%03d',i)])
saveas(gcf,['pdffig' sprintf('%03d',i) '.png'])
close
end

%%%%% to find the transient profile of a selected point
Xp=[0.0847 0.0847];
Yp=[0.06641 0.28641];
Yt={'YC' 'YG'};
figure
for j=1:length(Xp)
Xallmat=Xall{1,1};
diffX=abs(Xallmat-Xp(j));
[ip,jp]=find(diffX==min(min(diffX)));
jp1=jp(1); %%%Select only one as they are the same
```

```matlab
Yallmat=Yall{1,1};
diffY=abs(Yallmat-Yp(j));
[ip,jp]=find(diffY==min(min(diffY)));
ip1=ip(1); %%%Select only one as they are the same


for i=1:NfigsR
   Vp(i)=Vall{1,i}(ip1,jp1);

end



plot(tR,Vp)
title('Velocity')

itext=find(Vp==max(Vp));
text(tR(itext),Vp(itext),['\leftarrow ' Yt{j} ])
hold on

end
fid=fopen('Part950cough2vel.txt','w');
fprintf(fid, '%f %f \n', [ tR;VallMean]);
fclose(fid);true
```

Curriculum Vitae

Name: Ahmed Mohamed

Post-secondary   **-** Bright Star University of Technology

Education and   (Sirte University)

Degrees: Albrega- Libya

1987-1991***B.A.***

- University of Benghazi

Garyounis, Benghazi-Libya

1994-2007 ***M.Sc.***

- University of Western Ontario

2015-2017 ***M.E.Sc.***

London, Ontario - Canada

Related Work   - Assistant Lecturer

Experience: Mechanical Engineering Department

Faculty of Engineering

Omar Al-Mukhtar University

Albayda- Libya

2008-2014

- Graduate Research Assistant

The University of Western Ontario

London, Ontario, Canada

2015-2017

Publications:

- M. Ahmed, N. Dudalski, W. E. Lin, E. Savory, S. Mubareka (2017). The far field of coughs produced by healthy and influenza-infected human subjects, Physmod. 2017 – International Physical and Modelling of Flow and Dispersion Phenomena, Dynamics of Urban and Coastal Atmosphere - LHEEA - École Centrale de Nantes – France, 23 - 25 August 2017.

Poster Presentation:

- A. Mohamed, E. Savory," Investigation of Cough Flow and Bio-Aerosol Spread from Influenza Infected Persons"- CHRP Mini-symposium, University Institute of Cardiology and Pulmonology – Laval University, Québec- Canada, October 2016.

- A. Mohamed, N. Dudalski, E. Savory," Experimental Investigation of the Far - Field Flow of Coughs from Healthy and Influenza Infected Human Subjects", The annual CHRP meeting 2017, Department of Microbiology ; Division of Infectious Diseases; University of Toronto, Toronto- Canada June 2017